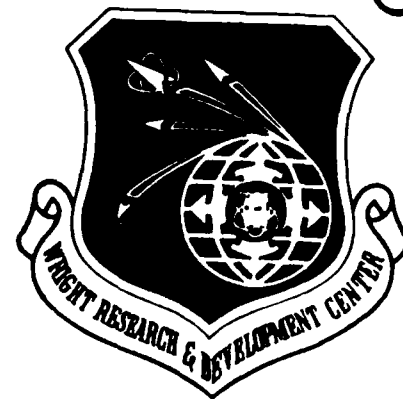


WRDC-TR-89-3123
Volume II

AD-A221 501



B-1B IMPROVED WINDSHIELD DEVELOPMENT
VOLUME II: MAGNA ANALYSIS: BASELINE AND PARAMETRIC

Michael P. Bouchard
William R. Braisted

University of Dayton Research Institute
300 College Park Avenue
Dayton, OH 45469

FEBRUARY 1990

Interim Report for Period Jun87 - Sep88

Approved for public release; distribution unlimited



FLIGHT DYNAMICS LABORATORY
WRIGHT RESEARCH AND DEVELOPMENT CENTER
AIR FORCE SYSTEMS COMMAND
WRIGHT-PATTERSON AIR FORCE BASE, OHIO 45433-6553

NOTICE

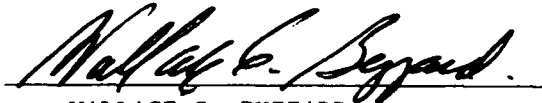
WHEN GOVERNMENT DRAWINGS, SPECIFICATIONS, OR OTHER DATA ARE USED FOR ANY PURPOSE OTHER THAN IN CONNECTION WITH A DEFINITELY GOVERNMENT-RELATED PROCUREMENT, THE UNITED STATES GOVERNMENT INCURS NO RESPONSIBILITY OR ANY OBLIGATION WHATSOEVER. THE FACT THAT THE GOVERNMENT MAY HAVE FORMULATED OR IN ANY WAY SUPPLIED THE SAID DRAWINGS, SPECIFICATIONS, OR OTHER DATA, IS NOT TO BE REGARDED BY IMPLICATION, OR OTHERWISE IN ANY MANNER CONSTRUED, AS LICENSING THE HOLDER, OR ANY OTHER PERSON OR CORPORATION; OR AS CONVEYING ANY RIGHTS OR PERMISSION TO MANUFACTURE, USE, OR SELL ANY PATENTED INVENTION THAT MAY IN ANY WAY BE RELATED THERETO.

THIS REPORT HAS BEEN REVIEWED BY THE OFFICE OF PUBLIC AFFAIRS (ASD/PA) AND IS RELEASABLE TO THE NATIONAL TECHNICAL INFORMATION SERVICE (NTIS). AT NTIS IT WILL BE AVAILABLE TO THE GENERAL PUBLIC INCLUDING FOREIGN NATIONS.

THIS TECHNICAL REPORT HAS BEEN REVIEWED AND IS APPROVED FOR PUBLICATION.



TONG C. CHOE, 2Lt, USAF
Project Engineer
B-1B Project



WALLACE C. BUZZARD
Chief, Aircrew Protection Branch
Vehicle Subsystems Division

FOR THE COMMANDER



RICHARD E. COLCLOUGH, JR.
Chief
Vehicle Subsystems Division

IF YOUR ADDRESS HAS CHANGED, IF YOU WISH TO BE REMOVED FROM OUR MAILING LIST, OR IF THE ADDRESSEE IS NO LONGER EMPLOYED BY YOUR ORGANIZATION PLEASE NOTIFY WRDC/FIVR, WRIGHT-PATTERSON AFB, OH 45433-6553 TO HELP MAINTAIN A CURRENT MAILING LIST.

COPIES OF THIS REPORT SHOULD NOT BE RETURNED UNLESS RETURN IS REQUIRED BY SECURITY CONSIDERATIONS, CONTRACTUAL OBLIGATIONS, OR NOTICE ON A SPECIFIC DOCUMENT.

REPORT DOCUMENTATION PAGE				Form Approved OMB No. 0704-0188	
1a. REPORT SECURITY CLASSIFICATION UNCLASSIFIED			1b. RESTRICTIVE MARKINGS		
2a. SECURITY CLASSIFICATION AUTHORITY			3. DISTRIBUTION/AVAILABILITY OF REPORT Approved for public release; distribution unlimited.		
2b. DECLASSIFICATION/DOWNGRADING SCHEDULE			4. PERFORMING ORGANIZATION/REPORT NUMBER(S) UDR-TR-88-129, Volume II		
5. MONITORING ORGANIZATION REPORT NUMBER(S) WRDC-TR-89-3123, Vol. II			6a. NAME OF PERFORMING ORGANIZATION University of Dayton Research Institute		
6b. OFFICE SYMBOL (If applicable)			7a. NAME OF MONITORING ORGANIZATION Flight Dynamics Laboratory (WRDC/FIVR) Wright Research and Development Center		
6c. ADDRESS (City, State, and ZIP Code) 300 College Park Ave. Dayton OH 45469			7b. ADDRESS (City, State, and ZIP Code) Wright-Patterson AFB, OH 45433-6553		
8a. NAME OF FUNDING/SPONSORING ORGANIZATION		8b. OFFICE SYMBOL (If applicable)		9. PROCUREMENT INSTRUMENT IDENTIFICATION NUMBER F33615-84-C-3404	
8c. ADDRESS (City, State, and ZIP Code)		10. SOURCE OF FUNDING NUMBERS			
		PROGRAM ELEMENT NO. 64212F	PROJECT NO. 1926	TASK NO. 01	WORK UNIT ACCESSION NO. 12
11. TITLE (Include Security Classification) B-1B IMPROVED WINDSHIELD DEVELOPMENT, VOLUME II - MAGNA ANALYSIS: BASELINE AND PARAMETRIC					
12. PERSONAL AUTHOR(S) Michael P. Bouchard and William R. Braisted					
13a. TYPE OF REPORT Interim		13b. TIME COVERED FROM JUN87 TO SEP88		14. DATE OF REPORT (Year, Month, Day) February 1990	
15. PAGE COUNT 147					
16. SUPPLEMENTARY NOTATION					
17. COSATI CODES			18. SUBJECT TERMS (Continue on reverse if necessary and identify by block number)		
FIELD 01	GROUP 03	SUB-GROUP	Nonlinear Static Analysis Nonlinear Dynamic Analysis Baseline Trade Study		
19. ABSTRACT (Continue on reverse if necessary and identify by block number) This report documents analyses which supported a study aimed at eliminating B-1B windshield problems which surfaced when the aircraft became operational. Optics and durability were immediately degraded by delamination. The many edge attachments made windshield changeout difficult and time-consuming, thereby affecting supportability. The objective of these analyses was to evaluate the impact of design configuration changes proposed to alleviate the in-service problems on the structural performance of the windshield system when subjected to birdstrike or internal cabin pressure. The MAGNA finite element analysis code was used to evaluate the structural performance of the current production configuration, which served as a baseline, and the alternate design configurations. The fasteners were evaluated based on the MAGNA output using additional computer programs. Computations were made first assuming all fasteners were present, then assuming every other fastener was removed. The models and analyses are discussed and summary results for each design (continued)					
20. DISTRIBUTION/AVAILABILITY OF ABSTRACT <input checked="" type="checkbox"/> UNCLASSIFIED/UNLIMITED <input type="checkbox"/> SAME AS RPT <input type="checkbox"/> DTIC USERS			21. ABSTRACT SECURITY CLASSIFICATION Unclassified		
22a. NAME OF RESPONSIBLE INDIVIDUAL Lt. Paul J. Kolodziejski			22b. TELEPHONE (Include Area Code) (513) 255-2916		22c. OFFICE SYMBOL WRDC/FIVR

CONTINUATION OF ITEM 19.

configuration presented. Conclusions are drawn regarding the viability of the proposed alternate design configurations in view of their impact on the structural performance of the windshield system. *REMARKS: As per drawing, the proposed alternate design configurations are not feasible due to the structural requirements of the windshield system.*

REMARKS: The proposed alternate design configurations are not feasible due to the structural requirements of the windshield system.

PREFACE

This final technical report was prepared by the University of Dayton Research Institute (UDRI), Dayton, Ohio, under contract F33615-84-C-3404, Project 1926, "Birdstrike Resistant Crew Enclosure Program," for the Flight Dynamics Laboratory, Wright Research & Development Center, Wright-Patterson Air Force Base, Ohio. Air Force administrative and technical support were provided by Lt. Paul Kolodziejwski, Capt. Steve Hargis, Capt. Steve Kolbow, and Lt. Tong Choe, WRDC/FIVR.

The effort documented herein was conducted during the period June 1987 to September 1988. Project supervision and technical assistance were provided through the Aerospace Mechanics Division of UDRI, with Mr. Dale H. Whitford, Supervisor, and Mr. Blaine S. West, Head, Structures Group. Technical effort was accomplished under Mr. K. I. Clayton as Principal Investigator, with Mr. M. P. Bouchard being responsible for the MAGNA finite element analyses. In addition, the authors wish to acknowledge the significant contributions made by the following program participants: B-1B SPO, ASD/EN, SAC, AAMRL, PPG Industries, Sierracin Research, Sierracin/Sylmar, and Rockwell International.

Accession For	
NTIS GRA&I	<input checked="checked" type="checkbox"/>
DTIC TAB	<input type="checkbox"/>
Unannounced	<input type="checkbox"/>
Justification	
By	
Distribution/	
Availability Codes	
Dist	Avail and/or Special
A-1	



TABLE OF CONTENTS

SECTION	PAGE
1 INTRODUCTION	1
2 MODELING	3
2.1 Procedure	3
2.2 Elements	11
2.3 Material Properties	13
2.4 Constraints	23
2.5 Loads	28
3 ANALYTICAL PROCEDURE	33
3.1 Eigenvalue Analysis	33
3.2 Nonlinear Static Analysis	33
3.3 Nonlinear Dynamic Analysis	35
3.4 Fastener Analysis	35
4 RESULTS AND DISCUSSION	46
4.1 Natural Frequency Analysis Results	46
4.2 Internal Pressure Analysis Results	48
4.3 Baseline Birdstrike Results	59
4.4 Trade Study Birdstrike Results	82
4.5 Fastener Tolerances	116
4.6 Summary of Results	118
5 CONCLUSIONS AND RECOMMENDATIONS	128
REFERENCES	131

LIST OF ILLUSTRATIONS

FIGURE	PAGE
2.1 Schematic of B-1B Windshield System	4
2.2 Windshield Cross-Section Geometry	5
2.3 Coarse Model of the Left Side B-1B Windshield Panel	7
2.4 Cross-Sections of Solid Element Support Structure	8
2.5 MAGNA Model for the Current Production Windshield System	9
2.6 MAGNA Model for the Split Structural Polycarbonate Windshield System	10
2.7 Location of Polycarbonate Edge Elements	21
2.8 Pull-out of Structural Ply in the Absence of Fastener Constraints	22
2.9 Modeling of a Fixed Edge Using Pinned Connections	24
2.10 Beam Elements with Fixed Nodes Indicated	25
2.11 Typical Linear Constraint	26
2.12 Situations Requiring Linear Constraints	27
2.13 Bird Impact Locations	30
2.14 Birdstrike Load Distributions	31
3.1 Fastener Analysis Procedure	38
3.2 Location of Element Faces that were Integrated to Obtain Stress Resultants for Fastener Analysis	39
3.3 Shear Loads Applied to Fastener	41
3.4 Axial Load Induced in Fastener	42
3.5 Windshield Perimeter Location System for Fastener Analysis	43
3.6 Fastener System Failure Modes	45
4.1 Mode Shape for Lowest Natural Frequency of the Left Side Windshield Panel	47

LIST OF ILLUSTRATIONS, continued

FIGURE		PAGE
4.2	Equivalent Stress Contours for the Outer Surface of the Structural Ply, Case 2	49
4.3	Equivalent Stress Contours for the Outer Surface of the Structural Ply, Case 8	50
4.4	Equivalent Stress Contours on the Centerpost Web, Case 2	52
4.5	Equivalent Stress Contours on the Centerpost Web, Case 8	53
4.6	Fastener Load Distribution, Case 2	55
4.7	Fastener Load Distribution, Case 8	56
4.8	Deformed Shape of the Left Side Windshield, Case 3, Increment 50	60
4.9	Deformed Shape of the Left Side Windshield, Case 4, Increment 35	61
4.10	Displacement Time Histories, Cases 3 and 4	62
4.11	Location of Maximum Displaced Nodes from Baseline Birdstrike Analyses	63
4.12	Superposition of Near-Center Bird Footprint Onto Windshield Finite Element Model	64
4.13	Equivalent Stress Contours on the Outer Surface of the Structural Ply, Case 3	66
4.14	Equivalent Stress Contours on the Inner Surface of the Spall Ply, Case 3	67
4.15	Equivalent Stress Contours on the Outer Surface of the Structural Ply, Case 4	68
4.16	Close-up of High Stress Regions (Upper Aft Corner) on the Outer Surface of the Structural Ply, Case 4	69
4.17	Equivalent Strain Contours Through the Thickness of the Structural Ply at the Upper Corner Windshield/Eyebrow Interface, Case 4	71

LIST OF ILLUSTRATIONS, continued

FIGURE		PAGE
4.18	Equivalent Stress Contours on the Centerpost Web, Case 3	72
4.19	Equivalent Stress Contours on the Centerpost Web, Case 4	73
4.20	Equivalent Stress Contours on the Eyebrow Web, Case 3	74
4.21	Equivalent Stress Contours on the Eyebrow Web, Case 4	75
4.22	Equivalent Strain Contours on Lower Portion of Eyebrow Web, Case 4	77
4.23	Fastener Load Distribution, Case 3	79
4.24	Fastener Load Distribution, Case 4	80
4.25	Displacement Time Histories, Cases 4, 5, 6, 7, and 9	84
4.26	Location of Node Having Maximum Displacement Relative to Upper Surface of the Structural Polycarbonate Ply, Cases 4-7, 9	85
4.27	Equivalent Stress Contours on the Outer Surface of the Structural Ply, Case 5	86
4.28	Close-up of Maximum Stress Region on the Outer Surface of the Structural Ply, Case 5	87
4.29	Equivalent Stress Contours on the Outer Surface of the Structural Ply, Case 6	88
4.30	Close-up of Maximum Stress Region on the Outer Surface of the Structural Ply, Case 6	89
4.31	Equivalent Stress Contours on the Outer Surface of the Structural Ply, Case 7	90
4.32	Close-up of the Maximum Stress Region on the Outer Surface of the Structural Ply, Case 7	91
4.33	Equivalent Stress Contours on the Outer Surface of the Upper Surface Ply, Case 9	92

LIST OF ILLUSTRATIONS, continued

FIGURE		PAGE
4.34	Close-up of the Maximum Stress Region on the Outer Surface of the Upper Structural Ply, Case 9	93
4.35	Equivalent Strain Contours Through the Thickness of the Structural Ply at the Upper Corner Windshield/Eyebrow Interface, Case 5	95
4.36	Equivalent Strain Contours Through the Thickness of the Structural Ply at the Upper Corner Windshield/Eyebrow Interface, Case 6	96
4.37	Equivalent Strain Contours Through the Thickness of the Structural Ply at the Upper Corner Windshield/Eyebrow Interface, Case 7	97
4.38	Equivalent Strain Contours Through the Thickness of the Structural Ply at the Upper Corner Windshield/Eyebrow Interface, Case 9	98
4.39	Equivalent Stress Contours on the Eyebrow Web, Case 5	99
4.40	Equivalent Stress Contours on the Eyebrow Web, Case 6	100
4.41	Equivalent Stress Contours on the Eyebrow Web, Case 7	101
4.42	Equivalent Stress Contours on the Eyebrow Web, Case 9	102
4.43	Equivalent Strain Contours on the Lower Portion of the Eyebrow Web, Case 5	104
4.44	Equivalent Strain Contours on the Lower Portion of the Eyebrow Web, Case 6	105
4.45	Equivalent Strain Contours on the Lower Portion of the Eyebrow Web, Case 7	106

LIST OF ILLUSTRATIONS, concluded

FIGURE		PAGE
4.46	Equivalent Strain Contours on the Lower Portion of the Eyebrow Web, Case 9	107
4.47	Fastener Load Distribution, Case 5	108
4.48	Fastener Load Distribution, Case 6	109
4.49	Fastener Load Distribution, Case 7	110
4.50	Fastener Load Distribution, Case 9	111
4.51	B-1B Fastener System Dimensions	117
4.52	Strain Summary, Polycarbonate Structural Ply	122
4.53	Strain Summary, Centerpost	123
4.54	Strain Summary, Eyebrow	124
4.55	Fastener Stress Summary	126

LIST OF TABLES

TABLE	PAGE
2.1 Windshield System Finite Elements	12
2.2 Elastic Material Properties	14
2.3 Shear Corrected Material Properties for Type 11 Elements	15
2.4 Post-Yield Stress-Strain Curves	18
2.5 Internal (Cabin) Pressures	29
2.6 Birdstrike Loads	32
3.1 MAGNA Analysis Cases	34
3.2 NAS1580C4 Fastener Data	36
4.1 Maximum Stresses in Support Structure Due to Internal Pressurization	54
4.2 Fastener Safety margins for the Internal Pressurization Analyses	58
4.3 Critical Fastener Loads and Safety Margins for the Baseline Birdstrike Analyses	81
4.4 Critical Fastener Loads for the Upper Corner Impact Analyses	112
4.5 Fastener Safety margins for the Upper Corner Impact Analyses	114
4.6 Summary of Results for MAGNA Pressurization Analyses	119
4.7 Summary of Results for MAGNA Birdstrike Analyses	121
4.8 Fastener Analysis Summary	125

SECTION 1

INTRODUCTION

This report discusses structural analyses performed in support of a study aimed at eliminating B-1B windshield problems which surfaced when the aircraft became operational. Optics and durability were immediately degraded by delamination. The many edge attachments made windshield changeout difficult and time-consuming, thereby affecting supportability. The overall objective of this study was to evaluate the impact of design configuration changes proposed to alleviate the in-service problems on the structural performance of the windshield system when subjected to birdstrike or internal cabin pressurization.

The study was conducted in two phases. The objective of Phase 1 was to establish the structural performance of the current production B-1B windshield system when subjected to internal pressure loading or birdstrike by a four pound bird impacting at either of two locations at 650 mi/hr. Birdstrike results were compared to birdstrike test results of the B-1A windshield system (no birdstrike tests of the B-1B system had been performed). In addition, the analytical results were reviewed to determine the more critical of the two bird impact locations (the near-center location, denoting the approximate windshield panel centroid location, or the upper corner location near the connection between the centerpost and the eyebrow frame). The Phase 1 results served as a baseline for the Phase 2 effort. The objectives of Phase 2 were to determine the structural performance of alternate configuration windshields subjected to the internal pressure loading or birdstrike at the critical location determined in Phase 1, and to compare the results with those of the baseline windshield system.

In evaluating the structural performance of the various windshield configurations, several items were deemed important.

First, deflections and stresses in the windshield panel (particularly in the structural polycarbonate plies) were important since the primary birdstrike protection is provided by this component. Second, the stresses in the frame members supporting the windshield were important, especially since fracture of a large portion of the eyebrow frame had occurred during testing of the B-1A windshield system.¹ Third, stresses in the fasteners joining the windshield to the immediate support structure were of importance since the fasteners must provide load transfer from the windshield to the frames and maintain the windshield pressure seal. Of special interest was checking the structural feasibility of removing every other fastener and of increasing the associated hole tolerances, both of which would significantly reduce windshield change-out time.

The study was performed using the MAGNA nonlinear finite element analysis program² as the major analysis tool. Additional computer programs were written or modified from existing ones to aid in analyzing the windshield fasteners. Owing to the large finite element model sizes, the ASD CRAY X-MP located at Wright-Patterson Air Force Base, Ohio was used for all MAGNA analyses. Preprocessing (model development), post-processing (data reduction), and fastener analysis were performed using the ASD CDC Cyber computers located at WPAFB and the UDRI Research VAX located at the University of Dayton in Dayton, Ohio.

SECTION 2

MODELING

Figure 2.1 is a schematic representation of the B-1B windshield system, showing the large left and right windshield panels, the aft windows, and the immediate support structure. Figure 2.2 depicts the cross sections of the various windshield panel configurations that were analyzed. The baseline windshield consisted of an outer thermally tempered glass ply, a single thick structural polycarbonate ply, and an inner spall polycarbonate ply, bonded together by silicone interlayers. The trade study alternate configuration windshield concepts included substituting acrylic for the glass outer ply, substituting urethane for silicone, substituting a coating for the inner spall polycarbonate ply, and splitting the single structural polycarbonate ply into two polycarbonate plies bonded together by a 0.060 inch layer of silicone. The use of silicone rather than urethane for this additional interlayer provided conservative results since the low modulus of the silicone leads to greater flexing, and therefore higher stresses, of the structural plies during bird impact.

2.1 Procedure

Because the bird impact locations were not along the windshield centerline (that is, along the centerpost -- see Section 2.5), no symmetry existed, therefore requiring both sides of the windshield to be modeled. A single windshield panel finite element grid was used for bird impact analyses of both impact sites and for the internal pressure analyses.

A coarse grid model of the left side windshield was first created using the MAGNA preprocessor module IJGEN³ and user subroutines CRDTRN, SURFAC, and UINPUT written by Robert E. McCarty of AFWAL/FIER.⁴ The subroutines were originally written

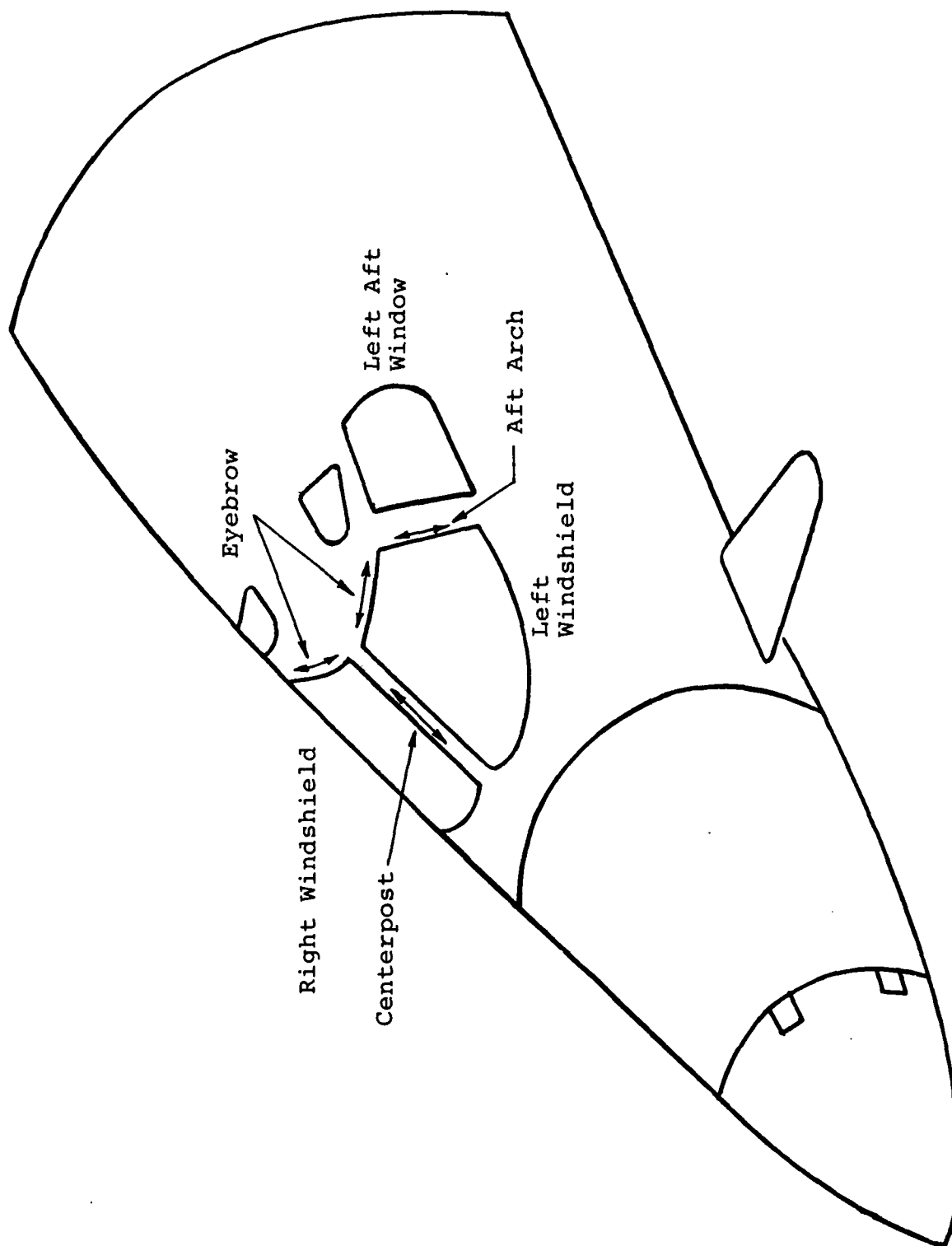


Figure 2.1 Schematic of B-1B Windshield System.

CASES 1-7

Layer 1:	0.12
Layer 2:	0.235
Layer 3:	0.87
Layer 4:	0.12
Layer 5:	0.15

CASES 8-9

Layer 1:	0.12
Layer 2:	0.235
Layer 3:	0.405
Layer 5:	0.405
Layer 6:	0.12
Layer 7:	0.15

Layer 6:
0.060

all dimensions in inches

Layer	Case 1-4	Case 5	Case 6	Case 7
1	GL	AC	GL	GL
2	SI	SI	UR	SI
3	PC	PC	PC	PC
4	SI	SI	UR	-
5	PC	PC	PC	-

Layer	Material
1	GL
2	SI
3	PC
4	SI
5	PC
6	SI
7	PC

AC = As-Cast Acrylic
 GL = Thermally Tempered Glass
 PC = Polycarbonate
 SI = Silicone
 UR = Urethane

Figure 2.2 Windshield Cross-Section Geometry.

to generate B-1A windshield geometry. UDRI modified the subroutines as needed to produce the correct B-1B geometry. The resulting model is shown in Figure 2.3.

The coarse windshield model was subsequently reflected to produce a coarse model of the right side windshield. The coarse models were merged and refined using the PREP module³ of the MAGNA preprocessor to produce the desired mesh of windshield finite elements. A coarse model of the left-side aft window was then created manually and subsequently refined and merged into the windshield model using PREP.

The support structure models were developed next. The centerpost and eyebrow frames in the vicinity of the bird impact sites were modeled with solid elements to give better stress results than simpler beam elements would. Both models were developed manually. Model cross sections are shown in Figure 2.4. The remaining frame elements (forward and aft centerposts, aft arch, right side eyebrow frame, and side window frame) were defined manually as beam elements and merged into the windshield.

At this point the basic model geometry (nodes, coordinates, and connectivity) was complete. The nodal bandwidth was then reduced by executing the RENUMBER option in PREP and then running the model through a stand-alone code that was modified for MAGNA by UDRI from a wavefront minimization code developed by Hoit and Wilson.⁵ The bandwidth reductions were performed to provide more efficient storage of the model, thus speeding execution of MAGNA.

To complete the model, material properties, boundary conditions, linear constraints, and run control data were added. Figure 2.5 shows the completed geometry used for the baseline and all but one of the trade studies. The geometry for the split polycarbonate structural ply trade study is shown in Figure 2.6.

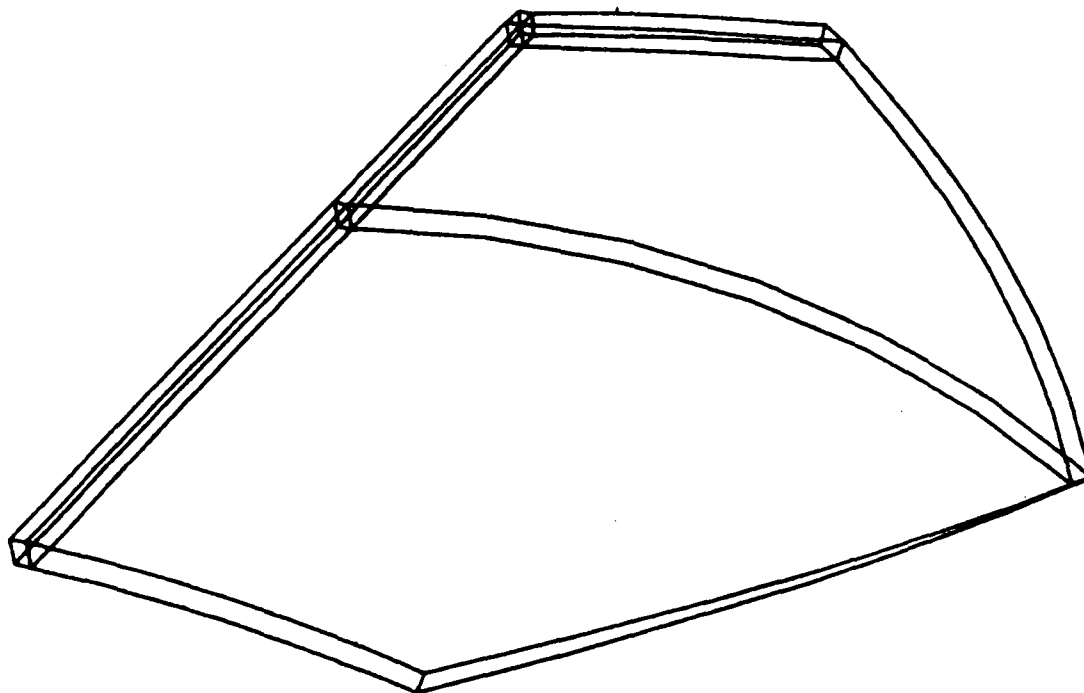


Figure 2.3. Coarse Model of the Left Side B-1B Windsheld Panel.

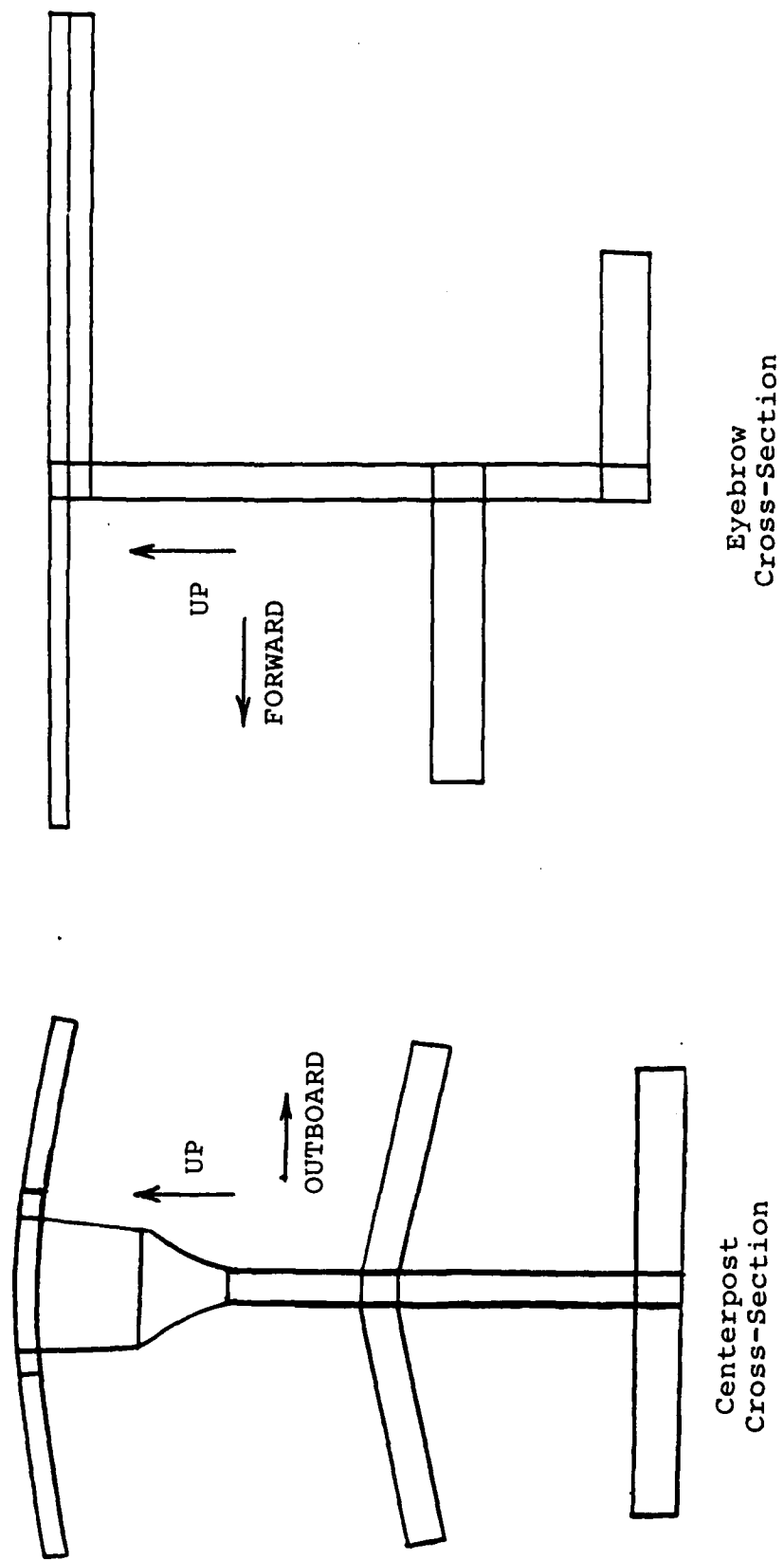


Figure 2.4. Cross-Sections of Solid Element Support Structure Models.

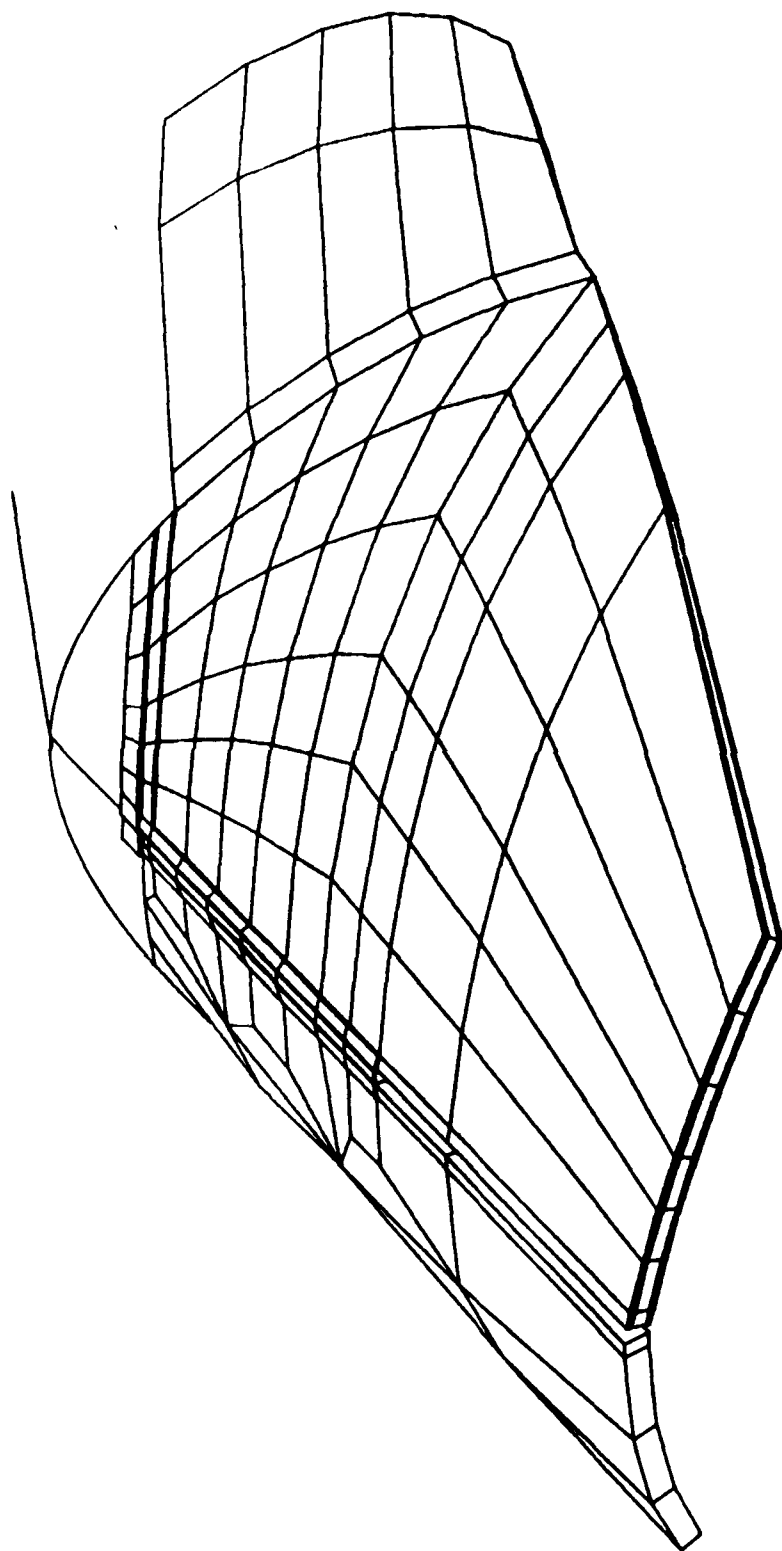


Figure 2.5. MAGNA Model for the Current Production Windshield System.

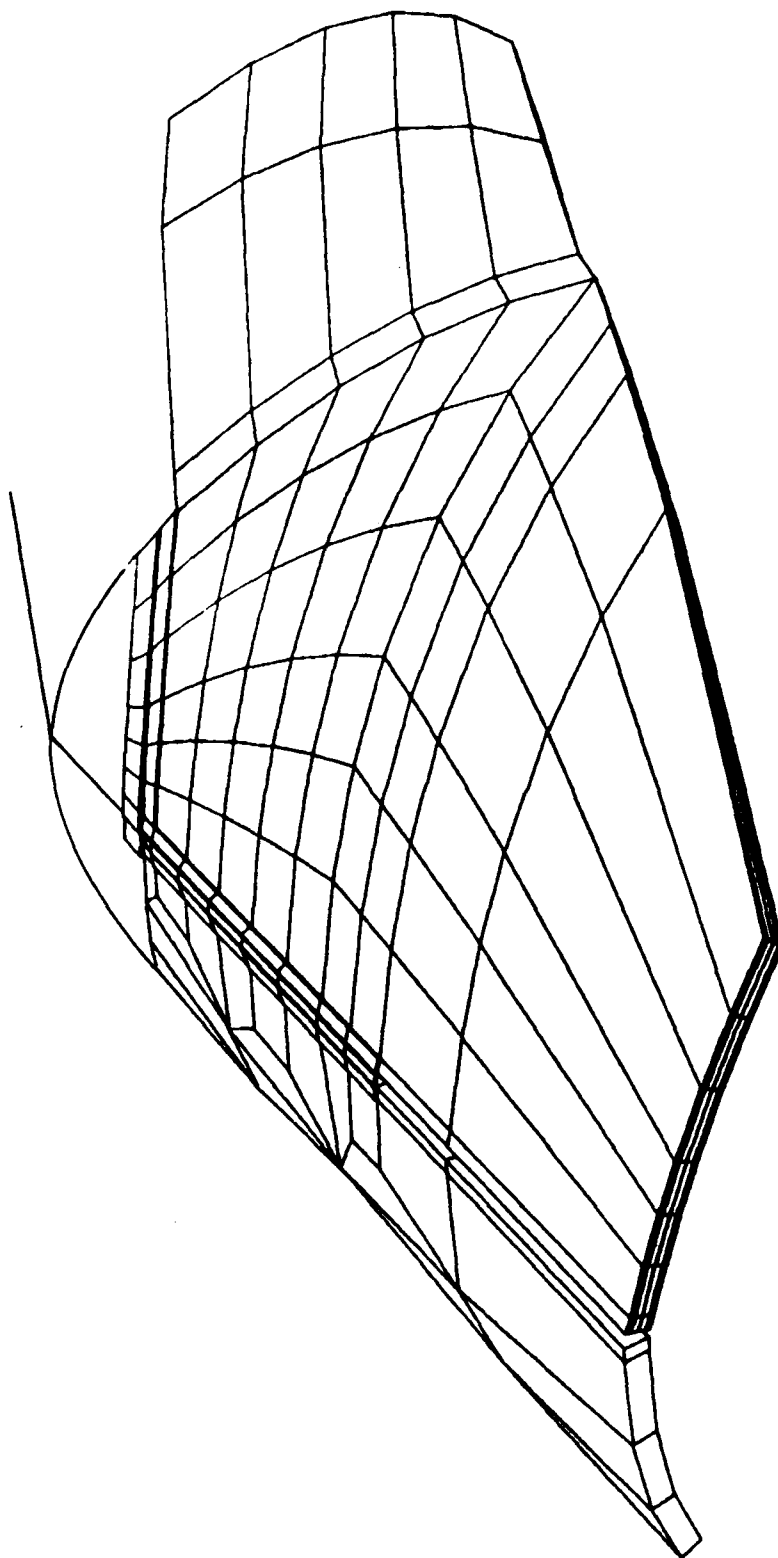


Figure 2.6. MAGNA Model for the Split Structural Polycarbonate Ply Windshield System.

2.2 Elements

Table 2.1 summarizes the elements used in the model. Element choices were governed by the output data required from each portion of the model. Good deflection data were required everywhere, while accurate stresses were needed only in the vicinity of the impact sites. Because the model was expected to be large and therefore expensive to run, economy of type and number of elements was also deemed important.

In keeping with these guidelines, the left side windshield and centerpost and eyebrow frames in the vicinity of the impact site were modeled with solid elements (MAGNA Types 6, 7, and 8) to obtain accurate stresses. One layer of solid elements was used for each layer of the left side windshield. The use of solid elements for frame members provided for accurate modeling of local effects such as flange bending. Fourteen-point integration was used for the solid elements to compute accurate stresses more economically than would be possible with full twenty-seven-point ($3 \times 3 \times 3$) integration.

For the right side windshield and side window, which are located away from the impact site, the laminated shell (Type 11) element was used. Only one layer of Type 11 elements was required to model all of the multiple windshield and window layers, thus leading to reduced model size and computation time. As discussed in Section 2.3, the material properties for this element had to be shear corrected to provide the correct stiffnesses (and therefore deflections). Eight-point integration ($2 \times 2 \times 2$) was used.

Finally, for the frame elements located away from the impact site, three-node curved beam elements (MAGNA Type 12) were used. This element provided good overall bending and twisting results, but did not model local effects like flange bending (a basic beam element assumption is that the cross section remains

TABLE 2.1
WINDSHIELD SYSTEM FINITE ELEMENTS

Structural Component	MAGNA Element Type	Quantity	Integration Scheme
Left Side Windshield	8	350 (490)*	14 point
Right Side Windshield	11	31 (31)	2x2x2
Aft Window	11	15 (15)	2x2x2
Centerpost Near Impact	6,7,8	164 (164)	14 point
Eyebrow Frame Near Impact	7,8	75 (75)	14 point
Frames Away from Impact	12	46 (46)	3 point

*Numbers in parentheses are for the split polycarbonate structural ply configuration (Case 9).

rigid, precluding flanges from moving independently of the rest of the cross section).

The resulting baseline model (also used for all but one of the trade studies) was quite large, having 589 solid elements, 46 laminated shell elements, and 46 beam elements. The model for the split polycarbonate ply trade study was even larger, containing 729 solid elements. The models were approximately three times larger than the largest models successfully analyzed on the ASD Cyber 845 computer,⁴ therefore requiring the use of the ASD CRAY X-MP computer for execution.

2.3 Material Properties

Table 2.2 summarizes the elastic material properties used in the various models. Isotropic properties were input for all solid and beam elements (Types 6, 7, 8, and 12), except for the interlayer elements. The tensile modulus, shear modulus, and Poisson's ratio were independent of each other for the interlayer materials. Therefore these properties were input in orthotropic format since this format allows for their independent entry.

Due to the assumption of perfect shear coupling between layers, the response of the Type 11 element is generally too stiff (deflections too small) when the tensile moduli vary considerably between adjacent layers. The layer-to-layer variation was large for the B-1B windshield, with the glass modulus being 3450 times larger than the silicone modulus. The tensile modulus, shear modulus, and Poisson's ratio were therefore multiplied by shear correction factors computed in accordance with Reference 6 using a program written by Dr. R. A. Brockman of UDRI. The resulting element stiffnesses were correct, therefore leading to accurate deflections. In the current version of MAGNA, however, stresses are not recovered properly for shear corrected elements, making the Type 11 element inappropriate for accurate stress analysis (such as was desired for the left side windshield). Table 2.3 summarizes the

TABLE 2.2

ELASTIC MATERIAL PROPERTIES

	Material	Tensile Modulus (kpsi)	Shear Modulus (kpsi)	Poisson's Ratio	Density (lb/in ³)	Yield Strength (kpsi)	References
Windshield Outer Ply	Thermally Tempered Glass	10,000	4,070	0.23	0.091	18.0	19, 22
Windshield Outer Ply	As-Cast Acrylic	450	167	0.35	0.043	10.0	19, 20
Windshield Structural Ply	Polycarbonate	355	130	0.37	0.043	12.1	19, 20, 21
Windshield Interlayer	Silicone	2.9	0.145	0.33	0.0385	*	19, 23
Windshield Interlayer	Urethane	8.7	0.895	0.43	0.0385	*	19, 23
Forward Centerpost and Aft Window Frame	2024-T62 Aluminum	10,600	3,980	0.33	0.1	50.	18
Aft Arch and Aft Centerpost	2124-T851 Aluminum	10,400	3,910	0.33	0.1	56.	18
Eyebrow	7075-T73 Aluminum	10,000	3,760	0.33	0.1	56.	18

*Arbitrarily large value of 1×10^{12} psi used--see text.

TABLE 2.3

SHEAR CORRECTED MATERIAL PROPERTIES FOR TYPE 11 ELEMENTS

CASE 4: CURRENT PRODUCTION CONFIGURATION
CORRECTION FACTOR = 0.00095

Material	E ₁ psi	E ₂ psi	E ₃ psi	G ₁₂ psi	G ₁₃ psi	G ₂₃ psi	ν_{12}	ν_{13}	ν_{23}
Glass	10x10 ⁶	10x10 ⁶	10x10 ⁶	4.07x10 ⁶	3867	3867	0.23	0.	0.
Polycarbonate	355000	355000	355000	130000	124	124	0.37	0.	0.
Silicone	2900	2900	2900	145	0.138	0.138	0.33	0.	0.

CASE 5: ACRYLIC OUTER PLY CONFIGURATION
CORRECTION FACTOR = 0.0093493

Material	E ₁ psi	E ₂ psi	E ₃ psi	G ₁₂ psi	G ₁₃ psi	G ₂₃ psi	ν_{12}	ν_{13}	ν_{23}
Acrylic	450000	450000	450000	167000	1561	1561	0.35	0.	0.
Polycarbonate	355000	355000	355000	130000	1215	1215	0.37	0.	0.
Silicone	2900	2900	2900	145	1.356	1.356	0.33	0.	0.

CASE 6: URETHANE INTERLAYER CONFIGURATION
CORRECTION FACTOR = 0.0057993

Material	E ₁ psi	E ₂ psi	E ₃ psi	G ₁₂ psi	G ₁₃ psi	G ₂₃ psi	ν_{12}	ν_{13}	ν_{23}
Glass	10x10 ⁶	10x10 ⁶	10x10 ⁶	4.07x10 ⁶	23603	23603	0.23	0.	0.
Polycarbonate	355000	355000	355000	130000	754	754	0.37	0.	0.
Urethane	8700	8700	8700	895	5.19	5.19	0.43	0.	0.

TABLE 2.3 (continued)

CASE 7: NO SPALL PLY CONFIGURATION
CORRECTION FACTOR - 0.00073913

Material	E ₁ psi	E ₂ psi	E ₃ psi	G ₁₂ psi	G ₁₃ psi	G ₂₃ psi	ν_{12}	ν_{13}	ν_{23}
Glass	10x10 ⁶	10x10 ⁶	10x10 ⁶	4.07x10 ⁶	3008	3008	0.23	0.	0.
Polycarbonate	355000	355000	355000	130000	96	96	0.37	0.	0.
Silicone	2900	2900	2900	145	0.107	0.107	0.33	0.	0.

CASE 9: SPLIT STRUCTURAL PLY CONFIGURATION
CORRECTION FACTOR - 0.00084879

Material	E ₁ psi	E ₂ psi	E ₃ psi	G ₁₂ psi	G ₁₃ psi	G ₂₃ psi	ν_{12}	ν_{13}	ν_{23}
Glass	10x10 ⁶	10x10 ⁶	10x10 ⁶	4.07x10 ⁶	3454	3454	0.23	0.	0.
Polycarbonate	355000	355000	355000	130000	110	110	0.37	0.	0.
Silicone	2900	2900	2900	145	0.123	0.123	0.33	0.	0.

correction factors and revised material properties used for the Type 11 elements. Note that all other Type 11 properties remained as listed in Table 2.2.

To simulate the removal of the spall polycarbonate ply, the inner ply of the Case 7 model was assigned a low tensile modulus value (1000 psi) to ensure that its stiffness would be negligible. In addition, it was assigned a low density value (4.29×10^{-4} lb/in³) to ensure that its inertia contributions would be small.

In addition to elastic material properties, it was important that the plastic stress-strain behavior be input for those materials for which yielding was a possibility. Table 2.4 gives the stress (Second Piola-Kirchoff)-versus-plastic strain (Green-St. Venant) curve values that were input into the MAGNA models.

Note that no plasticity was included for the interlayer materials. These materials were considered to be only load transfer mediums since material modeling of such viscoelastic materials is imprecise (due to the lack of accurate material properties and the inability of MAGNA to adequately model the bulk behavior of such materials). Thus the interlayers were modeled as elastic materials up to an arbitrarily high yield stress (chosen to ensure that yielding would not occur during the analyses).

Acrylic was modeled as an elastic-perfectly plastic material. In reality, acrylic is brittle compared to polycarbonate, and fractures with little plastic deformation. However, MAGNA cannot "turn off" an element once it reaches its ultimate strength, nor can the stress-versus-plastic strain curve be made to slope negatively (strain softening) down to a zero stress state, since numerical instabilities would result during analysis. The best recourse, then, was to use perfect plasticity in the post-yield range. The effect of this modeling decision was to enhance the stiffness and energy-absorbing ability of the

TABLE 2.4
POST-YIELD STRESS-STRAIN CURVES

Material	Total Strain ^a μin/in	Plastic Strain μin/in	Stress ^b kpsi
2024-T62	4728.	0.	49.8
Aluminum	5214.	290.	52.2
	5616.	550.	53.7
	6018.	860.	54.7
	7025.	1760.	55.8
	8032.	2680.	56.7
	9041.	3620.	57.5
	10050.	4520.	58.2
	105000.	99510.	58.7
7075-T73	5616.	0.	55.7
Aluminum	5817.	60.	57.6
	6018.	120.	59.0
	6219.	230.	59.9
	6622.	530.	61.0
	7025.	850.	61.7
	8032.	1700.	63.3
	9041.	2630.	64.1
	10050.	3560.	64.9
	116050.	109560.	64.9
Polycarbonate	35150.	0.	12.0
	644368.	605700.	13.7
Acrylic	22222.	0.	10.0
	10022222.	10000000.	10.0

^a Green-St. Venant Strain

^b Second Piola-Kirchoff Stress

model acrylic compared to actual acrylic. The improvement did not adversely affect the accuracy of the analytical results because the thick polycarbonate structural ply (plies) still provided the largest influence on the windshield behavior, and because the soft, thick interlayer immediately below the acrylic ply tended to uncouple the acrylic ply response from the remainder of the windshield model.

Initially the glass outer ply was modeled like the acrylic outer ply, namely, elastic-perfectly plastic. In studying the results of an initial near-center birdstrike analysis, it was apparent that this technique did not best represent the glass ply behavior and adversely affected the analytical results. The maximum deflection obtained from the birdstrike run was less than 1 inch, less than half the deflection that was recorded during birdstrike testing of the B-1A.⁷ In addition, the region of glass that had reached the ultimate strength was relatively small, being limited to the vicinity of the impact point. In birdstrike testing of glass-faced windshields, such as the B-1A simulated windshield test articles,⁸ the entire glass ply shatters into very small pieces almost instantaneously on impact by the bird. Thus the stiffness contribution of the B-1B glass ply was assumed to be negligible during the impact event. The failure model used by MAGNA is only appropriate for materials which fail in ductile fashion, and thus cannot model shattering of glass. In effect, then, the initial B-1B model was performing as though the outer ply was a sheet of aluminum (moduli for glass and aluminum are nearly identical, and sheet aluminum would deform plastically under similar loading).

Since the stiffening effect of the glass ply was small after shattering, and since the shattering failure mode could not be correctly modeled, the left side glass ply was assigned a low modulus (1000 psi) for the birdstrike analyses. The glass remained bonded to the windshield after shattering, so that its mass influenced the dynamic response of the windshield.

Therefore the correct density for glass was assigned to the outer ply of the models. The glass ply modulus for the Type 11 elements was not changed because it was not expected to fail since it was located away from the impact location. In addition, the left-side glass ply was assigned the full tensile modulus for the natural frequency and pressure analyses, since glass ply failure was not expected.

For the windshield edge elements shown in Figure 2.7, all layers were assigned the tensile modulus of polycarbonate and an arbitrarily high yield strength to prevent yielding from occurring. These properties were used in an effort to simulate the constraints on the windshield due to the bolted connections along the edges. As Figure 2.8 demonstrates, without any restraint the structural polycarbonate ply could have pulled out away from the edge in an unrealistic fashion that would have relieved the stresses at the edges of the structural polycarbonate ply. The use of linear constraints to simulate the bolted connections was considered to be too restrictive, leading to higher-than-actual stresses in the structural ply (because the constraints are applied at points, not distributed, and because the constraints are rigid, not elastic). By making the edge interlayers stiffer, the bolted connection was simulated in a distributed and elastic manner. Stresses in the edge elements were not of concern for the edge member analysis (see Section 3.4 for details), so that this method of constraint was acceptable from an edge member analysis standpoint.

Finally, it was found necessary to increase the tensile modulus of the silicone for the left side windshield when acrylic was used for the outer ply. The relatively flexible acrylic was pushed through the soft silicone into the structural polycarbonate ply, resulting in unreasonable deformation and plasticity of the acrylic ply, thus causing numerical instabilities in the birdstrike analysis. This phenomena occurred because there was no means to incorporate the silicone

NOTES:

- Cross-hatched elements assigned polycarbonate material properties to represent constraint due to fasteners.
- Only upper layer of elements shown for clarity (elements below cross-hatched elements treated in similar fashion).

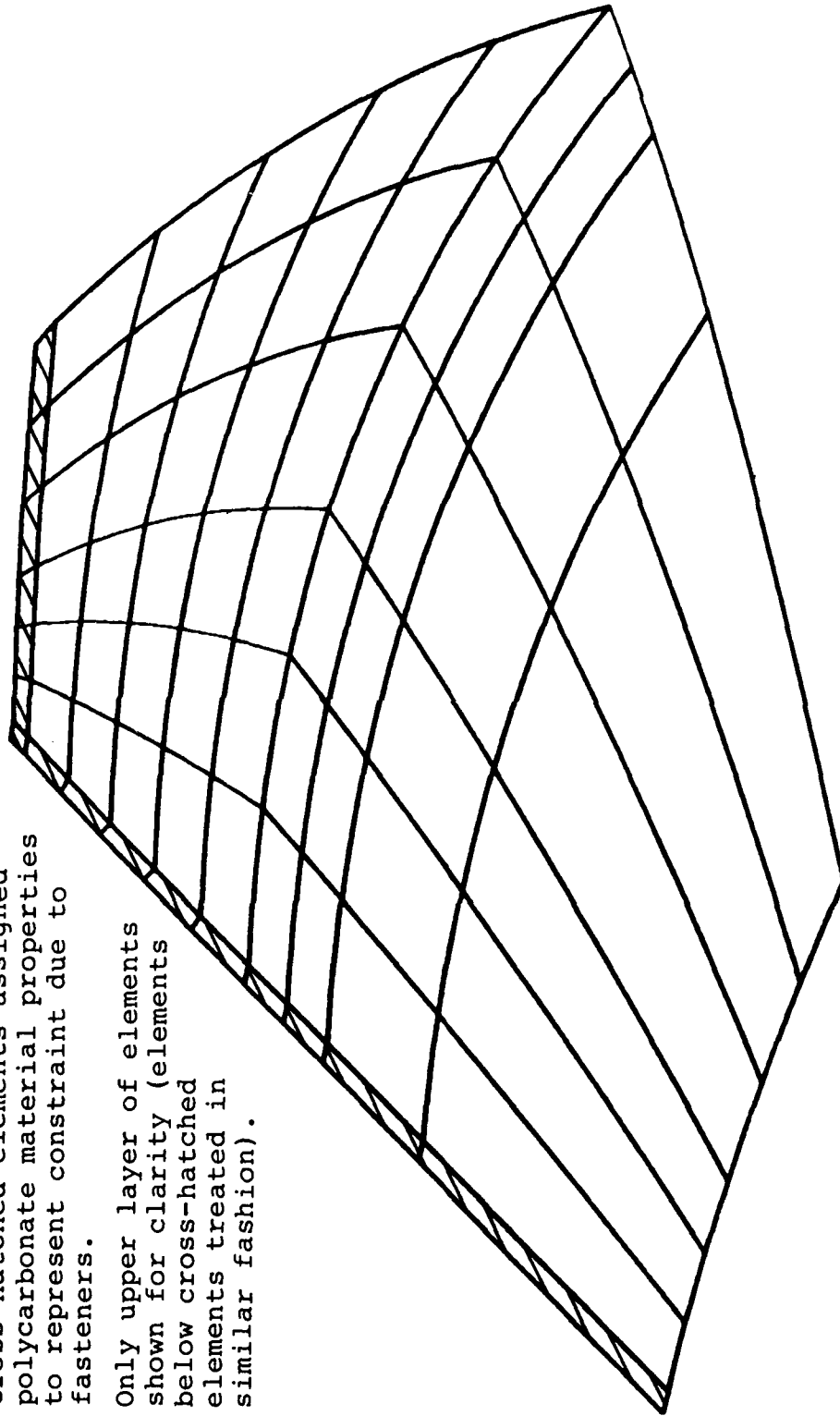


Figure 2.7. Location of Polycarbonate Edge Elements.

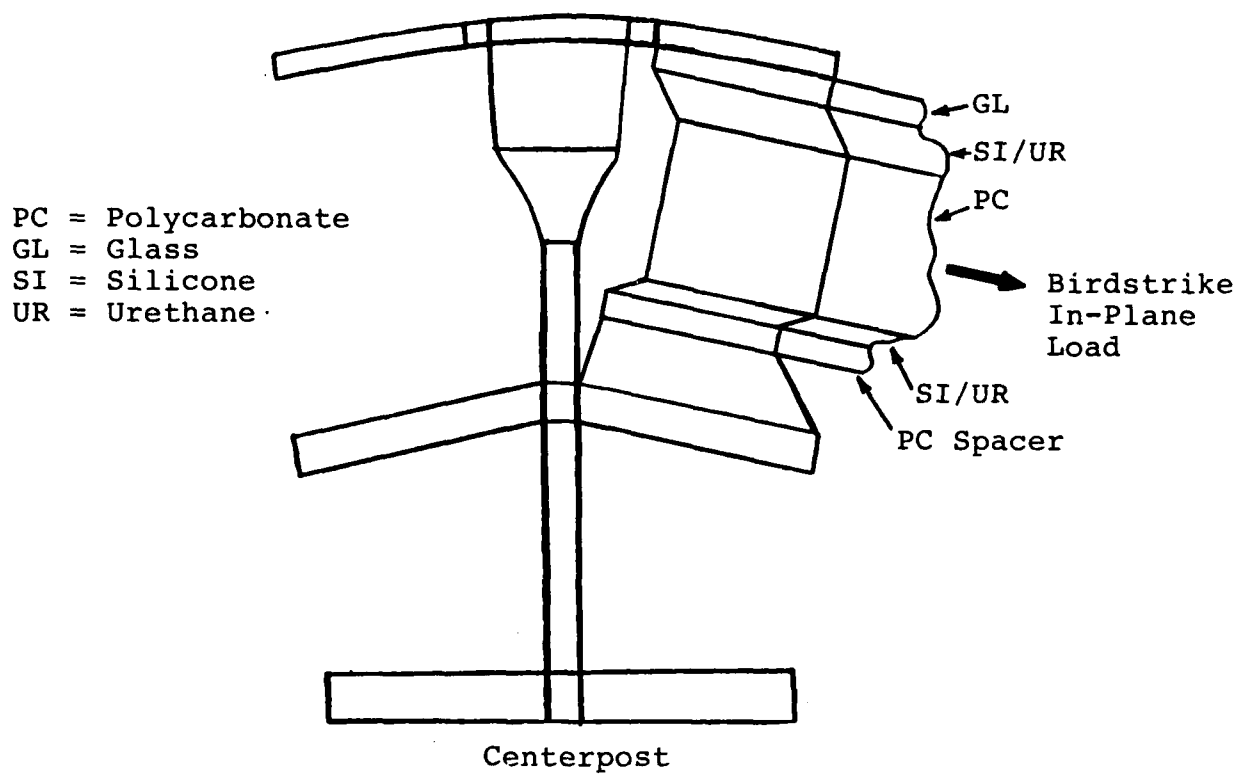


Figure 2.8. Pull-out of Structural Ply in the Absence of Fastener Constraints.

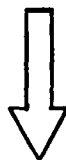
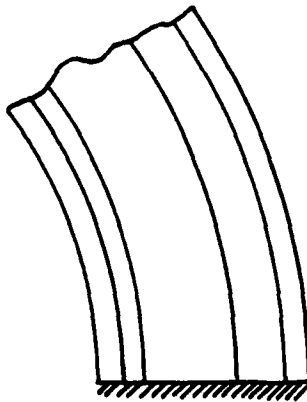
bulk properties (for example, bulk modulus), which govern material compression, into the computer model. Increasing the tensile modulus to 10,000 psi compensated for this limitation and allowed for a numerically stable solution. No adverse effects on the results were expected since the load transfer from the acrylic ply to the structural polycarbonate ply was acceptable, and since the added stiffness of the silicone layers was still relatively small compared to that of the structural polycarbonate ply (tensile modulus ratio of 35.5 to 1 for polycarbonate compared to silicone).

2.4 Constraints

Fixed boundary conditions were used to model the windshield-to-fuselage connections, simulating the rigidity of the actual connections. Rigid connections were modeled along the sill and forward arch by pinning (constraining x, y, and z translations) all nodes along these edges, as sketched in Figure 2.9. The end nodes of some of the beam elements (see Figure 2.10) were fully constrained to prevent translation and rotation at the point of connection with other portions of the aircraft.

Linear constraints were necessary to properly couple the motion of the beam elements to the solid elements to which they joined. Specifically, these constraints ensured that the beam elements and solid elements would rotate (twist or bend) together, not independently. (Note that the beams and solids already translated together where they shared common nodes.) A typical constraint is shown in Figure 2.11. Three computer codes (one each for three different model situations, as shown in Figure 2.12) were written to generate the linear constraints. Each code computed the constraints in local coordinates, translated them into global coordinates, and wrote them in MAGNA format to files which were later merged into the MAGNA models.

Fixed
Edge



Finite Element
Model Simulating
Fixed Edge by
Pinned Connections

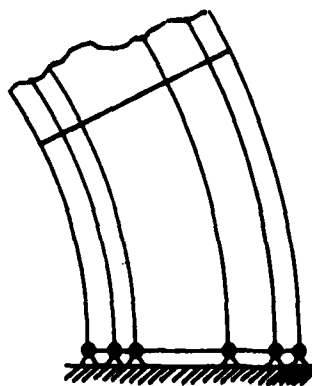
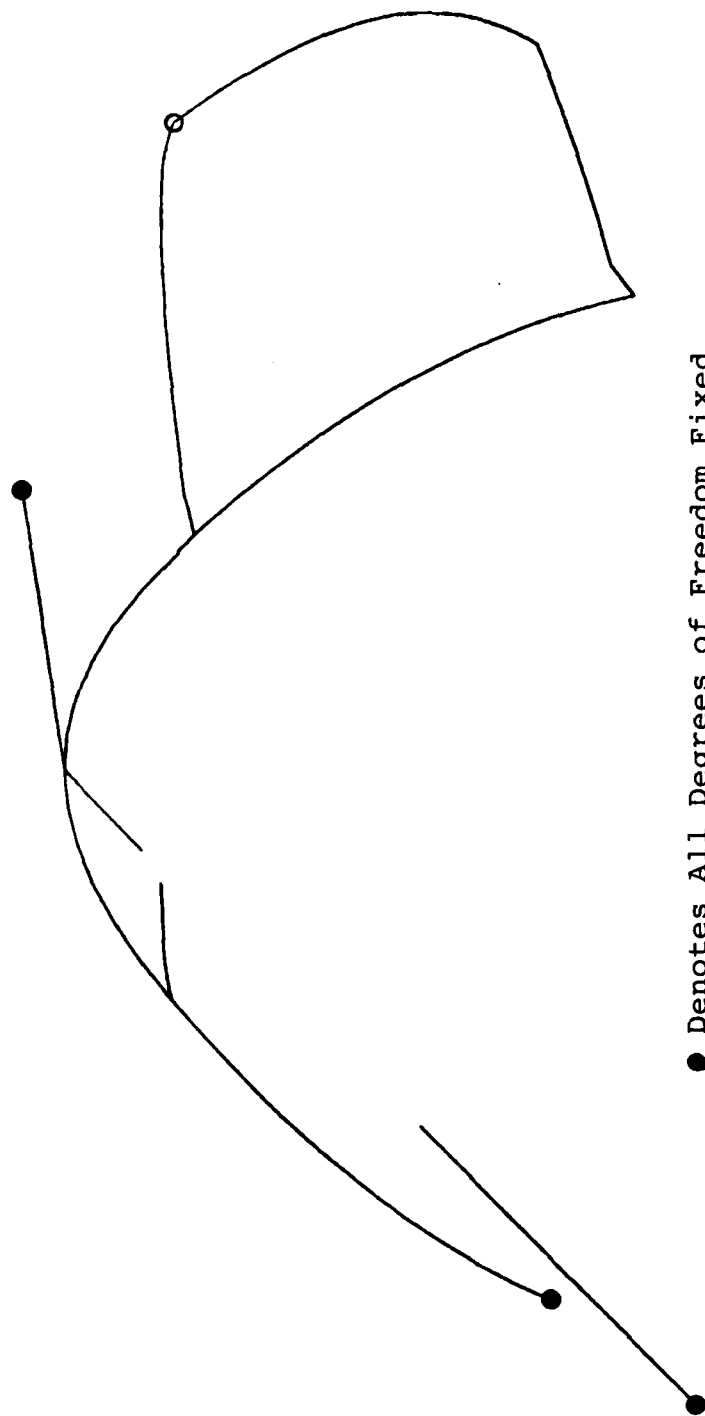


Figure 2.9. Modeling of a Fixed Edge Using Pinned Connections.

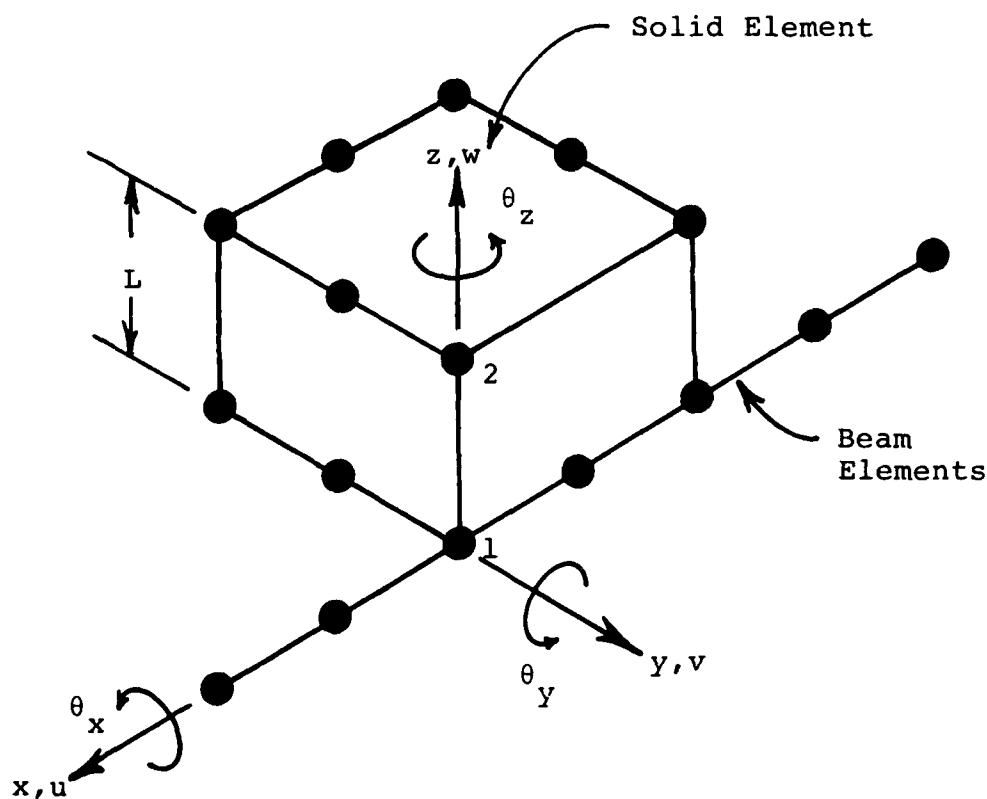


- Denotes All Degrees of Freedom Fixed
- Denotes Translation Degrees of Freedom Fixed

Figure 2.10. Beam Elements with Fixed Nodes Indicated.

NOTES:

1. Constraints as shown are written in local coordinates. Must be transformed to global coordinates.
2. The "w" equation is not necessary if the solid element already connects the vertical translations of nodes 1 and 2 with sufficient stiffness.



$$u_2 = u_1 + L \sin \theta_y$$

$$v_2 = v_1 - L \sin \theta_x$$

$$w_2 = w_1$$

Linearize
($\sin \theta \approx \theta$)

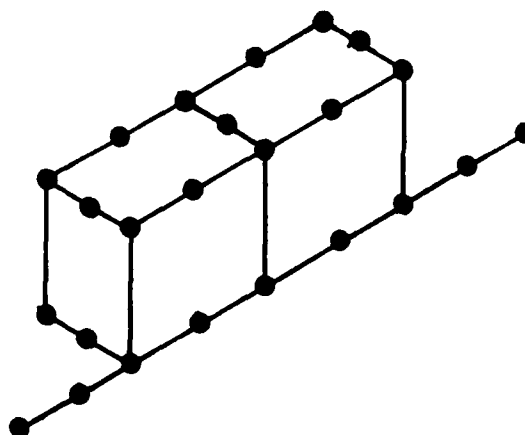
$$u_2 - u_1 - L \theta_y = 0$$

$$v_2 - v_1 + L \theta_x = 0$$

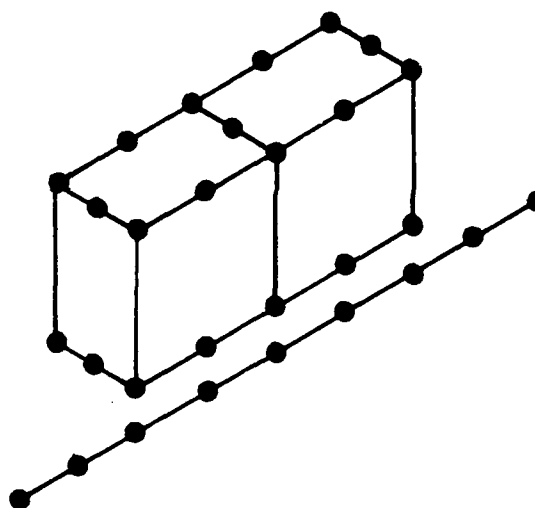
$$w_2 - w_1 = 0$$

Figure 2.11. Typical Linear Constraint.

Matching Rotations of
Parallel Beams and Solids
(Aft Arch, Right Side
Eyebrow to Windshield)



Matching Translations and
Rotations of Parallel
Beams and Solids
(Forward Centerpost to
Windshield)



Matching Rotations of
Perpendicular Beams and
Solids
(Centerpost Beams to Solids)

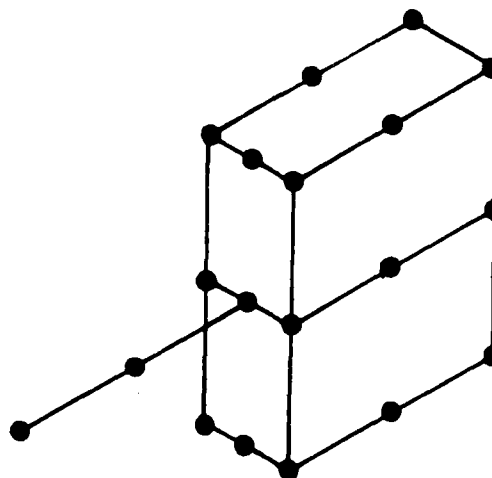


Figure 2.12. Situations Requiring Linear Constraints.

2.5 Loads

For the internal pressure analyses, the windshields were subjected to three different pressure loads, as outlined in Table 2.5. All pressures were gauge pressures, that is, pressure above atmospheric (the pressure difference between the cockpit and outside the aircraft). All interior, inward-facing solid and layered shell element surfaces were loaded.

Two bird impact sites were used for the baseline birdstrike analyses, as shown in Figure 2.13. For the trade studies, only the "worst case" site was used, which was determined from the baseline analyses. Bird impact was by a 4-pound bird impacting at 650 mi/hr. Two user subroutines, ULOAD and USRL0D, were developed using the method discussed in Reference 9 to compute and apply to the models the loads due to birdstrike. The method computed loads based on the results of flat panel testing,^{10,11} and featured the correct spatial and time distribution of pressure and force (see Figure 2.14), as well as "hands-off" operation by the user during MAGNA runs. The method assumed that the bird was a right, circular cylinder having a length-to-diameter ratio of 2:1 and density of 0.03433 lb/in³, that the maximum pressure point (located at the first point of contact between the bird and windshield) remained stationary, and that no bird spreading occurred (constant width footprint). Table 2.6 presents the pertinent data describing the geometry, magnitude, and timing of both the near-center and corner impact loads.

TABLE 2.5
INTERNAL (CABIN) PRESSURES

Designation	Pressure (psig)	Structural Pass/Fail Criterion
Limit Pressure	10.6	Maintain pressure without yielding of windshield or support structure
Proof Pressure	14.1	Maintain pressure without significant yielding of windshield or support structure
Ultimate Pressure	21.2	Maintain pressure

A = Impact Site A, "Near-Center"
B = Impact Site B, "Upper-Corner"

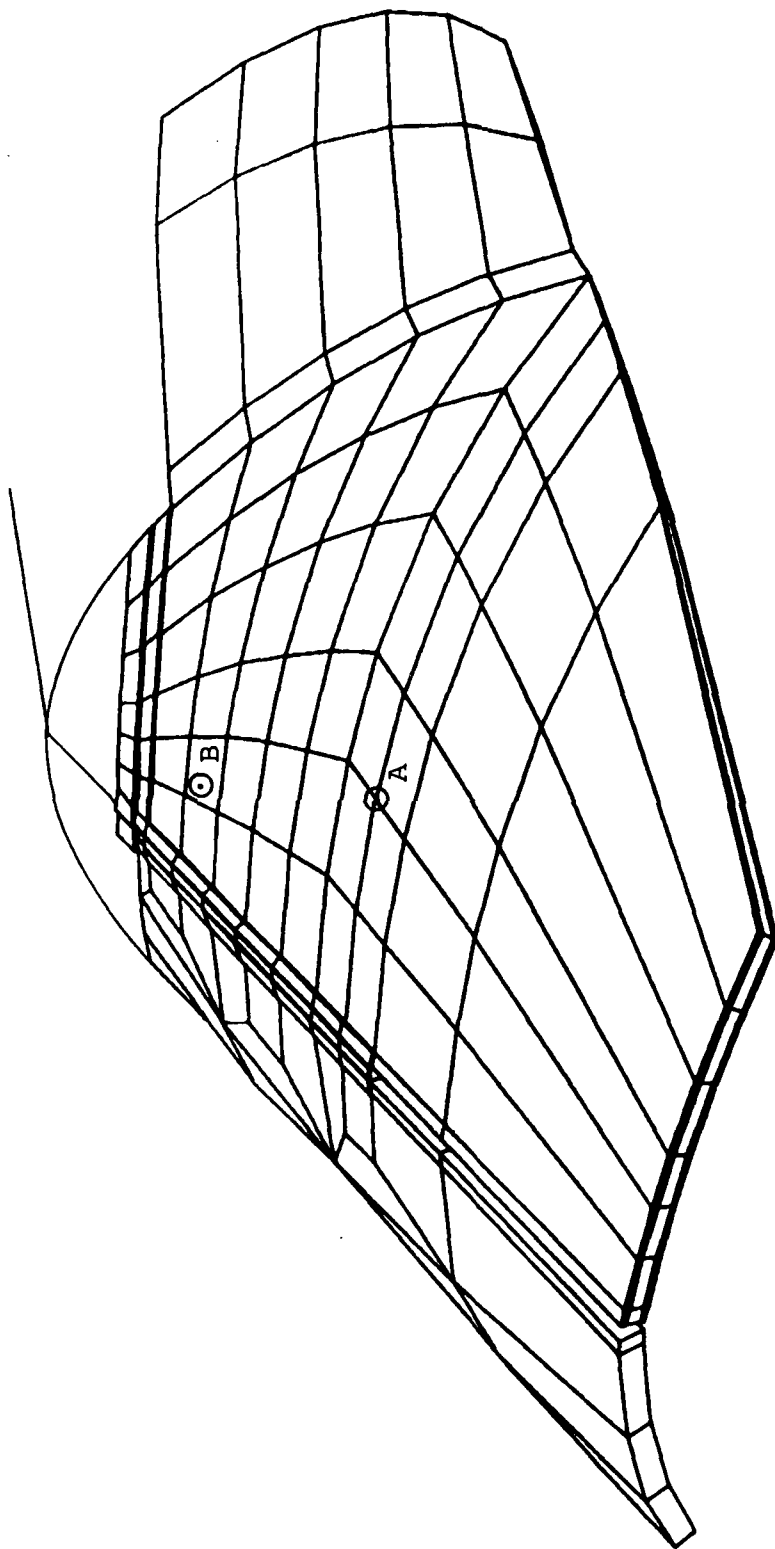


Figure 2.13. Bird Impact Locations.

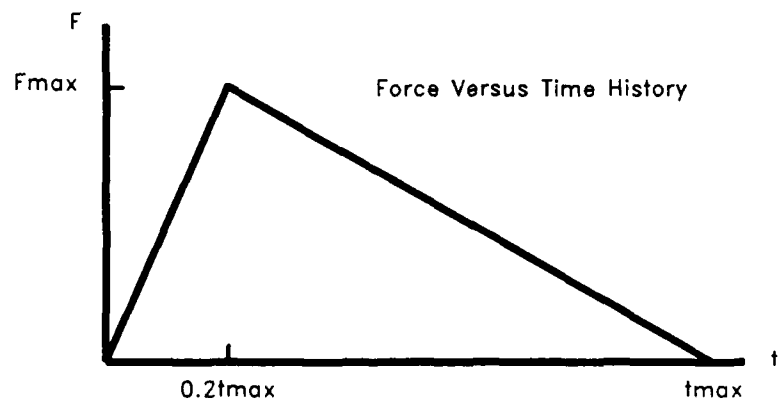
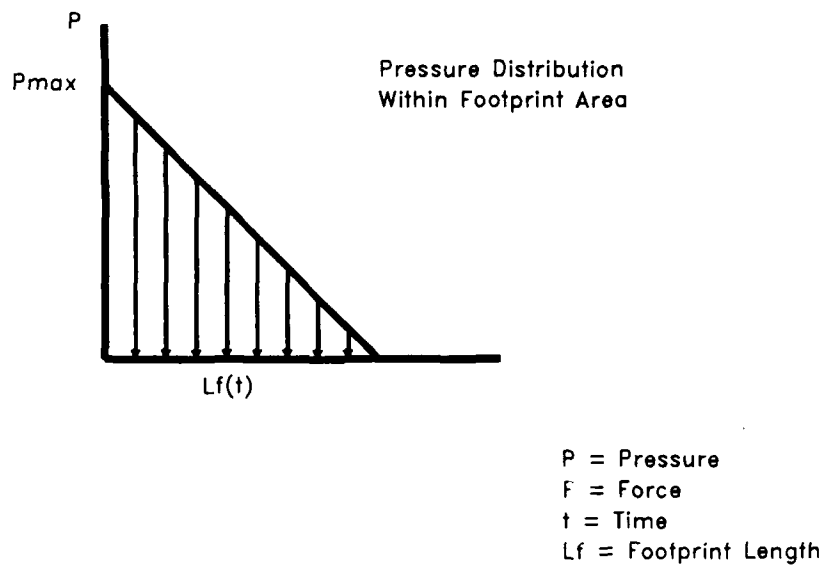


Figure 2.14. Birdstrike Load Distributions.

TABLE 2.6
BIRDSTRIKE LOADS

	Near Center Impact	Upper Corner Impact
Impact Angle (deg)	20.5714	25.0
Bird Diameter (in)	4.201672	4.20167
Effective Bird Length (in)	19.5987	17.4139
Max. Footprint Length (in)	30.3068	25.7243
Impact Velocity (in/sec)	11,447.8	11,447.8
Normal Velocity (in/sec)	4,022.47	4,838.06
Tangential Velocity (in/sec)	10,717.9	10,375.3
Impact Duration (msec)	1.712	1.52115
Pressure Rise Time (msec)	0.3424	0.30423
Peak Total Force (lb)	48,695.9	65,917.8
Peak Pressure (psi)	1,483.2	2,395.5

SECTION 3

ANALYTICAL PROCEDURE

Table 3.1 summarizes the various MAGNA analyses that were conducted. The Phase I (baseline) effort consisted of Cases 1-4, while the Phase II (trade study) effort consisted of Cases 5-9.

This section briefly describes the three different types of MAGNA analyses that were performed, namely, natural frequency, nonlinear static (pressurization), and nonlinear dynamic (birdstrike) analyses. The reader is referred to the MAGNA Finite Element Analysis Manual² for additional detailed information. The analytical procedure used to evaluate the windshield edge fasteners is also described, though in somewhat more detail, since this analysis is not a standard MAGNA capability.

3.1 Eigenvalue Analysis

Eigenvalue analysis (natural frequency analysis) was performed as a means to check the MAGNA models and as an aid in selecting a time step for nonlinear dynamic birdstrike analysis. The frequency and mode shapes generated were studied to reveal any anomalies due to boundary conditions, linear constraints, or material properties. The period of the lowest vibration mode of the left side windshield panel was divided by 100 to give an estimate of the time step for nonlinear dynamic analysis. The consistent mass matrix formulation was used in the analyses.

3.2 Nonlinear Static Analysis

Nonlinear static analysis was performed for the internal pressure loading cases. The material nonlinearity option was selected because, as noted in Table 2.5, the proof and ultimate pressure definitions included the possibility of yielding. Displacements were, however, expected to be small. Static analysis was appropriate since the time history of the

TABLE 3.1
MAGNA ANALYSIS CASES

Case	Windshield Configuration	Loads
1	Current Production	Natural Frequency
2	Current Production	Internal Pressure
3	Current Production	Bird Impact at A ^a
4	Current Production	Bird Impact at B ^b
5	Acrylic Outer Ply	Bird Impact at B
6	Urethane Interlayer	Bird Impact at B
7	No Spall Ply	Bird Impact at B
8	Split Structural Ply	Internal Pressure
9	Split Structural Ply	Bird Impact at B

NOTES:

^a Location A is near the windshield geometric center

^b Location B is near the centerpost-to-eyebrow joint

loading and response was not important. The internal pressure was applied in four successive increments of 5.3 psi, 5.3 psi, 3.5 psi, and 7.1 psi, resulting respectively in total internal pressures of 5.3 psi, 10.6 psi, 14.1 psi, and 21.2 psi. Iteration was performed at every increment to obtain convergence of the solution. The combined Newton-Raphson iteration technique and default displacement and residual force tolerances were used.

3.3 Nonlinear Dynamic Analysis

Nonlinear dynamic analysis was performed for all birdstrike analyses. The large displacement and material nonlinearity options were required in anticipation of deflections of approximately two inches (similar to deflections of the B-1 windshield panel⁷) and yielding of the windshield plies and/or frame members. The time step for all analyses was 0.04 millisecond, which was chosen based on the time of contact of the bird on the windshield (the period of vibration technique discussed in Section 3.2 above was used only for comparison and verification to the impact time result). Combined Newton-Raphson iteration was performed during every fifth increment to ensure convergence of the solution. Default displacement and residual stress convergence tolerances were used. The analyses were stopped and restarted after every fifth increment so that the convergence and results (displacements and stresses) could be checked. The analyses were terminated when the displacements and stresses in the structural polycarbonate ply began to decrease after having reached their maximum values.

3.4 Fastener Analysis

Table 3.2 presents data pertinent to the NAS1580C4 fasteners used to attach the windshield to the support structure. The fasteners joining the windshield to the supporting structure were not modeled explicitly in the MAGNA analyses. Therefore, the MAGNA results did not provide loads acting on the fasteners.

TABLE 3.2
NAS1580C4 FASTENER DATA

Material:	A286 Steel
Threads per Inch:	28
Diameter:	0.2491±0.0005 inches
Tensile Diameter:	0.20238 in
Shear Diameter:	0.25 in
Tensile Area:	0.0364 in ²
Shear Area:	0.04909 in ²
Ultimate Tensile Stress:	180,000 psi
Ultimate Shear Stress:	108,000 psi

However, it was possible to reduce the available MAGNA data into the desired fastener loads. The process outlined in Figure 3.1 required that several computer programs be written or modified. The following paragraphs briefly describe the process by which the MAGNA results are converted into loads on the fasteners. A more complete explanation of the fastener analysis procedure is provided in a separate report (Ref. 12).

The results obtained from the MAGNA analyses were collected on MAGNA post-processor, or MPOST, files. At each time increment during each analysis, the stress state in the transparency model was recorded on an MPOST file. Stress results contained on the MPOST file were computed at integration points located on the interior of each element. These values were a direct result of the numerical analysis using the finite element method. However, integration point stresses were not appropriate for subsequent data reduction; nodal stresses were necessary. Extrapolation from integration point stresses to nodal stresses occurred in the stress averaging program, STRAVG, which is a utility in the MAGNA post-processing software package (Ref. 13). Note that it is these nodal stresses, written to an averaged post-processor or APOST file, that are displayed in stress contour plots appearing in Section 4.

Safety margins for the fasteners were determined as a function of the forces and moments acting on the fasteners, not directly from the transparency nodal stresses. The computer program STRSLT, which was modified from a previous version, converted stresses at node points into equivalent forces and moments per unit length (stress resultants) by integrating the nodal stresses through the transparency thickness. Figure 3.2 shows the faces that were integrated.

Written for this analysis, the computer program XFER converted STRSLT stress resultant information into loads acting on the fasteners. The stress resultants acting along the windshield edge were assumed to cause bushing rotation relative

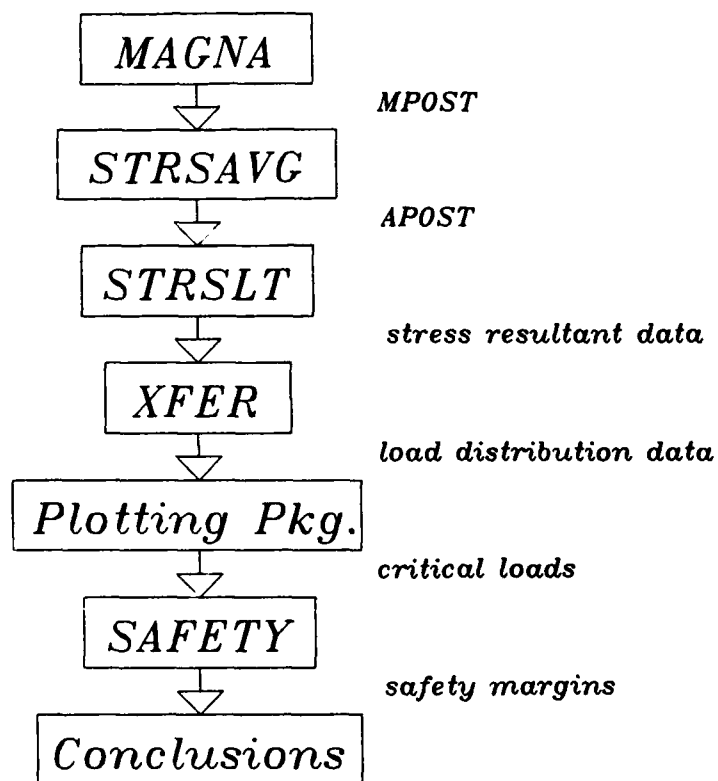
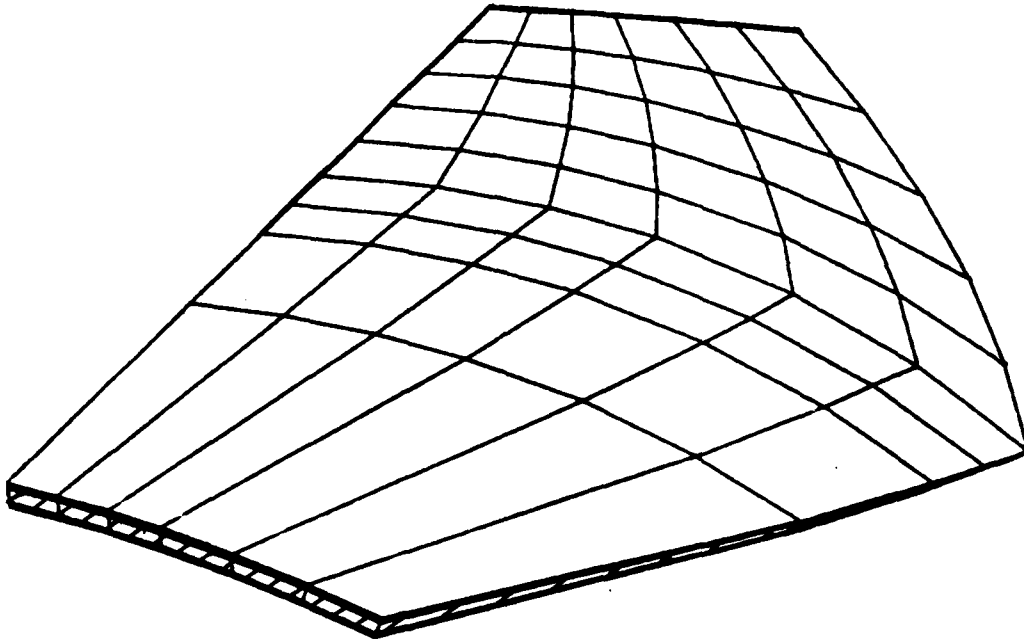


Figure 3.1. Fastener Analysis Procedure.



All outward-facing element faces through the windshield thickness around the perimeter of the panel shown above were integrated to obtain stress resultants. The visible faces are cross-hatched.

Figure 3.2. Location of Element Faces that were Integrated to Obtain Stress Resultants for Fastener Analysis.

to the fastener due to the clearance between these components. Such rotation produced shear forces on the upper and lower portions of the fastener grip length as indicated in Figure 3.3. Shear resultants acting through the transparency thickness were transferred to the frame flanges through the fasteners, resulting in an axial force in the fastener as shown in Figure 3.4.

The loads (axial, upper shear, and lower shear) were calculated as a combination of the stress resultants for each of the five plies in the transparency (seven plies for Case 9) at every perimeter location. Perimeter locations corresponded directly with the corner and midside node positions of each element edge on the transparency perimeter. Figure 3.5 defines the perimeter location (p) as the distance in inches from the centerpost-forward arch connection increasing along the centerpost (p=0 in. to p=54 in.), eyebrow (54-74), aft arch (74-106), sill (106-157), and forward arch (157+) respectively.

Plot files written by XFER contained the axial and shear load components as functions of the perimeter position. Sigma-Plot,¹⁴ a commercially available scientific graph plotting program for IBM PC and compatible computers, was used to display the load resultants graphically, although any stand-alone plotting package could have been used. One plot was generated for each fastener load component (axial, upper shear, and lower shear) for each baseline and trade study analysis.

Since the fasteners were always loaded in tension, negative axial loads did not indicate compression. The sign of the axial load only indicated the direction of load application, which was the direction of the windshield shear load shown in Figure 3.4. The magnitude of the upper and lower fastener shear loads were displayed on the graphs, but the directions of the shear loads were not output from XFER.

The critical loads acting on the fasteners were taken directly from the plots. Shear and axial effects were considered both independently and together. The combined effects of shear

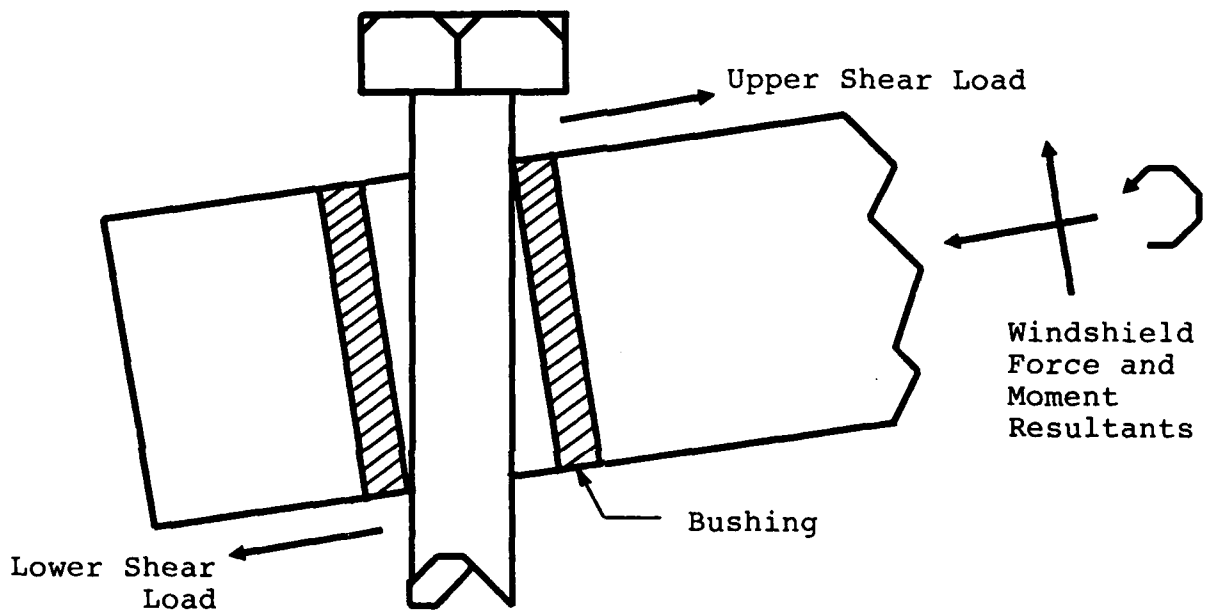


Figure 3.3. Shear Loads Applied to Fastener.

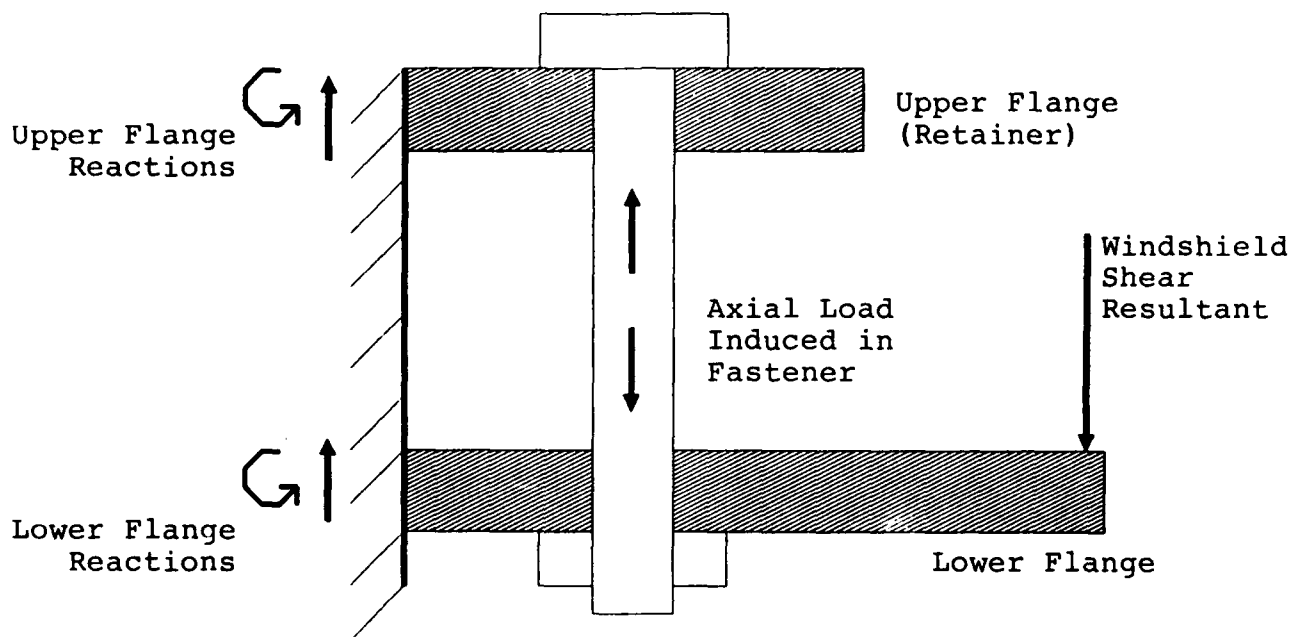


Figure 3.4. Axial Load Induced in Fastener.

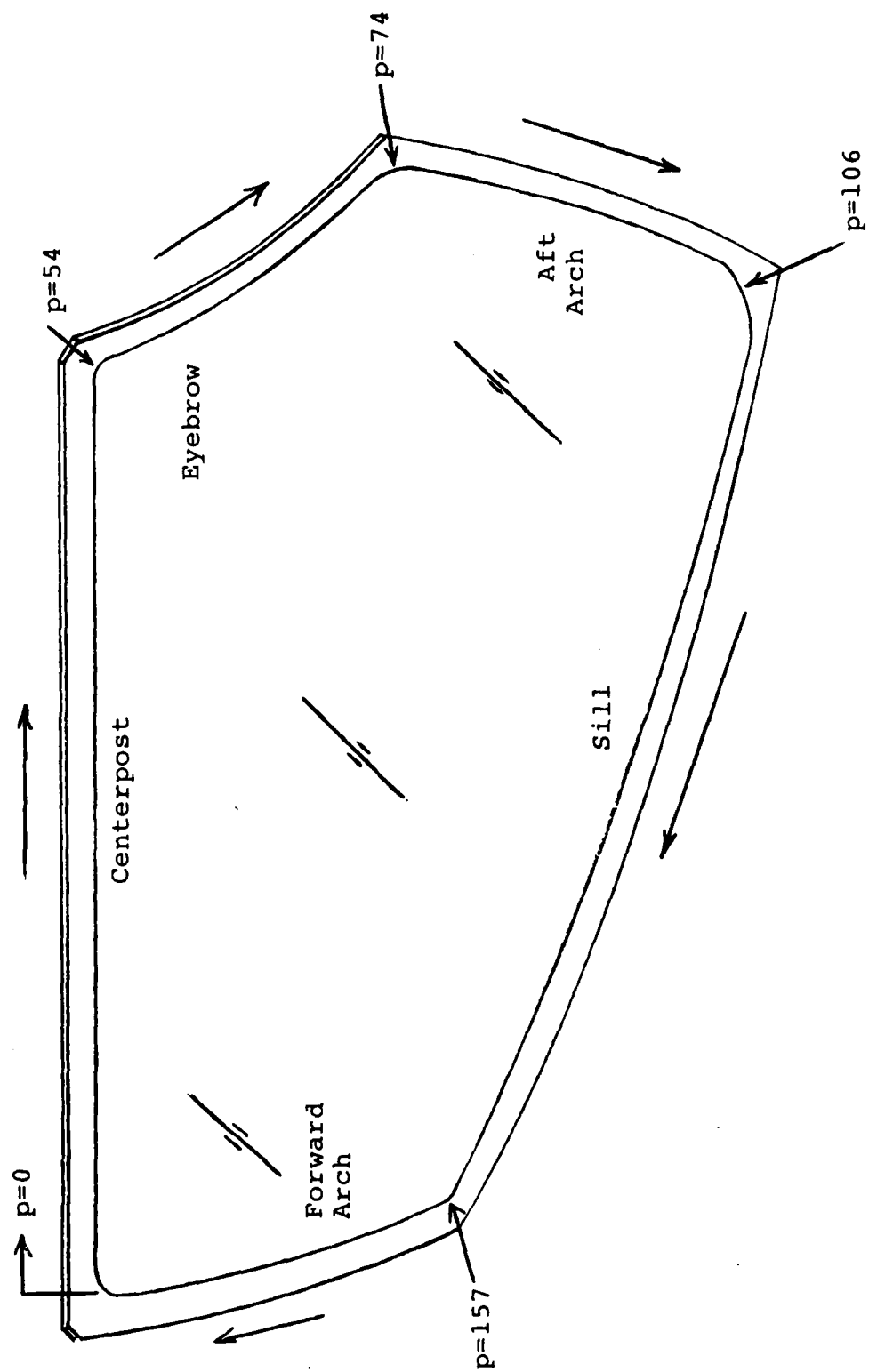


Figure 3.5. Windshield Perimeter Location System for Fastener Analysis.

and tension were accounted for, using the following interaction equation:²³

$$(S_t/S'_t)^2 + (S_s/S'_s)^3 \leq 1$$

where

- S_t = actual tensile stress on fastener, psi,
- S'_t = allowable tensile stress on fastener, psi,
- S_s = actual shear stress on fastener, psi,
- S'_s = allowable shear stress on fastener, psi.

Combined values greater than one imply fastener failure. The computer program SAFETY was written to determine the margins of safety against various failure modes (fastener tension and shear, transparency bearing and rupture) for given geometry and critical load conditions. Figure 3.6 describes each of the four failure modes considered in the analysis. SAFETY also computed fastener margins assuming every other fastener was deleted. Note that fastener preload was considered in performing all calculations.

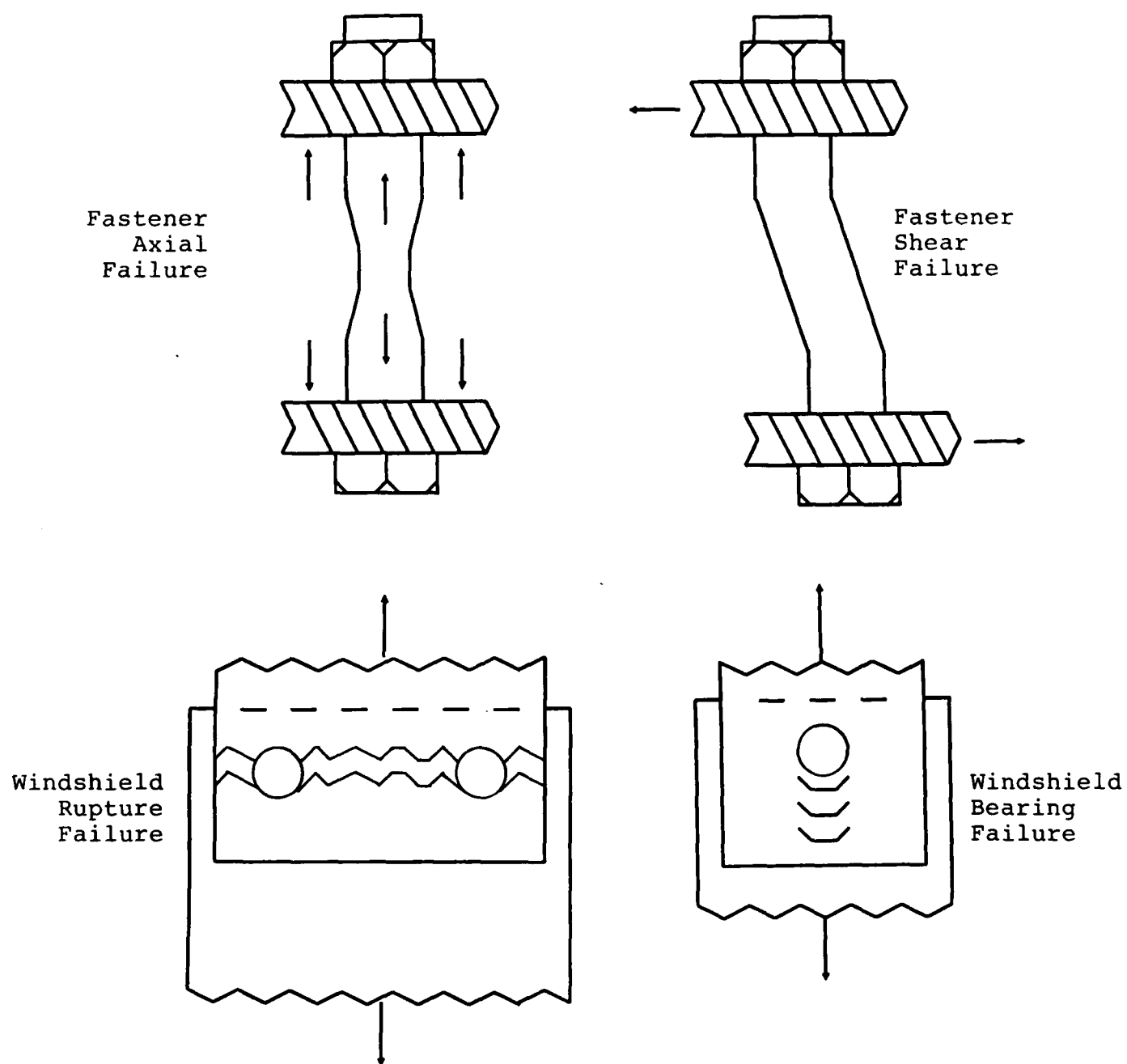


Figure 3.6. Fastener System Failure Modes.

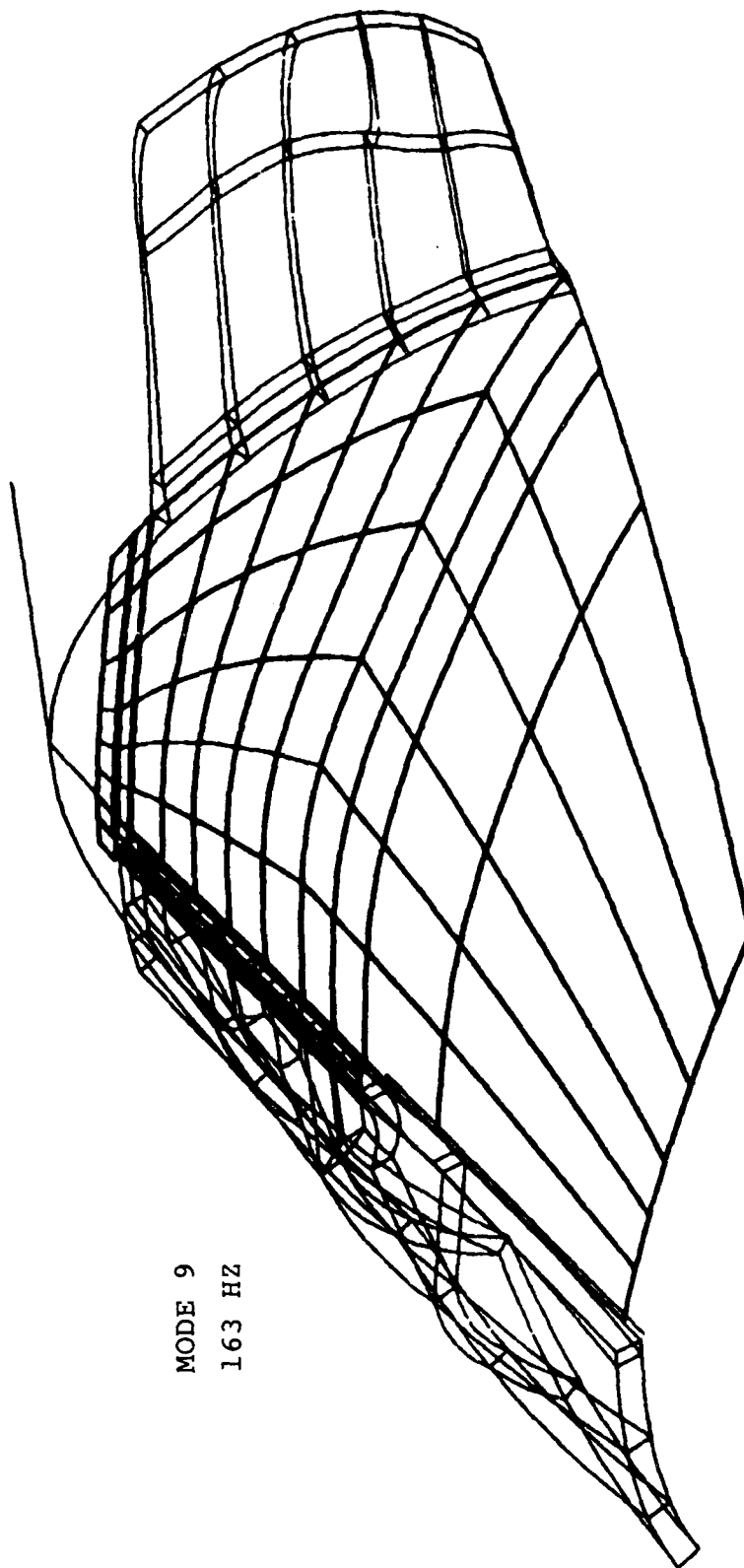
SECTION 4

RESULTS AND DISCUSSION

Four categories of results were obtained: natural frequencies and mode shapes, deformed shapes and displacement time histories, stress contours, and fastener loads and margins of safety. The appropriate results are presented by category for each analysis type (natural frequency, internal pressure, and birdstrike) to facilitate comparison and discussion among the different run cases. Discussion of fastener performance, including the effects of removing every other fastener, is included in the pressure and birdstrike discussions. Fastener tolerance is discussed separately in Section 4.5. For quick reference and comparison, Section 4.6 provides a concise summary of all results without detailed discussion.

4.1 Natural Frequency Analysis Results

The lowest vibration mode of the Case 1 left side windshield occurred at 163 Hz. Figure 4.1 shows the vibration mode shape. The corresponding period of vibration was calculated as the reciprocal of the natural frequency, resulting in a period of 0.0061 second. Dividing by 100 to obtain an estimate of the time step for nonlinear dynamic birdstrike analysis resulted in a step size of 0.000061 second. The order of magnitude of this estimate is the same as that of the chosen step size of 0.00004 second, verifying this choice. However, the value of 0.000061 was considered too large in view of the brief time the bird would be in contact on the windshield (see Table 2.6) and in view of the high stiffness of the windshield, which would tend to respond closely in phase with the loading (compared with a flexible windshield, like the F-16, in which the response would lag well behind the loading because of the greater influence of inertia).



MODE 9
163 HZ

Figure 4.1. Mode Shape for Lowest Natural Frequency of the Left Side Windshield Panel.

4.2 Internal Pressure Analysis Results

Maximum displacements for the internal pressure analyses occurred at approximately the centroid location of the left side windshield panel and were small, as expected. The total displacement was 0.104 inch for node 2029 of Case 2 and 0.107 inch for node 2740 of Case 8 (node located on the outer surface of the structural ply) at the maximum (ultimate) pressure of 21.2 psi.

Figures 4.2 and 4.3 present Von Mises equivalent stress contours for the structural polycarbonate ply (plies) of the Case 2 and Case 8 analyses at the ultimate pressure. The maximum stress was approximately 500 psi, well below the 12,000-psi yield stress of polycarbonate. In addition, the maximum equivalent stress in the glass ply was 11,850 psi for Case 2 and 9,933 psi for Case 8, below the ultimate stress of 18,000 psi, implying that the glass ply remained intact. Therefore both the current production and split polycarbonate ply windshield panel configurations were adequate for resisting the internal pressure loads. Since the Case 5-7 windshields used the same structural polycarbonate ply configuration as the current production windshield, the windshield panels for these cases should also be adequate for resisting all internal cabin pressure up to the ultimate pressure.

As a simple qualitative check on the results, the windshield was analyzed as a portion of a thin-walled monolithic polycarbonate cylindrical pressure vessel (the windshield panel geometry is, in fact, that of a right circular cylinder of 50 inch outer mold line radius). The stresses were computed from:¹⁵

$$\text{Hoop Stress: } S_h = pr / t$$

$$\text{Axial Stress: } S_a = pr / (2t)$$

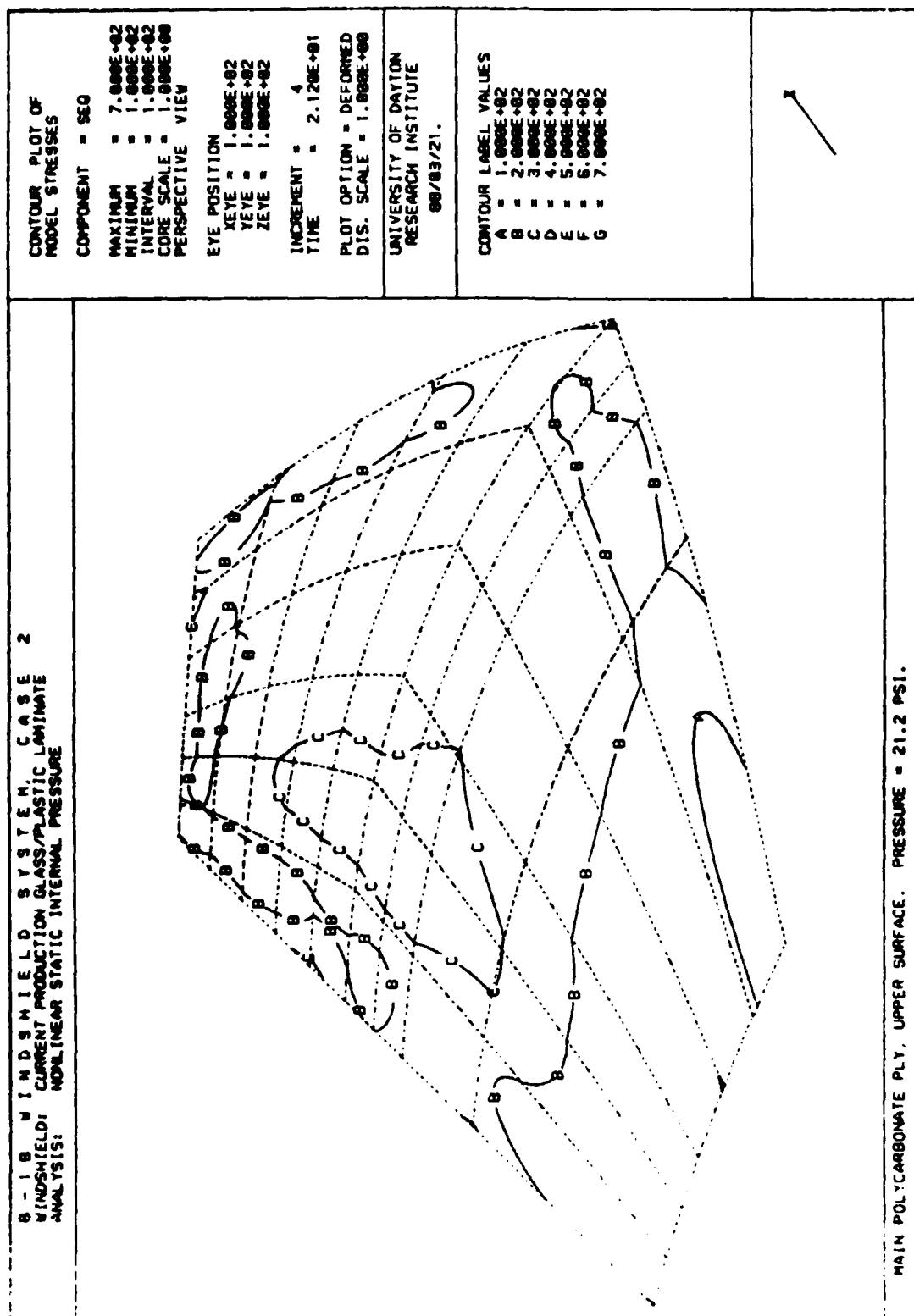


Figure 4.2. Equivalent Stress Contours for the Outer Surface of the Structural Ply, Case 2.

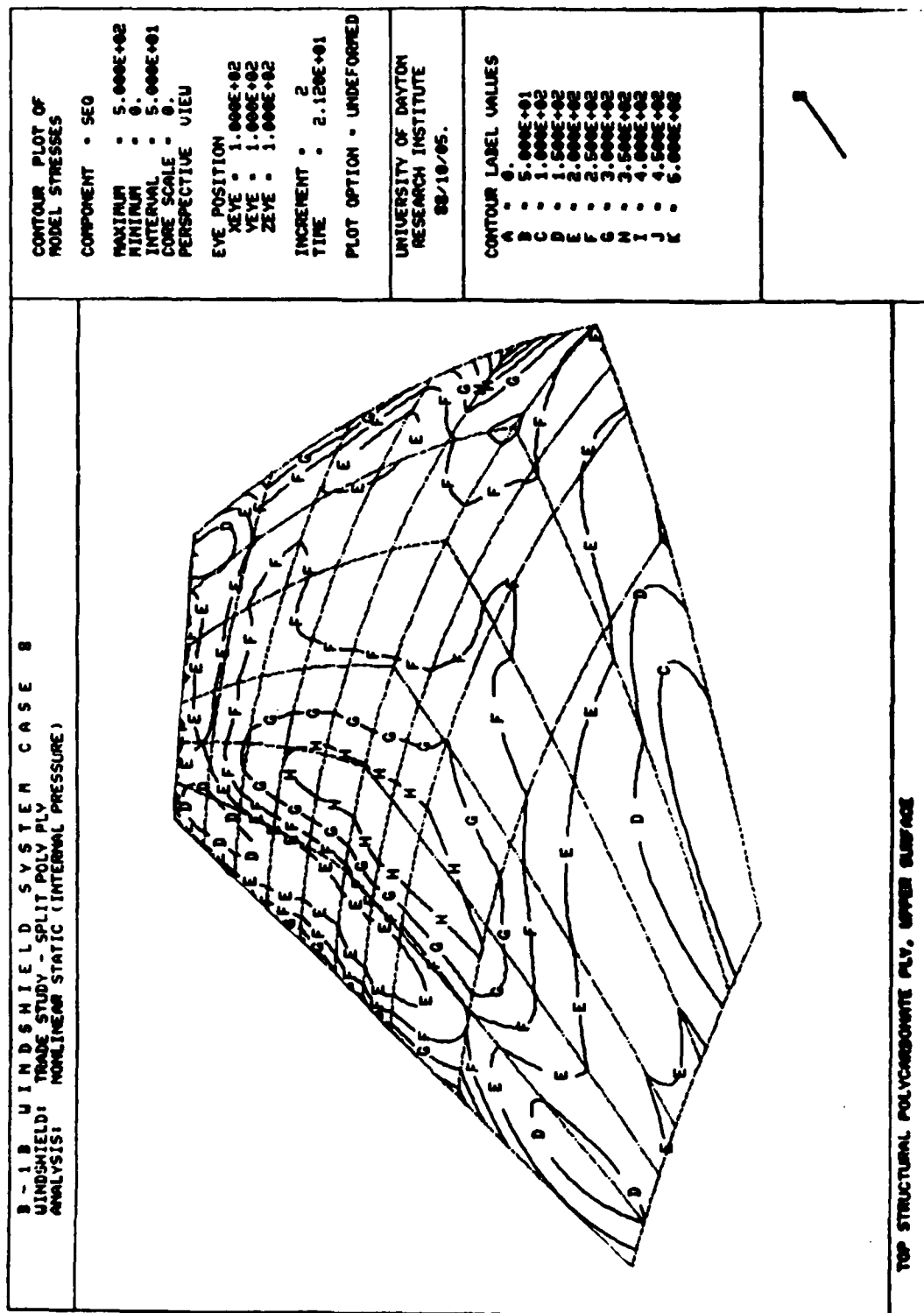


Figure 4.3. Equivalent Stress Contours for the Outer Surface of the Structural Ply, Case 8.

where p = internal pressure, psig
 r = nominal radius, in
and t = windshield thickness, in.

For Case 2, $p = 21.2$ psig, $r = 49.21$ in, and $t = 0.87$ in. The resulting hoop stress was 1,200 psi while the axial stress was 600 psi. The order of magnitude of these numbers agreed well with the MAGNA stress results, verifying the computer analysis. (Note that the MAGNA results were lower because the other windshield layers and the support structure helped resist the pressure load.)

Figures 4.4 and 4.5 show equivalent stresses in the centerpost frame for Case 2 and Case 8 at 21.2 psi. The stresses were low (4,000 - 5,000 psi), well below the yield stress of 50,000 psi. Note that the stresses in the forward-most centerpost solid elements rose sharply to 20,000 to 25,000 psi. This stress gradient was artificial, occurring due to the linear constraints joining the centerpost beam elements to the centerpost solid elements. The actual stresses in this region should have been similar to those for the remaining portions of the centerpost. In addition to the centerpost, stresses in the eyebrow and aft arch were also well below yield, as shown in Table 4.1. Thus the centerpost, eyebrow, and aft arch were adequate for resisting internal pressures of up to 21.2 psig.

Figures 4.6 and 4.7 describe the loads acting on the fasteners for the baseline and trade study internal pressurization analyses, respectively. For the baseline case, the largest axial and shear loads were found along the eyebrow near the aft arch connection ($p=74$ in.). For the trade study case, the largest fastener shear loads were located in the forward-most section of the centerpost where the linear constraints used in the modeling produced artificially high values (see previous paragraph). The largest axial load was along the eyebrow in a position similar to the baseline case.

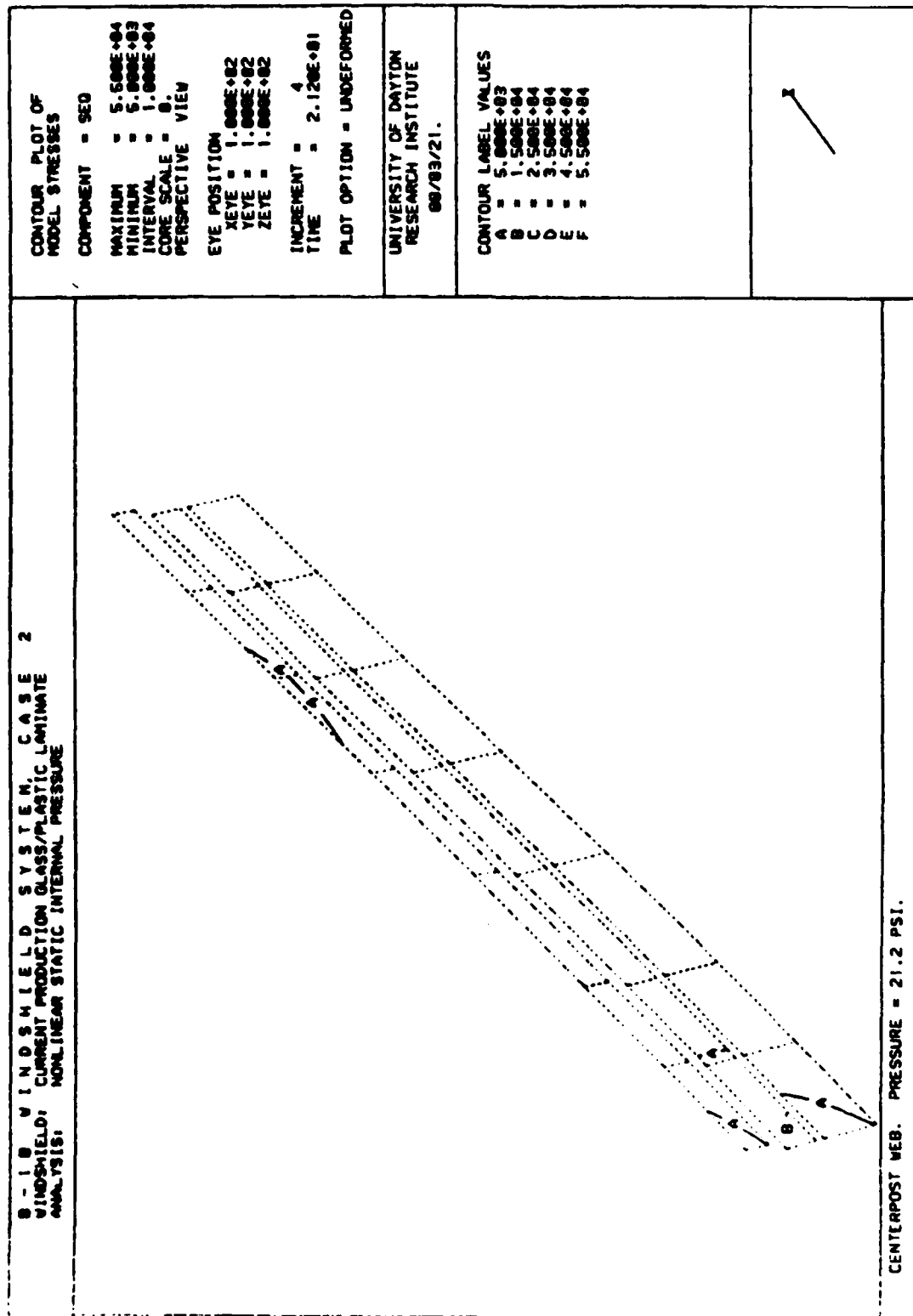


Figure 4.4. Equivalent Stress Contours on the Centerpost Web, Case 2.

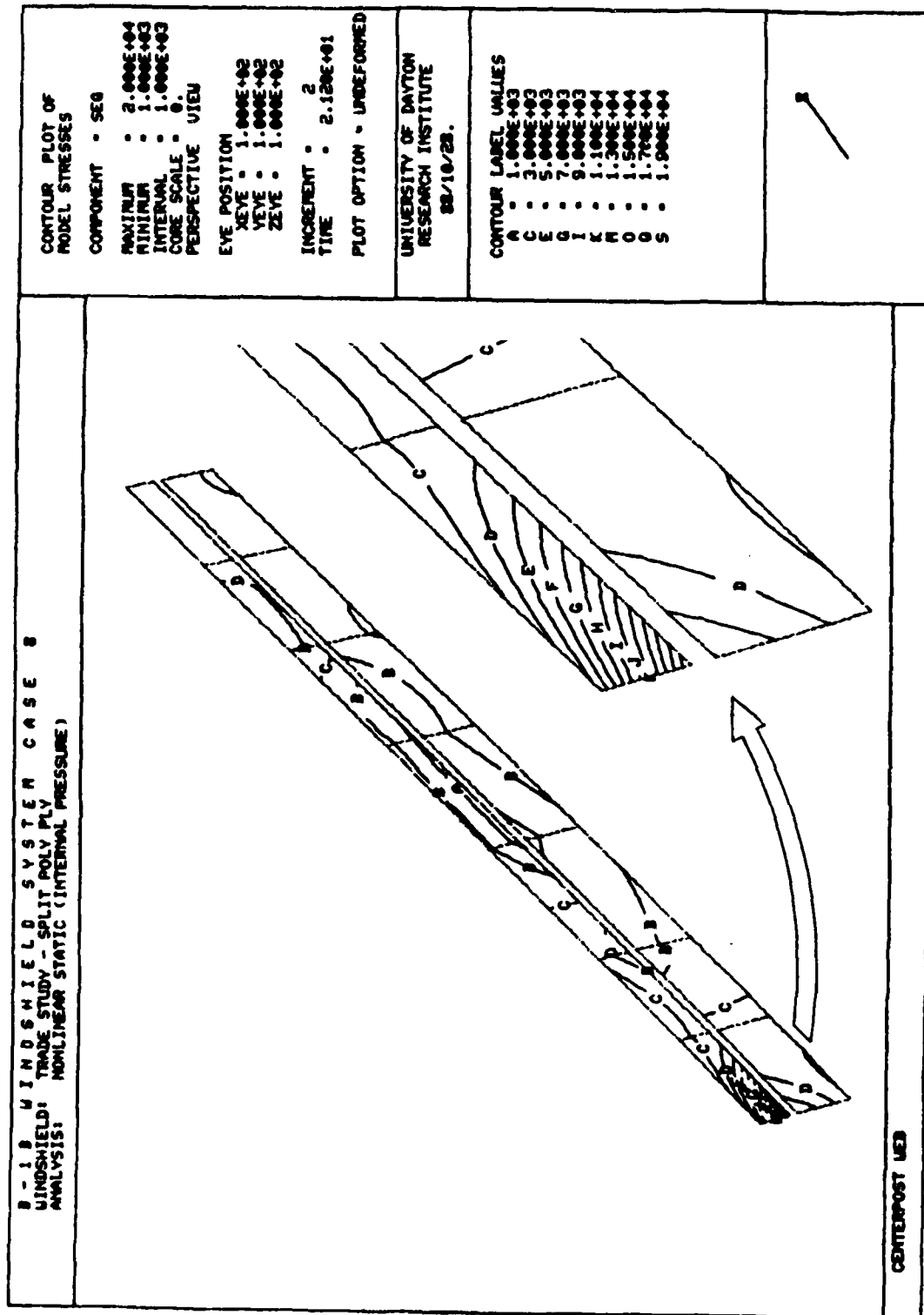


Figure 4.5. Equivalent Stress Contours on the Centerpost Web, Case 8.

TABLE 4.1
MAXIMUM STRESSES IN SUPPORT STRUCTURE
DUE TO INTERNAL PRESSURIZATION

Component	Yield Stress (kpsi)	Maximum Component Stress (ksi)	
		Case 2	Case 8
Forward Centerpost	50.	5.	4.
Aft Centerpost	56.	7.4	3.4
Eyebrow	56.	4.5	6.5
Aft Arch	56.	5.8	2.9

B-1 B Case 2 Incr 4

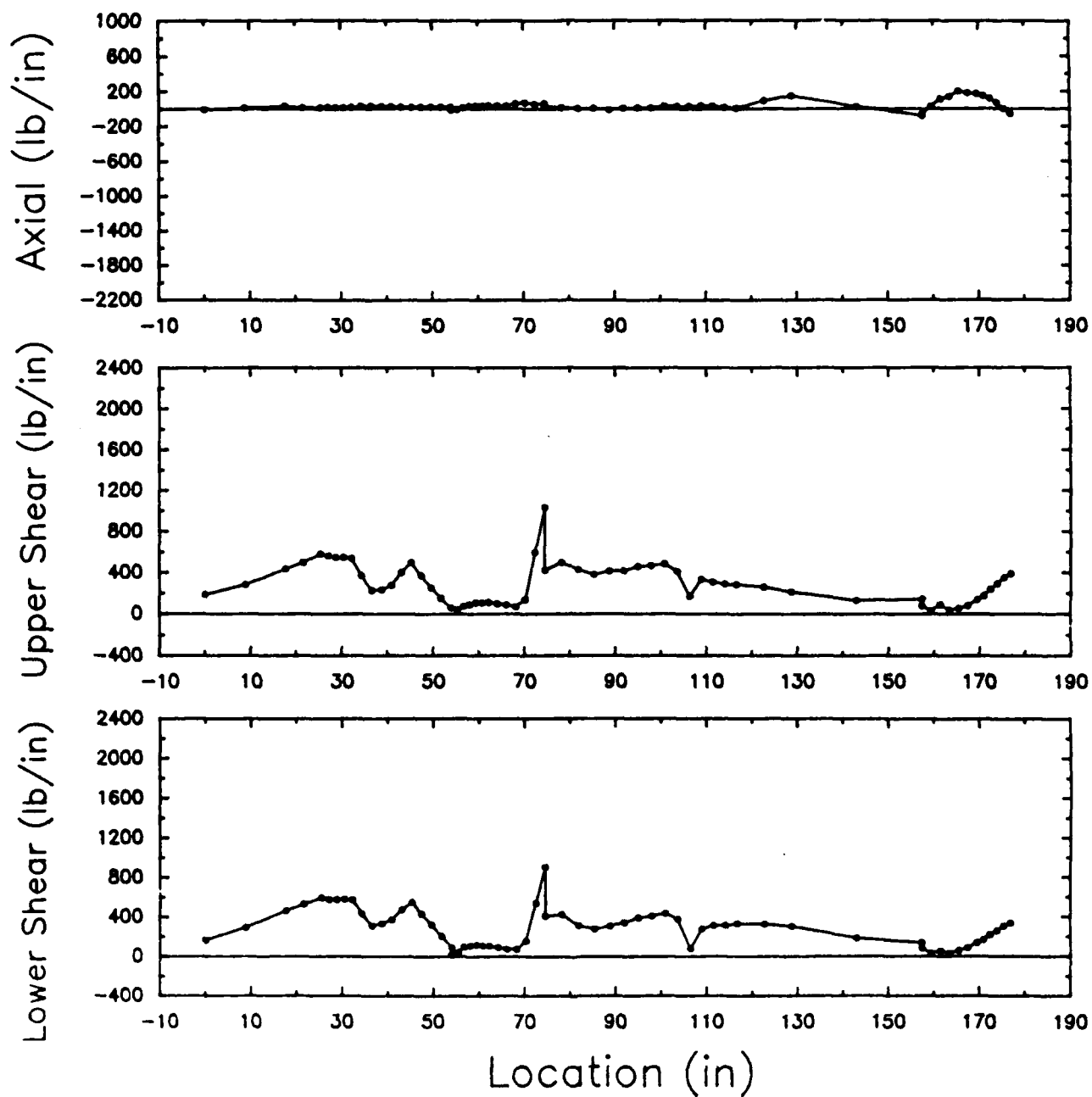


Figure 4.6. Fastener Load Distribution, Case 2.

B-1 B Case 8 Incr 2

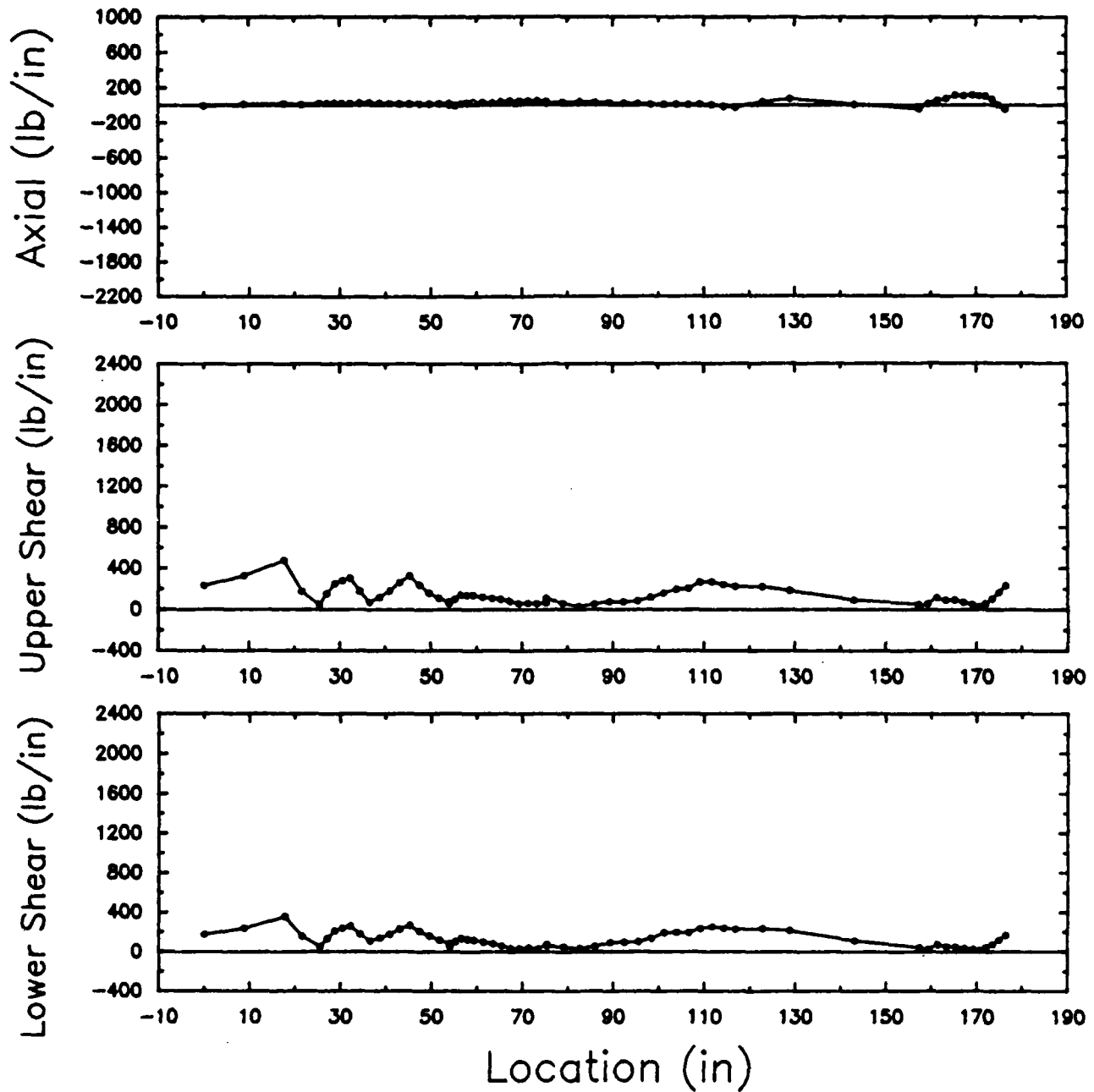


Figure 4.7. Fastener Load Distribution, Case 8.

The load distribution plots for both of the pressurization analyses were plotted with the same scaling used in the subsequent birdstrike analyses. The 21.2 psig internal pressure produced fastener loads which were relatively insignificant compared with the loads due to birdstrike. The axial loads for both pressurization cases were positive, indicating that the axial load in the fasteners acted toward the upper surface, as was expected. Note that the "spike" in the load plots near $p=74$ inches was due to linear constraints and was thus artificially high. These values were therefore ignored in determining the maximum fastener loads.

Table 4.2 shows the critical pressure loads and the percent change in these loads resulting from the split structural ply windshield configuration. The pressurization trade study analysis exhibited a load distribution character similar to the baseline case, but the loads were diminished by 21% to 40%. These loads were used to calculate the safety margins and interaction numbers indicated in Table 4.2.

The large safety margins indicated that the pressure loads were significantly below critical. The smallest safety margin for baseline study (4.64 in fastener shear) indicated that the fasteners were more than 4.64 times stronger than necessary for such loading. The trade study safety margins were more than three times larger than the baseline values. Even with every other fastener removed from the current windshield configuration, the minimum safety margins for Cases 2 and 8 were 1.82 and 2.58, respectively. Note that the combined tension/shear results follow the same trends as the individual tension and shear margins of safety.

All of the analyses conducted had a main structural ply identical to that of Case 2 or Case 8. Since the majority of the applied load (70%-80%) was carried by this ply to the fasteners, the results for Cases 2 and 8 were representative of all the baseline and trade studies. Thus the fasteners for all

TABLE 4.2

FASTENER SAFETY MARGINS FOR THE
INTERNAL PRESSURIZATION ANALYSES

	Case 2	Case 8
Critical Loads		
Axial (lb/in)	200.	130.
Upper Shear (lb/in)	610.	480.
Lower Shear (lb/in)	600.	360.
Percent Change in load from the baseline values		
Axial	-	-35.0
Upper Shear	-	-21.3
Lower Shear	-	-40.0
Safety Margins		
Fastener Tension	3.12	3.30
Fastener Shear	4.64	6.17
Transparency Bearing	6.50	8.53
Transparency Rupture	20.91	26.84
Safety Margins (50% fastener removal)		
Fastener Tension	1.06	1.15
Fastener Shear	1.82	2.58
Transparency Bearing	2.75	3.77
Transparency Rupture	24.66	31.61
Interaction Relation		
All Fasteners Present	0.06	0.06
50% Fastener Removal	0.28	0.24

Note: Safety margins < 0.0 indicate failure

Interaction relation values > 1.0 indicate failure

cases were adequate to resist internal pressures up to 21.2 psig.

In conclusion, the current production windshield system and each of the trade study windshield system configurations were sufficiently designed to resist internal cabin pressures of up to 21.2 psi above outside atmospheric pressure without permanent deformation to the windshield and immediate support structure and without failure of the fasteners.

4.3 Baseline Birdstrike Results

Figures 4.8 and 4.9 present the deformed shapes of the left side windshield panels for the near-center (Case 3) and upper corner (Case 4) analyses. The deformed shapes looked as expected, with the pocket formed due to bird impact being rather shallow because of the high stiffness of the windshield.

Figure 4.10 shows the displacement time histories for the nodes experiencing the greatest displacement during the analyses. (The node locations are shown in Figure 4.11.) The maximum displacement for the near-center analysis was 1.4 inches compared to 1.0 inch for the upper corner shot. Maximum displacement during birdstrike testing of the B-1A windshield was 2.15 inches for near-center impact.⁷ The lower analytical near-center displacement may have resulted in part from the differences in planform and cross-sectional geometry and outer ply materials between the B-1A and B-1B windshield systems. In addition, mapping of the near-center bird loads over too large an area contributed to the smaller analytical displacement. Figure 4.12 illustrates this situation. The bird footprint was assumed to be a constant width (equal to the diameter of the bird) for computing the impact loads. But the computed loads then had to be mapped onto the finite elements, which, because of the rather coarse element mesh used, were significantly wider than the bird footprint. Thus, though the total load applied to

NOTE: For clarity, only
upper layer of
elements shown.

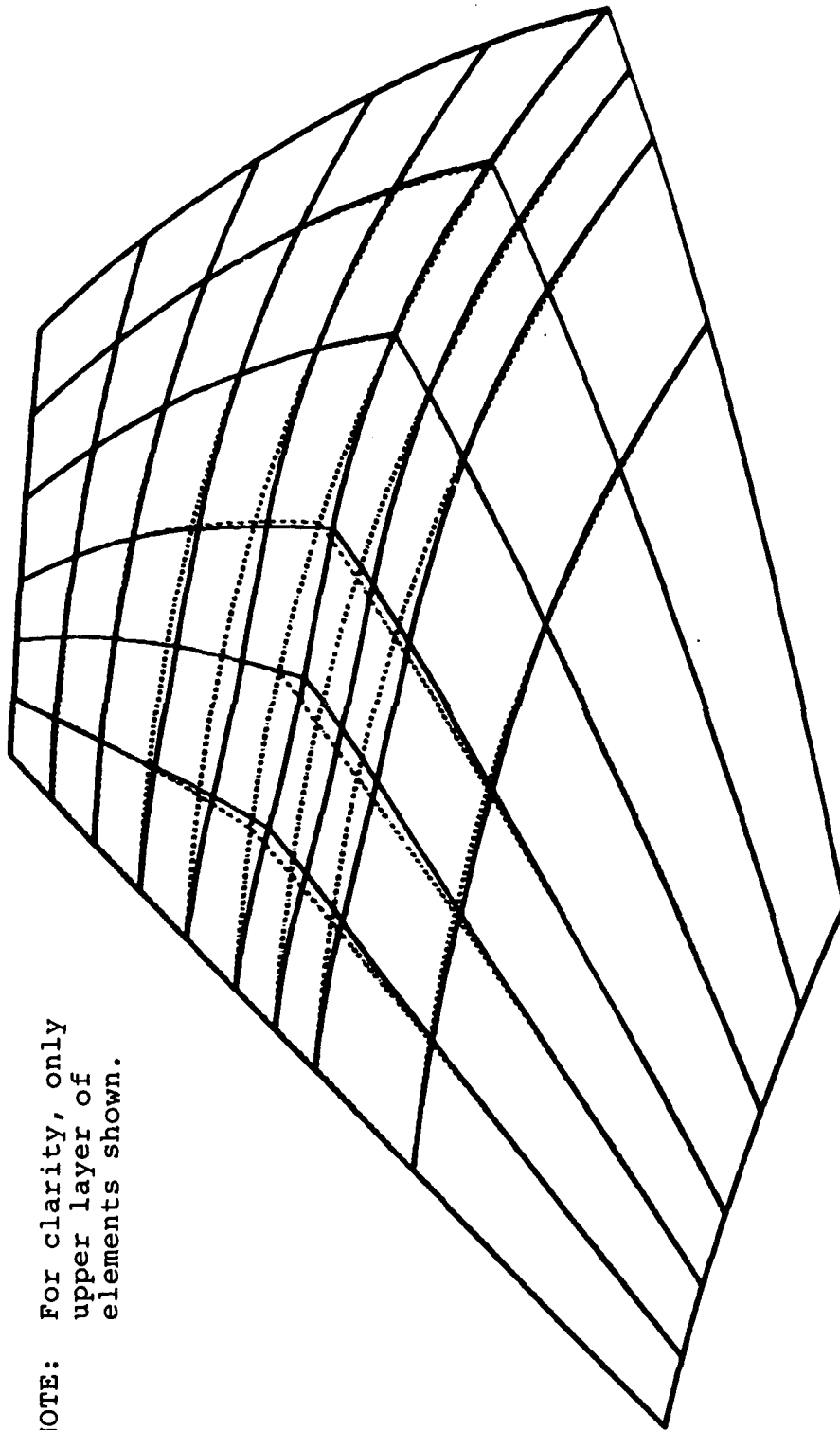


Figure 4.8. Deformed Shape of the Left Side Windshield,
Case 3, Increment 50.

NOTE: For clarity, only
upper layer of
elements shown.

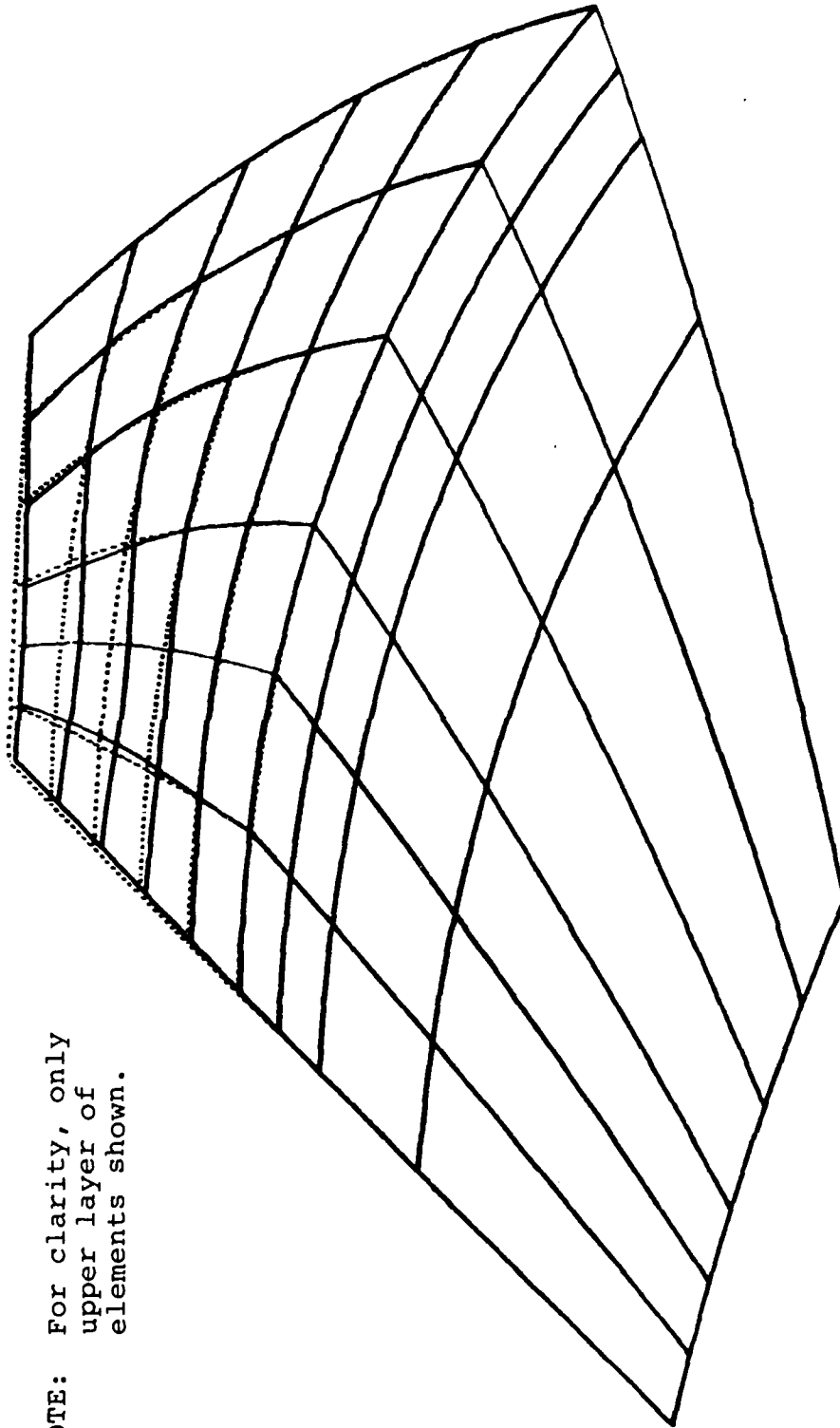


Figure 4.9. Deformed Shape of the Left Side Windshield,
Case 4, Increment 35.

B-1 B Windshield Displacement Time History Baseline Study

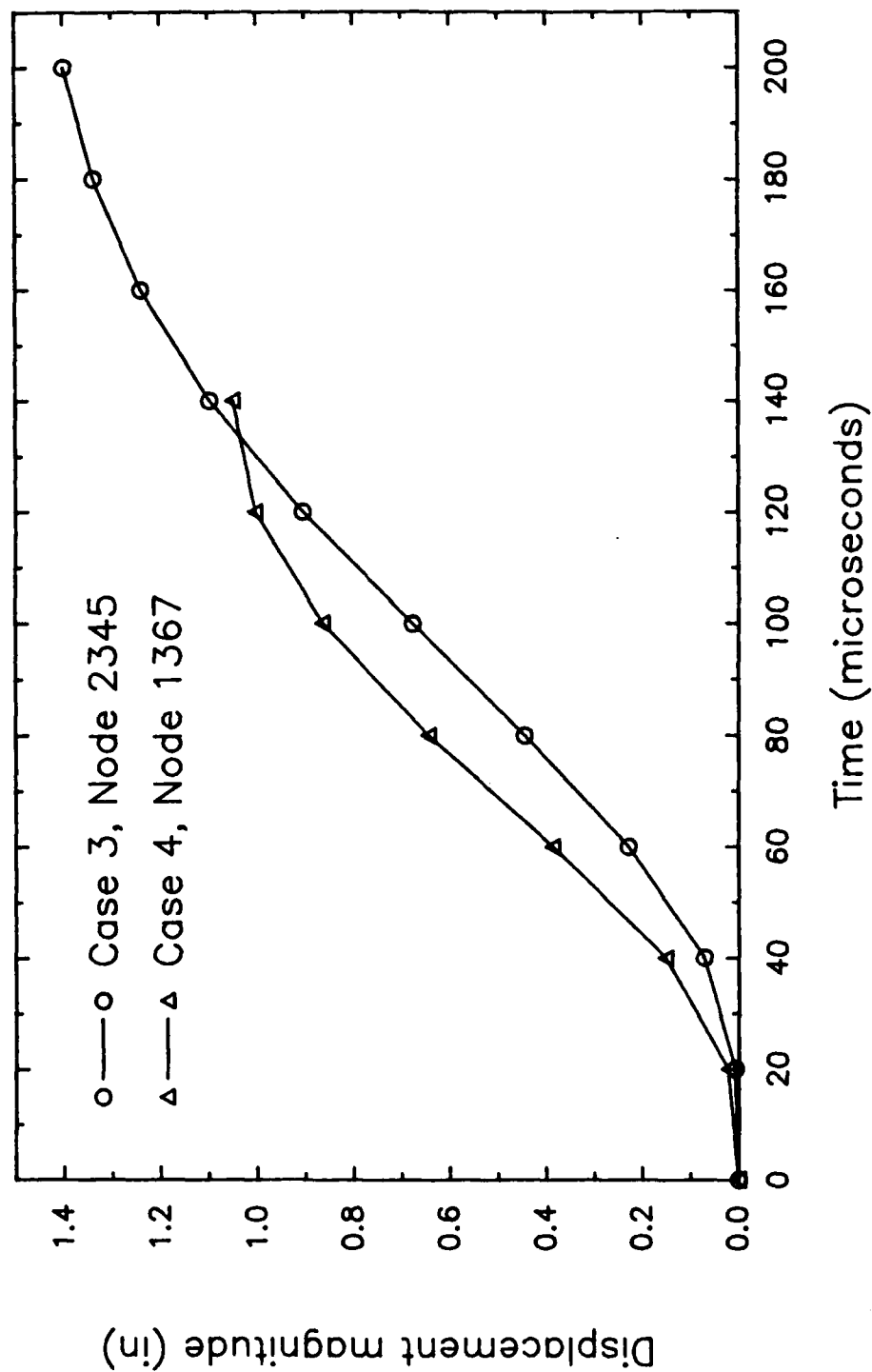


Figure 4.10. Displacement Time Histories, Cases 3 and 4.

C = Node 1367 (Maximum Displaced Node,
Upper Corner Impact)

D = Node 2345 (Maximum Displaced Node,
Near-Center Impact)

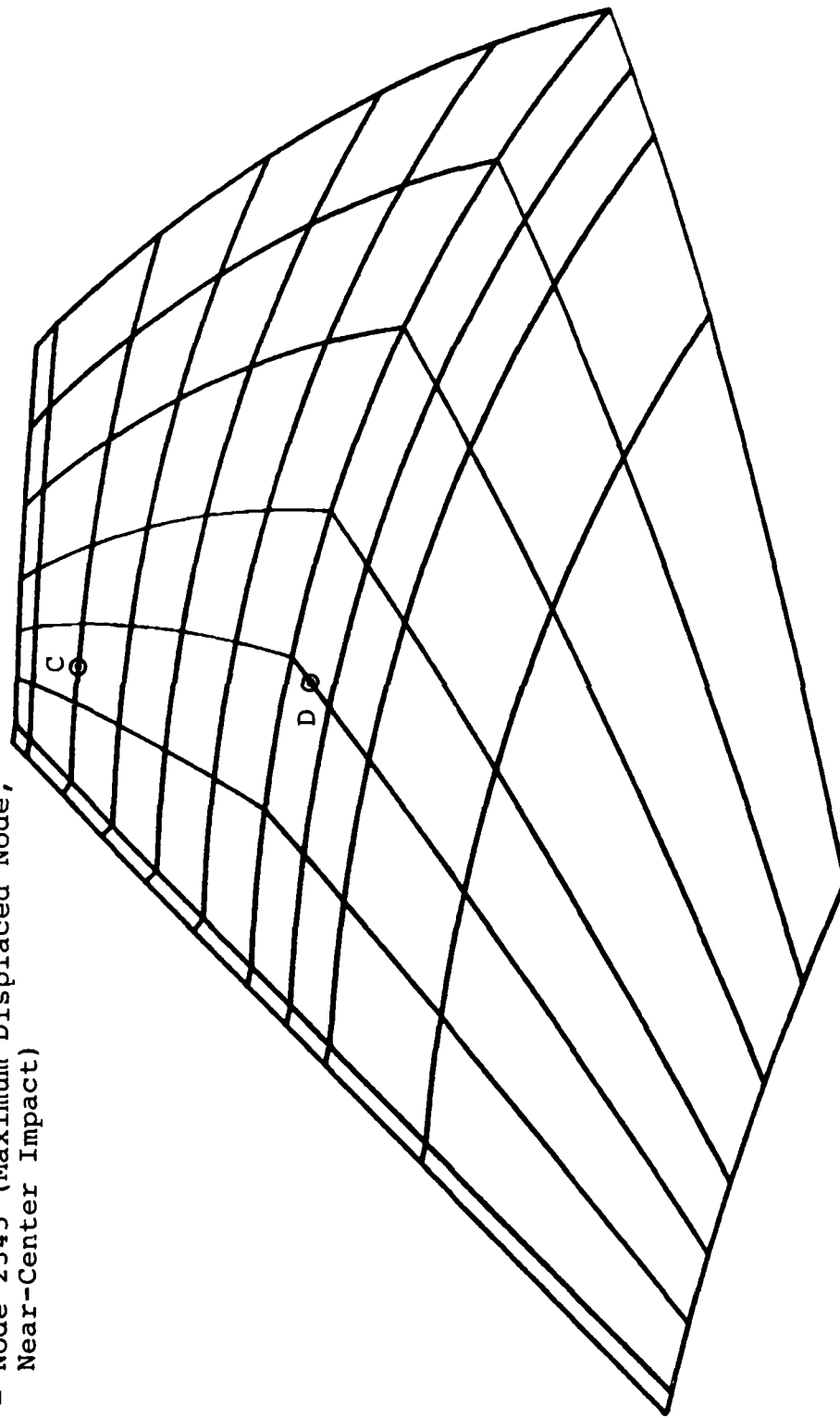


Figure 4.11. Location of Maximum Displaced Nodes from Baseline Birdstrike Analyses.

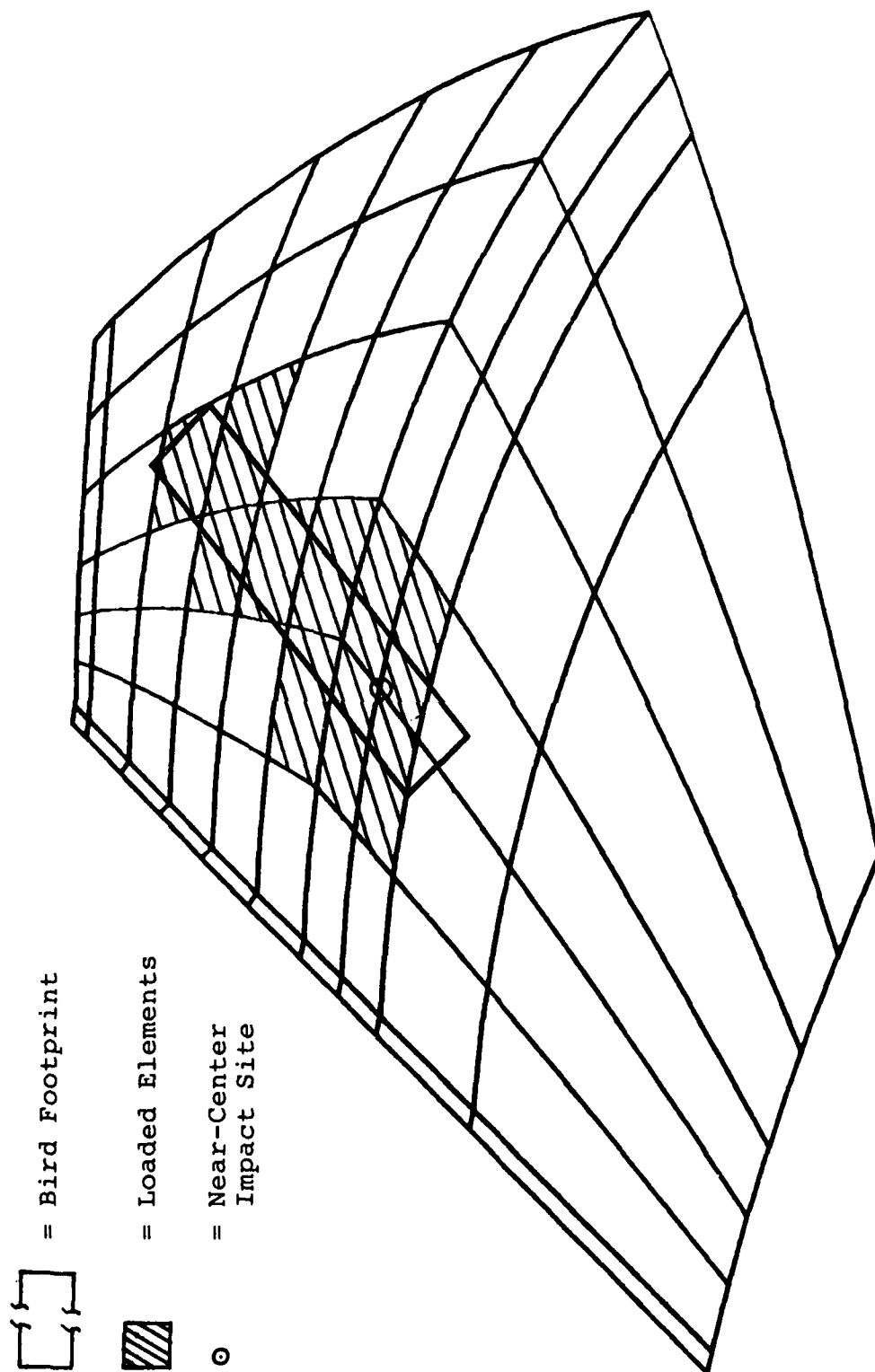


Figure 4.12. Superposition of Near-Center Bird Footprint Onto Windshield Finite Element Model.

the windshield was correct, the intensity of the loading (that is, the pressure) for the near-center shot was too small, leading to reduced displacements. For purposes of these analytical studies these differences should not effect the validity of the results. However, actual stresses resulting from near-center birdstrike could be slightly higher than computed values. The geometry of the loaded upper corner finite elements better matched the bird footprint geometry, resulting in more accurate values of applied pressure and therefore more accurate displacements.

Finally, it should be noted that the time required to reach peak displacement for the upper corner analysis was only approximately seventy percent of the time required for the near-center analysis. This more rapid response was indicative of the higher stiffness in the upper corner windshield panel due to the constraint of the frame members.

Figures 4.13 and 4.14 present equivalent stress contours on the highest stressed surfaces of the structural and spall polycarbonate plies for the near-center birdstrike analysis at the increment of maximum stress in the structural ply. The highest polycarbonate stresses for the near-center shot were 5,000 psi for the structural ply located at the impact site, and 6,000 psi for the spall ply located four inches aft of the impact site. These stresses were well below yield for polycarbonate, indicating that the current production windshield panel successfully defeated a near-center impact by a 4-pound bird at 650 mi/hr with no permanent deformation.

Figures 4.15 and 4.16 show that the peak structural ply stresses for the upper corner impact occurred at the interface between the windshield and eyebrow frame, and that the magnitude was twice that for the near-center shot. It was apparent that the constraint due to the frame member caused concentration of the stresses at the edge of the windshield when the bird impacted near the edge. The maximum stress magnitude in

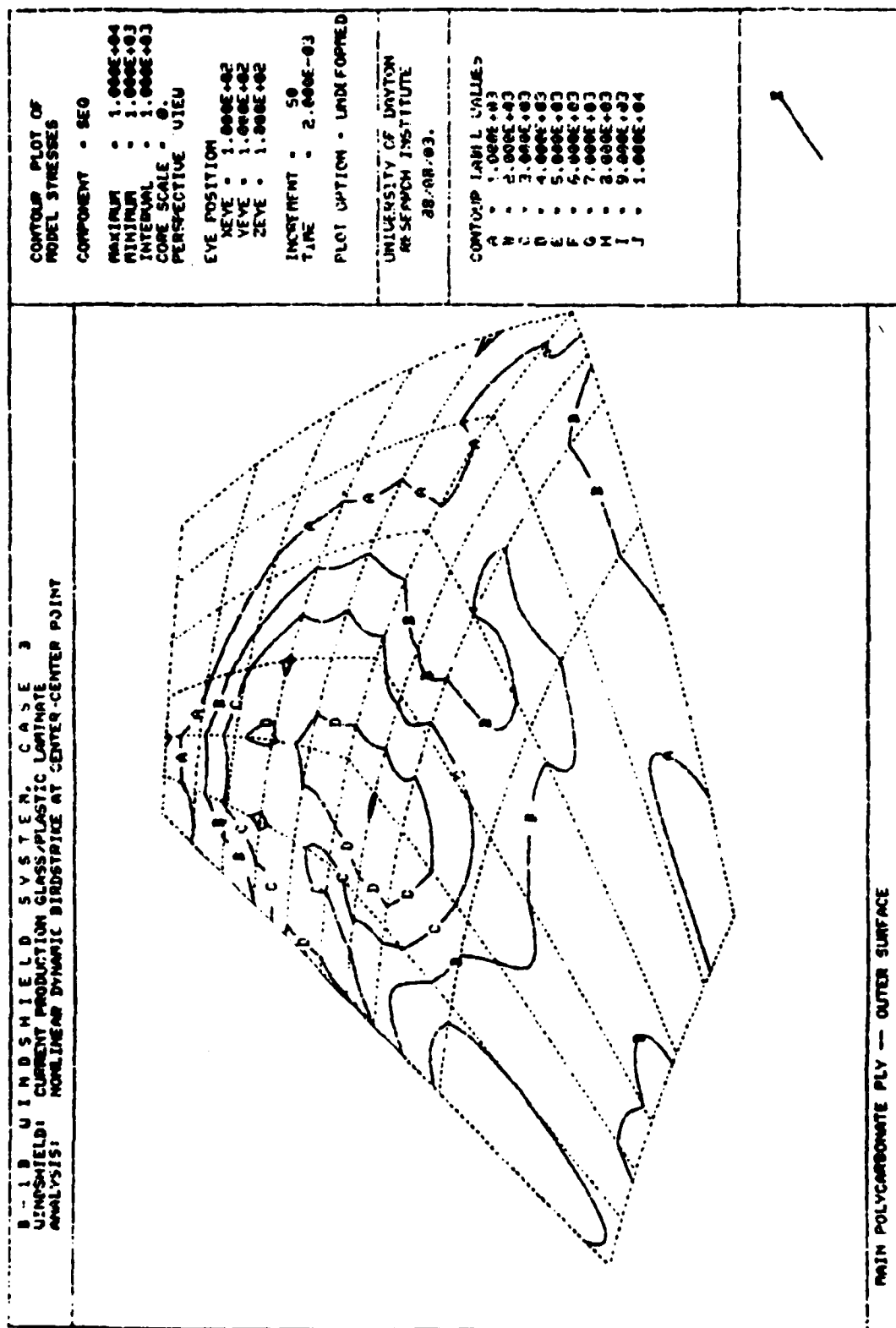


Figure 4.13. Equivalent Stress Contours on the Outer Surface of the Structural Ply, Case 3.

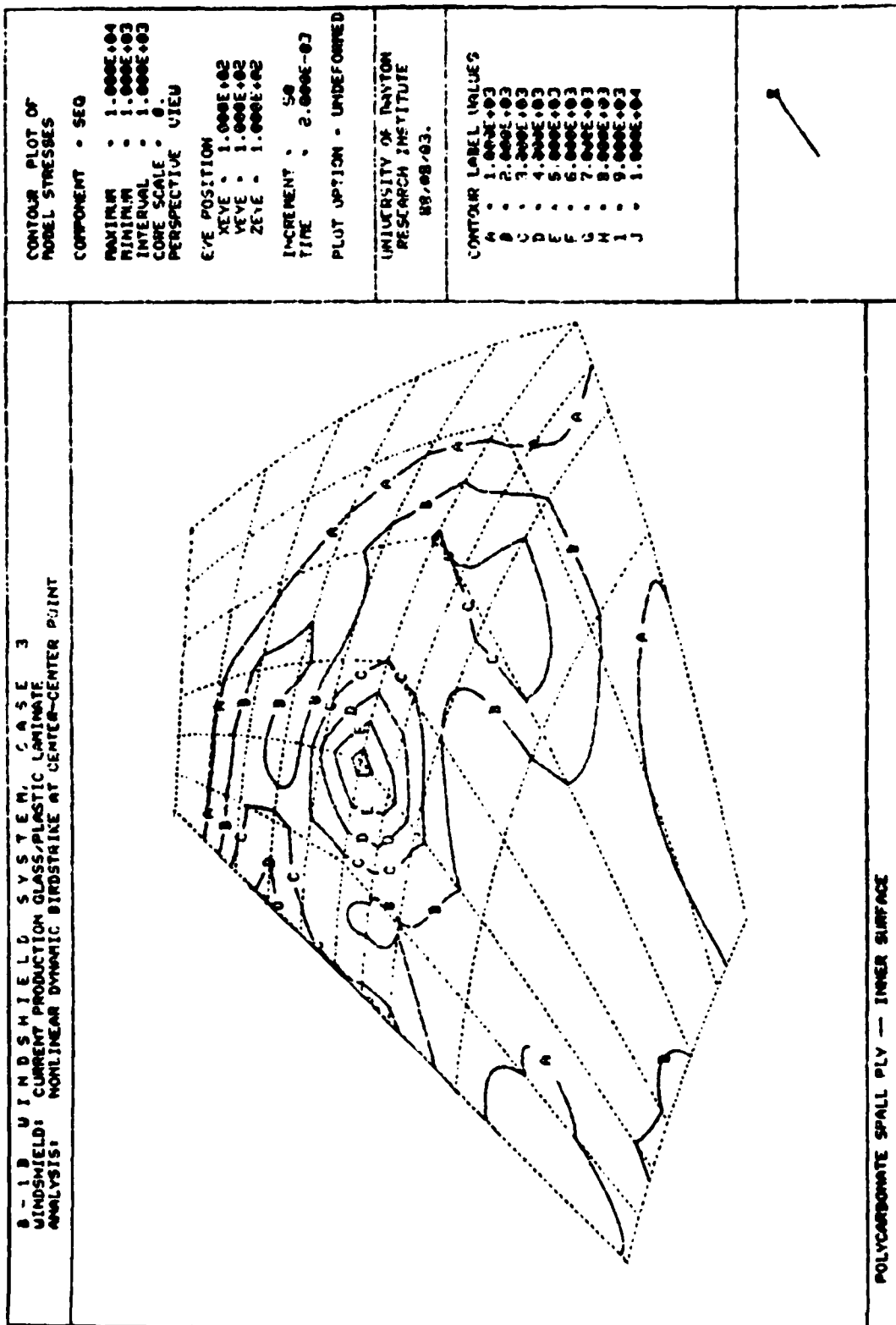


Figure 4.14. Equivalent Stress Contours on the Inner Surface of the Spall Ply, Case 3.

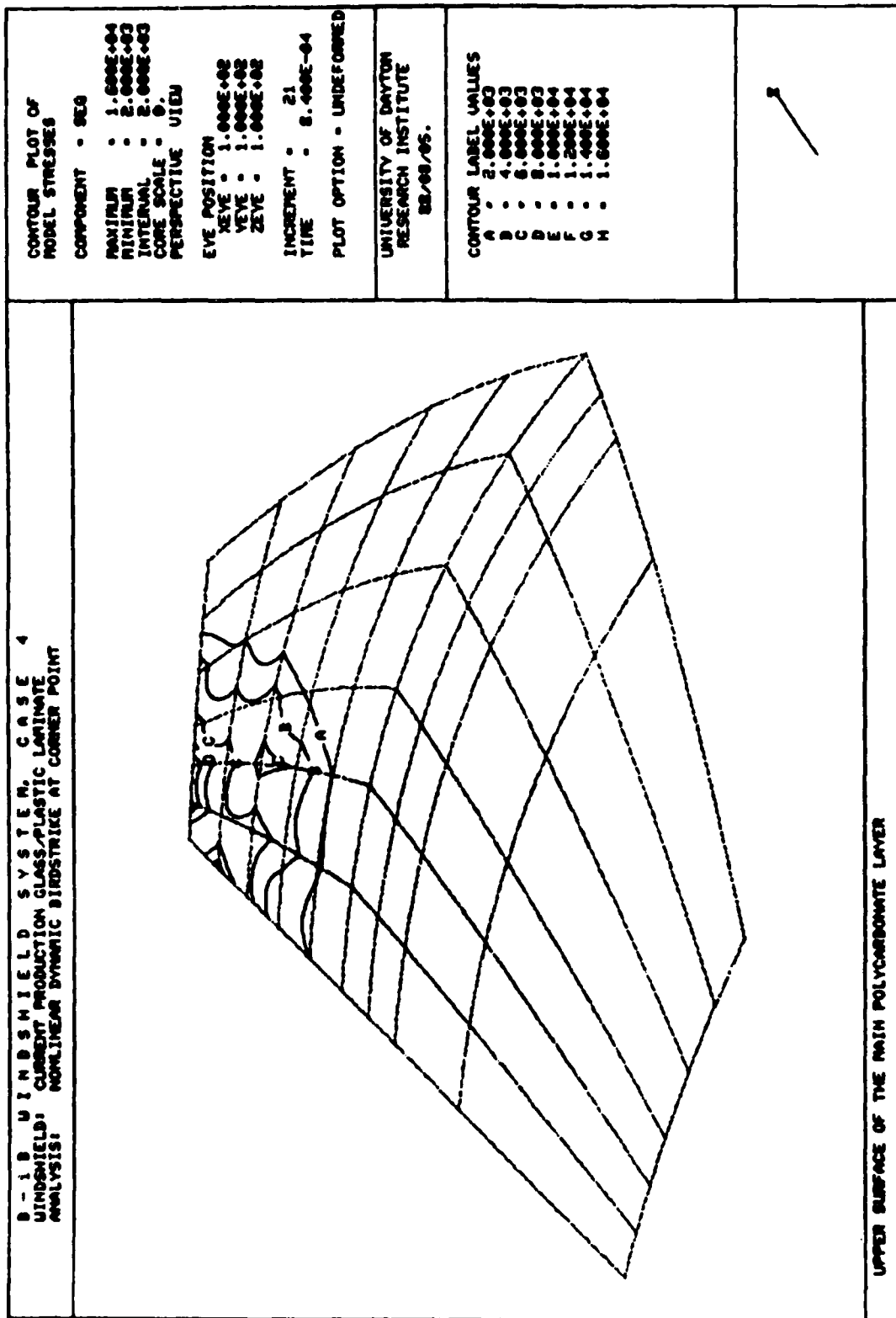


Figure 4.15. Equivalent Stress Contours on the Outer Surface of the Structural Ply, Case 4.

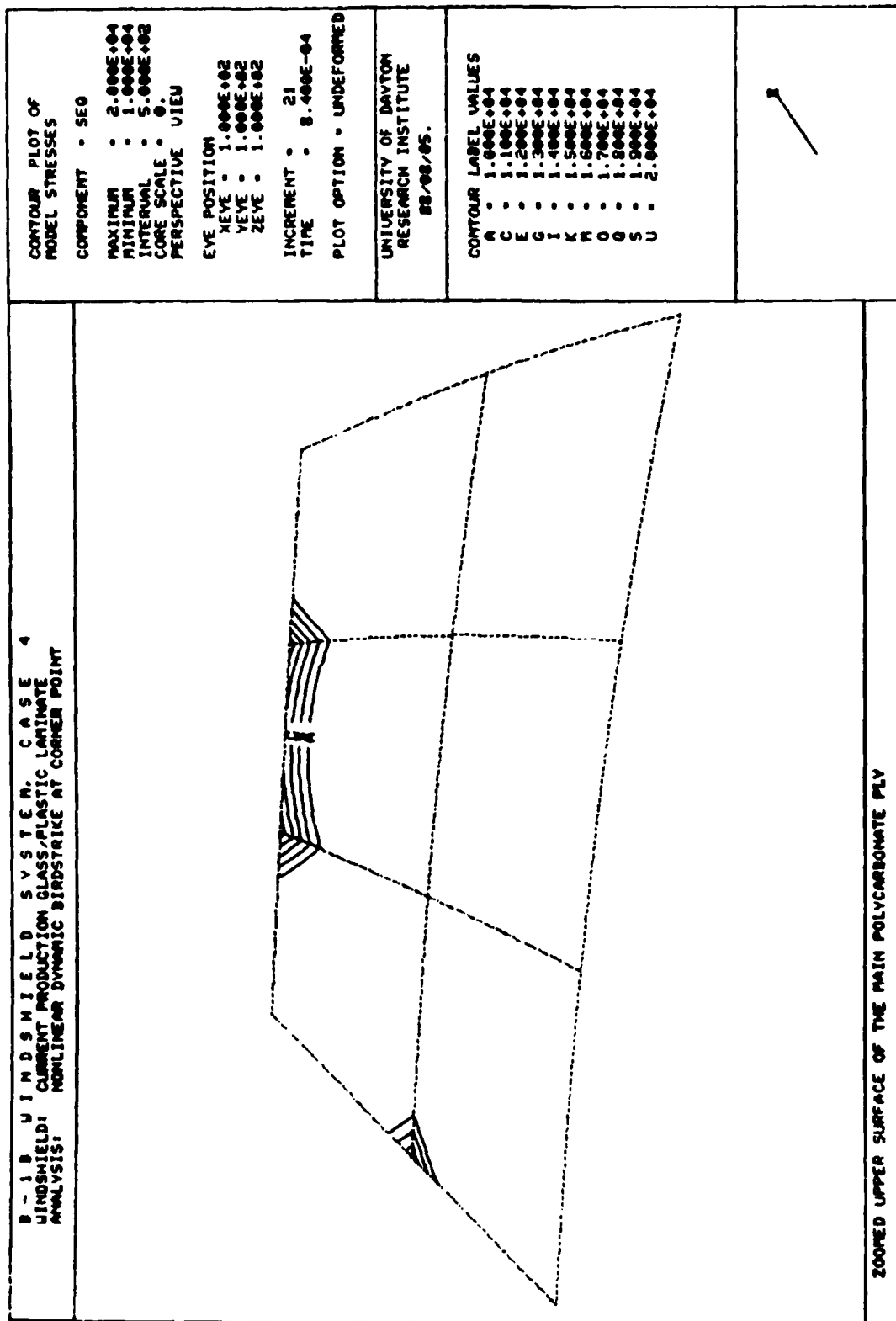


Figure 4.16. Close-up of High Stress Regions (Upper Aft Corner) on the Outer Surface of the Structural Ply, Case 4.

the structural ply was 12,000 psi, indicating that the polycarbonate had yielded. Figure 4.17 shows that the maximum equivalent strain in the structural ply due to upper-corner impact was 0.080 - 0.085 in/in (8.0% - 8.5% strain), exceeding the yield strain for polycarbonate of 3.38% (see Table 2.4). The fact that the structural polycarbonate ply yielded did not mean that the windshield was on the verge of failure. Polycarbonate exhibits high post-yield elongation to ultimate failure (115% - 125% plastic strain¹⁵), so that substantial yielding would occur prior to fracture. The contour plots therefore indicated that the current production windshield panel successfully defeated an upper corner impact by a 4-pound bird at 650 mi/hr without fracture and with little-to-no permanent deformation.

Figure 4.18 indicates that the stresses in the centerpost web were below yield for the near-center shot (12,000 - 20,000 psi). Again, stresses were artificially high at the forward-most edge due to linear constraints applied to nodes along this edge. Eyebrow stresses (Figure 4.20) were even lower, so that these frame members were sufficient to resist impact by a 4-pound bird striking the near-center impact location at 650 mi/hr.

Figures 4.19 and 4.21 present equivalent stress contours for the centerpost and eyebrow frames resulting from upper corner impact. The centerpost web stresses were significantly higher than those for the near-center impact, although the maximum stress was still below the yield point for 2024-T62 (40,000 psi computed versus 50,000 psi yield). The eyebrow stresses were very high, especially in the web between the lower and middle flanges (contour value of 70,000 psi). The yield and ultimate stresses for 7075-T73 were assigned values of 64,851 psi for the MAGNA model. The maximum integration point stresses in the web (elements 363 and 364) was 67,100 psi. Extrapolation of the integration point stresses to the nodes to obtain surface contour stress plots resulted in a maximum stress

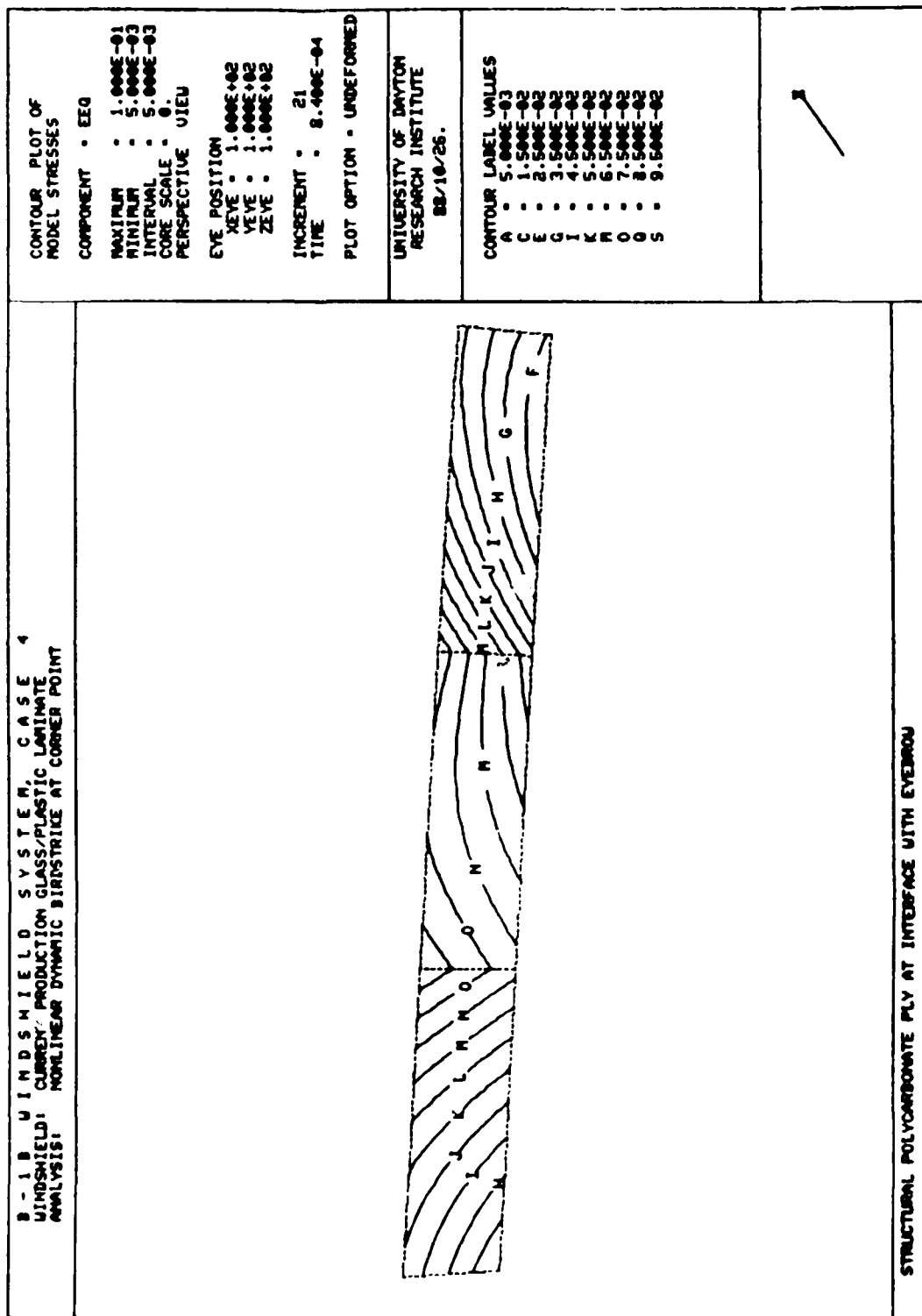


Figure 4.17. Equivalent Strain Contours Through the Thickness of the Structural Ply at the Upper Corner Windshield/Eyebrow Interface, Case 4.

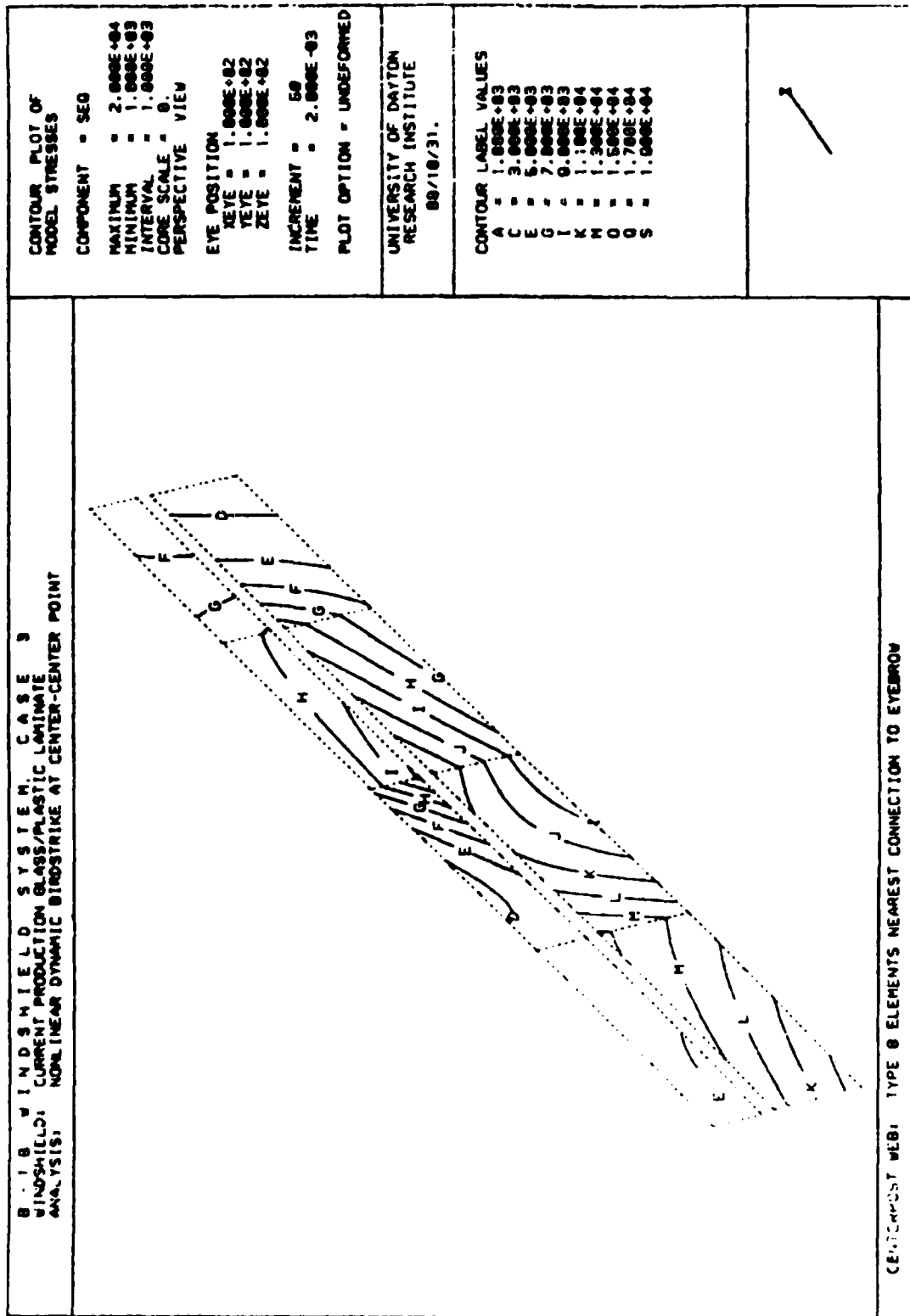


Figure 4.18. Equivalent Stress Contours on the Centerpost Web, Case 3.

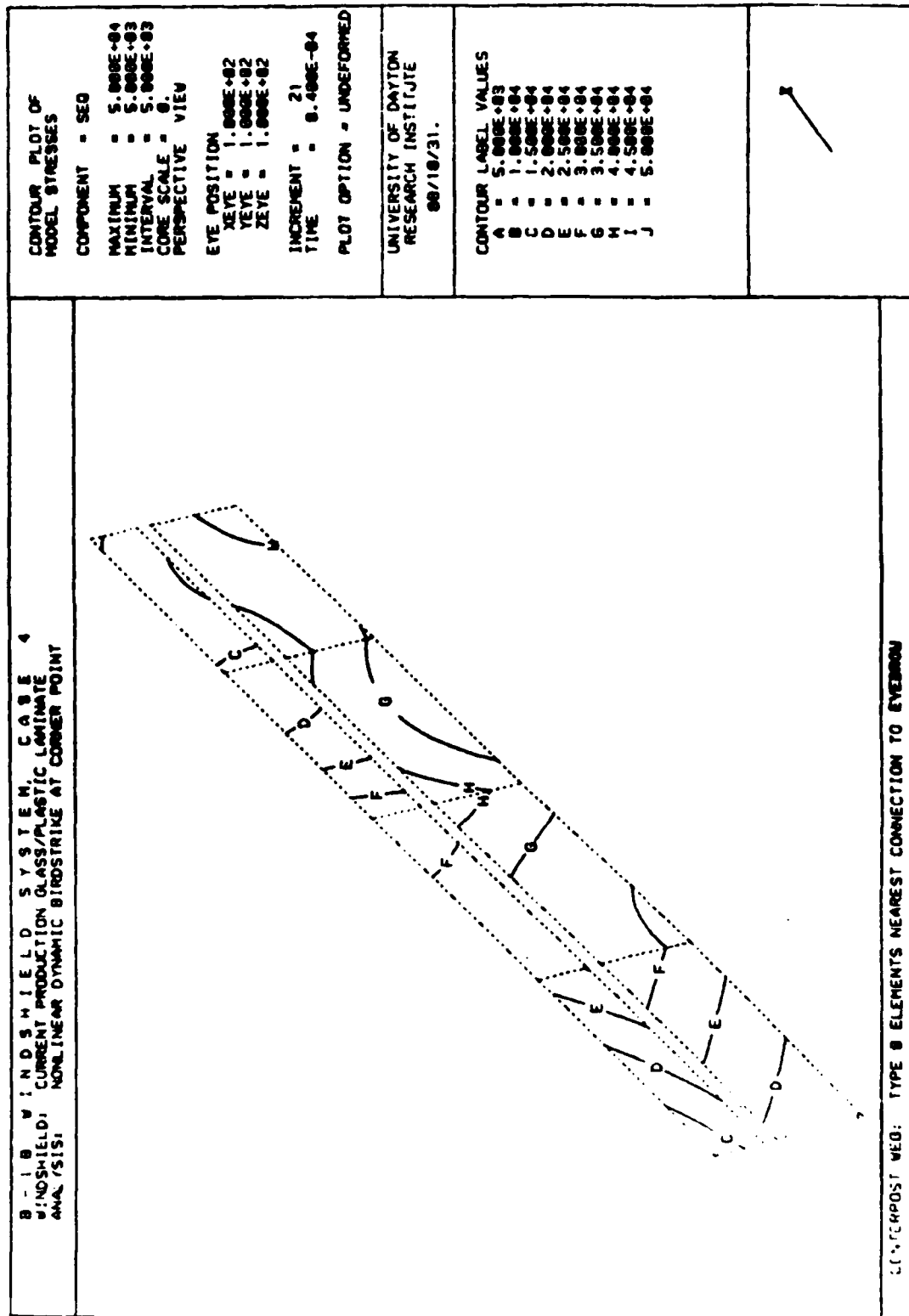


Figure 4.19. Equivalent Stress Contours on the Centerpost Web, Case 4.

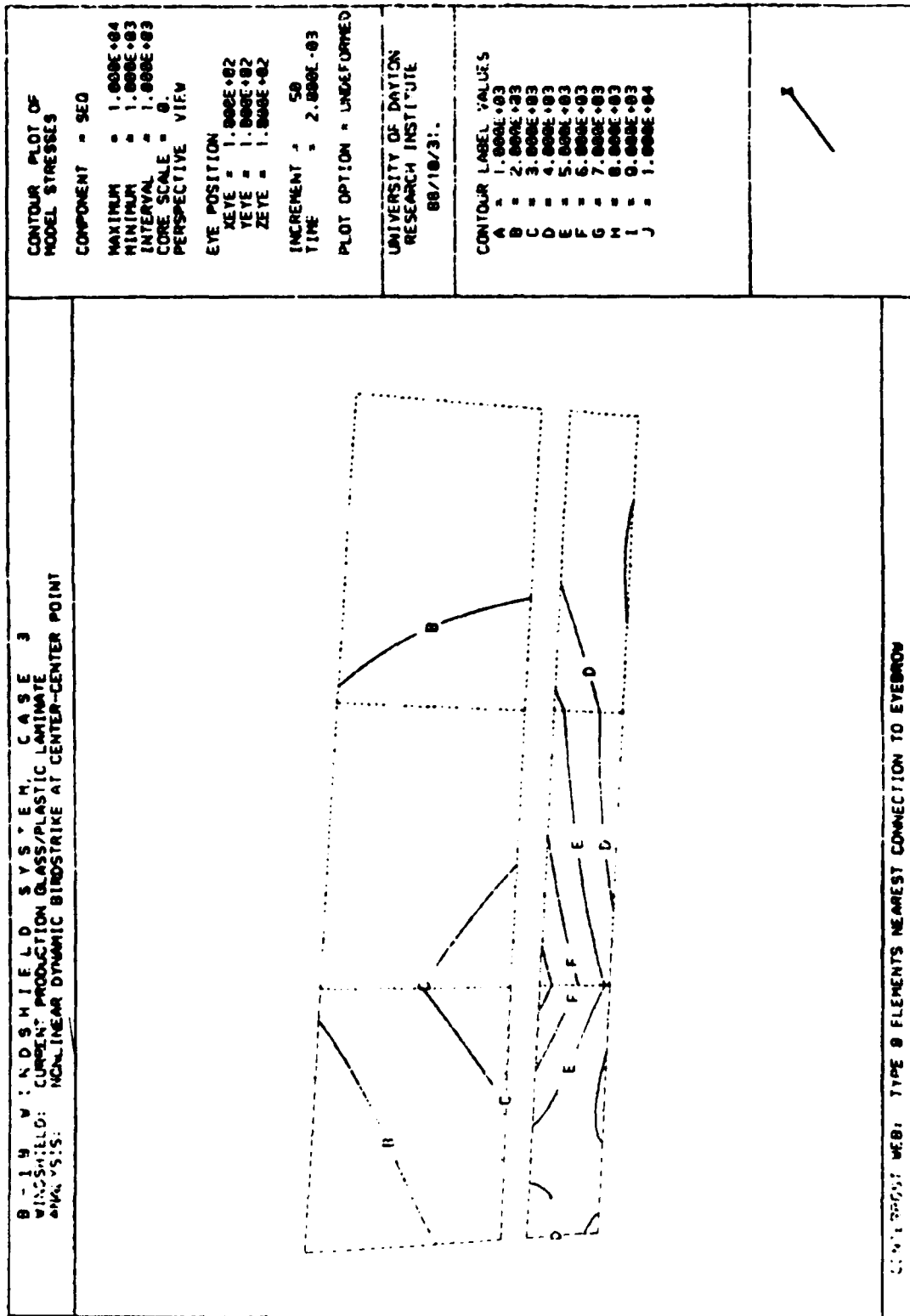


Figure 4.20. Equivalent Stress Contours on the Eyebrow Web, Case 3.

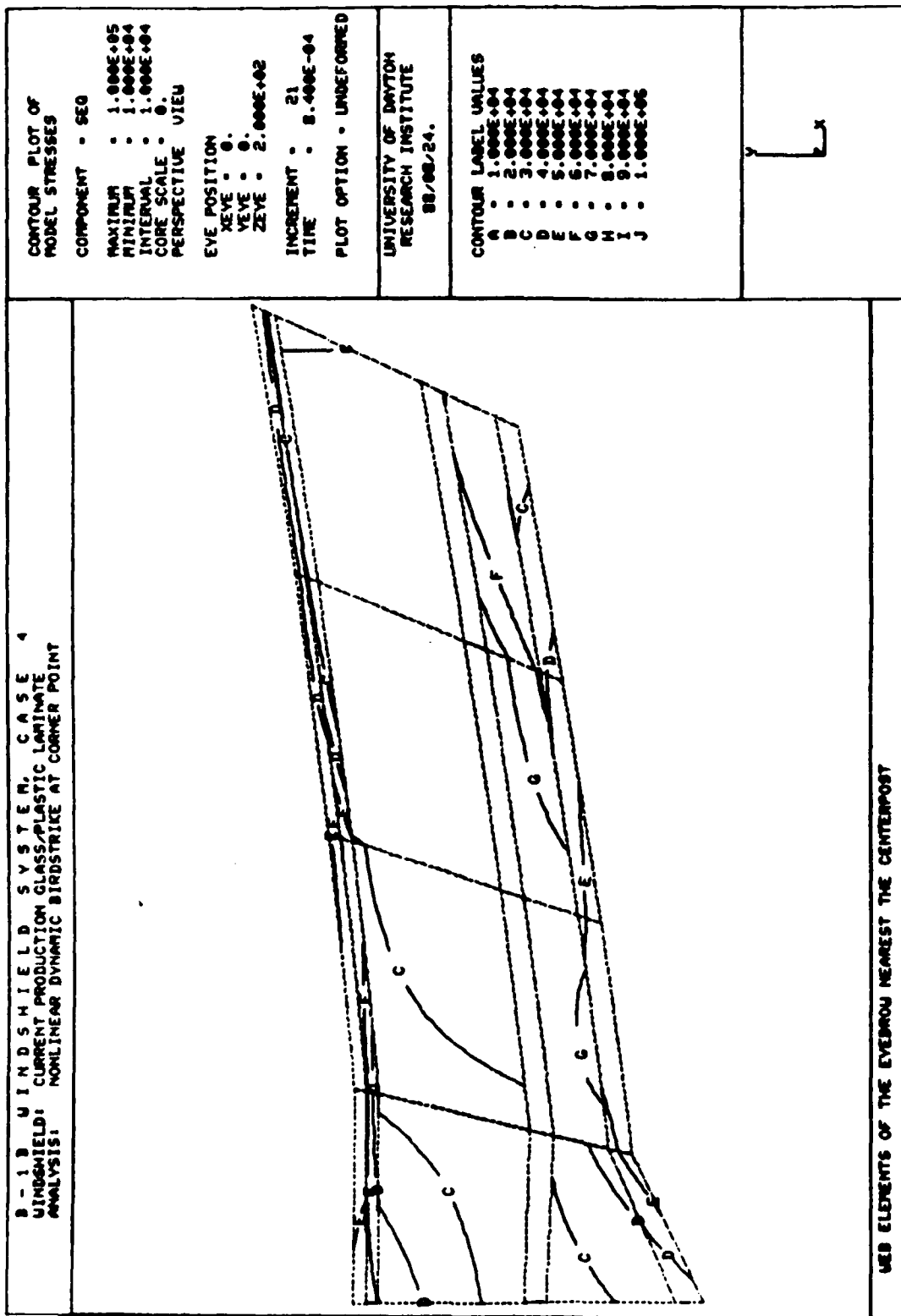


Figure 4.21. Equivalent Stress Contours on the Eyebrow Web, Case 4.

contour of 70,000 psi. These stresses were higher than the yield and ultimate stresses because the time step and strain subincrement used did not allow precise tracking of the stress-strain curve when it abruptly changed slopes from the elastic (slope equal to the modulus of 10×10^6 psi) to the perfectly plastic (slope of 0 psi) region. These stress values were therefore artificially high, making it impossible, without additional information, to determine whether the web was fractured or just permanently deformed.

The additional information needed was the equivalent strain corresponding to the equivalent stresses. Figure 4.22 presents these strains for the eyebrow web. The maximum equivalent strain was 0.035 in/in (3.5% strain). From MIL-HDBK-5D¹⁸, the ultimate elongation for a 7075-T73 die forging, such as the eyebrow frame, is 7% in the longitudinal direction and 3% in the transverse direction. (High strain rate data from Reference 24 and similar undocumented in-house data shows that the elongations for the various aluminum alloys tested in these programs were as great or greater than the elongations obtained from quasi-static tests. Therefore, it was reasonable to assume that the high strain rate elongations for the 7075-T73 eyebrow material, which was not tested in these programs, were at least equal to the low strain rate handbook values.) The difference in elongation is due to the formation of grains parallel to the longitudinal axis of the part due to the die forming process. The value of the analytical equivalent strain lies between the two allowable elongation values, indicating a marginal pass/fail condition in the eyebrow web. Additional comparison of individual stress and strain components with handbook allowables verified a marginal pass/fail condition in the eyebrow web near the connection to the centerpost.

It should be noted that this critical location was the same location where the B-1A eyebrow failed during birdstrike testing at the upper corner impact site.¹ However, due to the

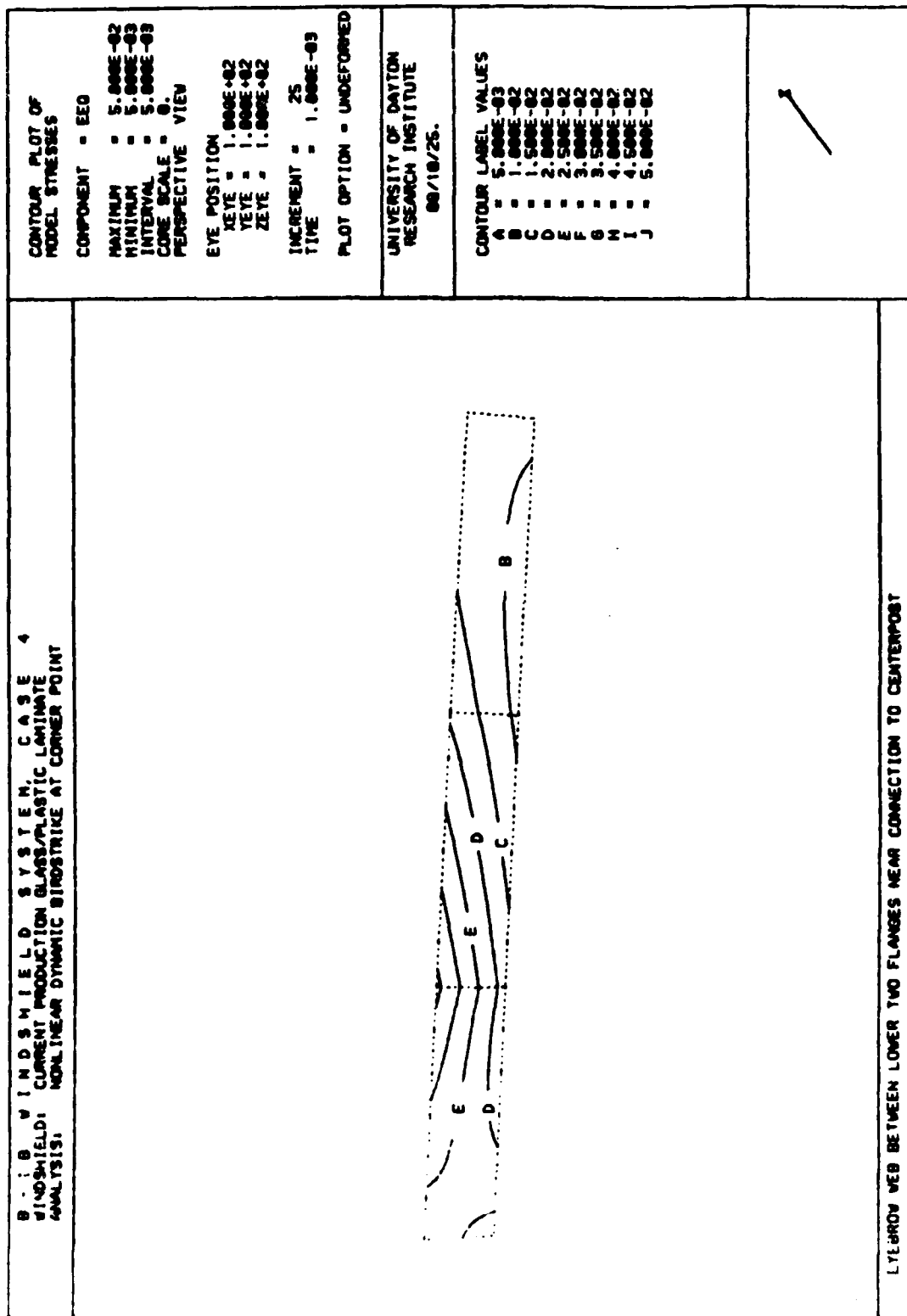


Figure 4.22. Equivalent Strain Contours on Lower Portion of Eyebrow Web, Case 4.

borderline pass/fail nature of the MAGNA results and the simplifications of the MAGNA model compared with the actual hardware, no definite conclusion can be drawn regarding whether or not the B-1B eyebrow will pass upper corner birdstrike without failure. The results do indicate that fracture of the eyebrow web is possible due to birdstrike in the upper corner of the windshield by a 4-pound bird impacting at 650 mi/hr.

Fastener load distribution curves for the baseline near-center impact (Case 3) and the baseline upper corner impact (Case 4) are presented in Figures 4.23 and 4.24, respectively. The loads for both birdstrike simulations were several times greater than those for the internal pressurization analysis of Case 2 (see Figure 4.6) which had the same geometry. The impact loads for the near-center impact dispersed widely over the transparency. The loads were carried predominantly by the fasteners along the centerpost and sill in shear and to a lesser extent by the fasteners of the forward arch in tension. In contrast, the loads resulting from the upper corner impact were highly localized near the centerpost-eyebrow connection (p=54) due to the high stiffness of the support structure in close proximity to this region.

The geometry and rigidity of the centerpost-eyebrow connection reduced the loads in the fasteners nearest the corner of the joint. This produced the double spike in the load distribution curves for Case 4. The double spike behavior was also evident in the contour plots of Figures 4.15 and 4.16. Note the high stresses in the polycarbonate on either side of the centerpost-eyebrow corner, but the relatively low stresses nearest the corner. Both baseline cases produced negative axial loads near the impact indicating that the fastener axial loads were directed inboard toward the crew enclosure.

Table 4.3 shows the critical axial and shear loads and the corresponding safety margins and interaction numbers for both baseline birdstrike studies. The fastener loads generated

B-1 B Case 3 Incr 50

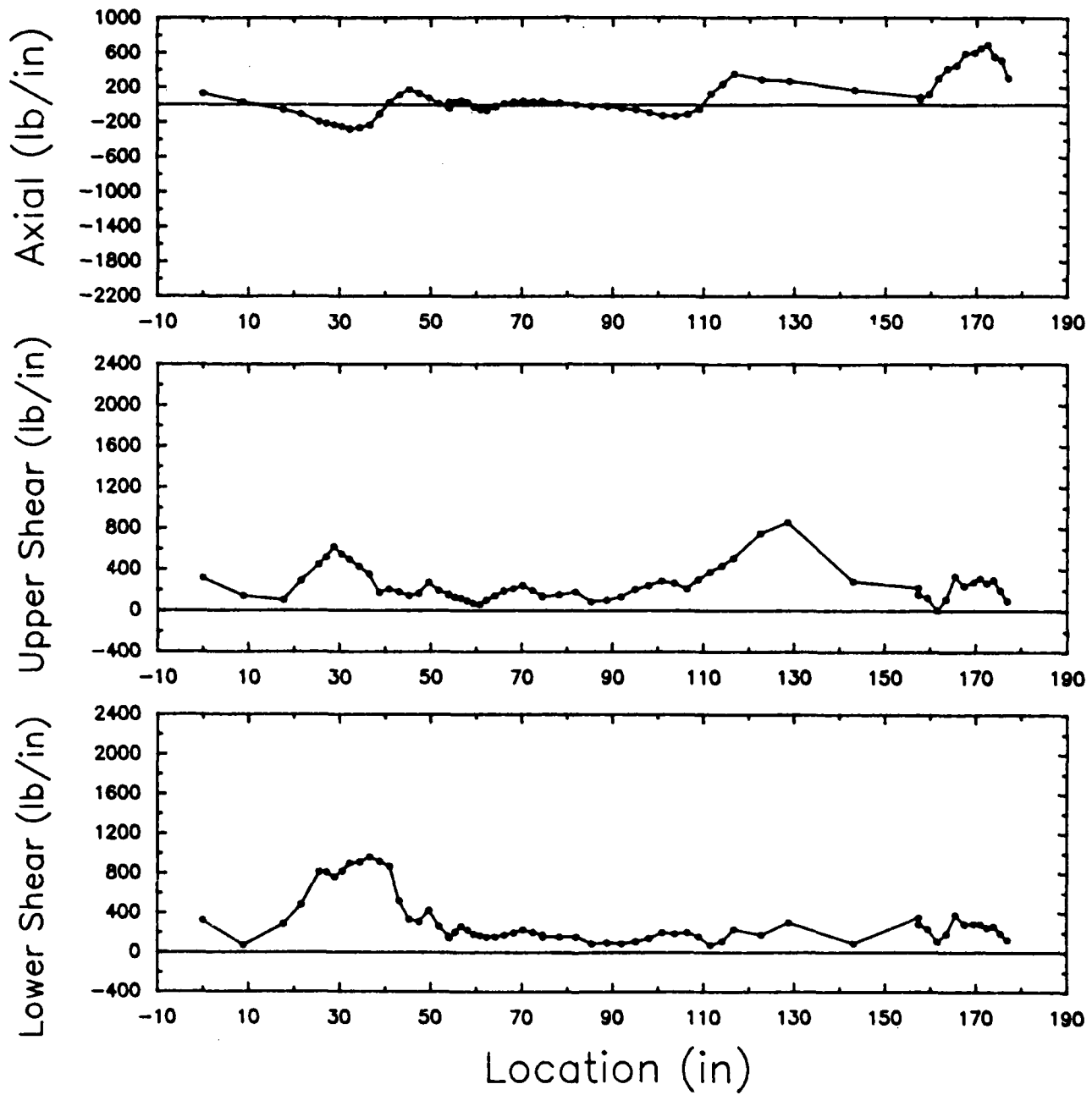


Figure 4.23. Fastener Load Distribution, Case 3.

B-1 B Case 4 Incr 21

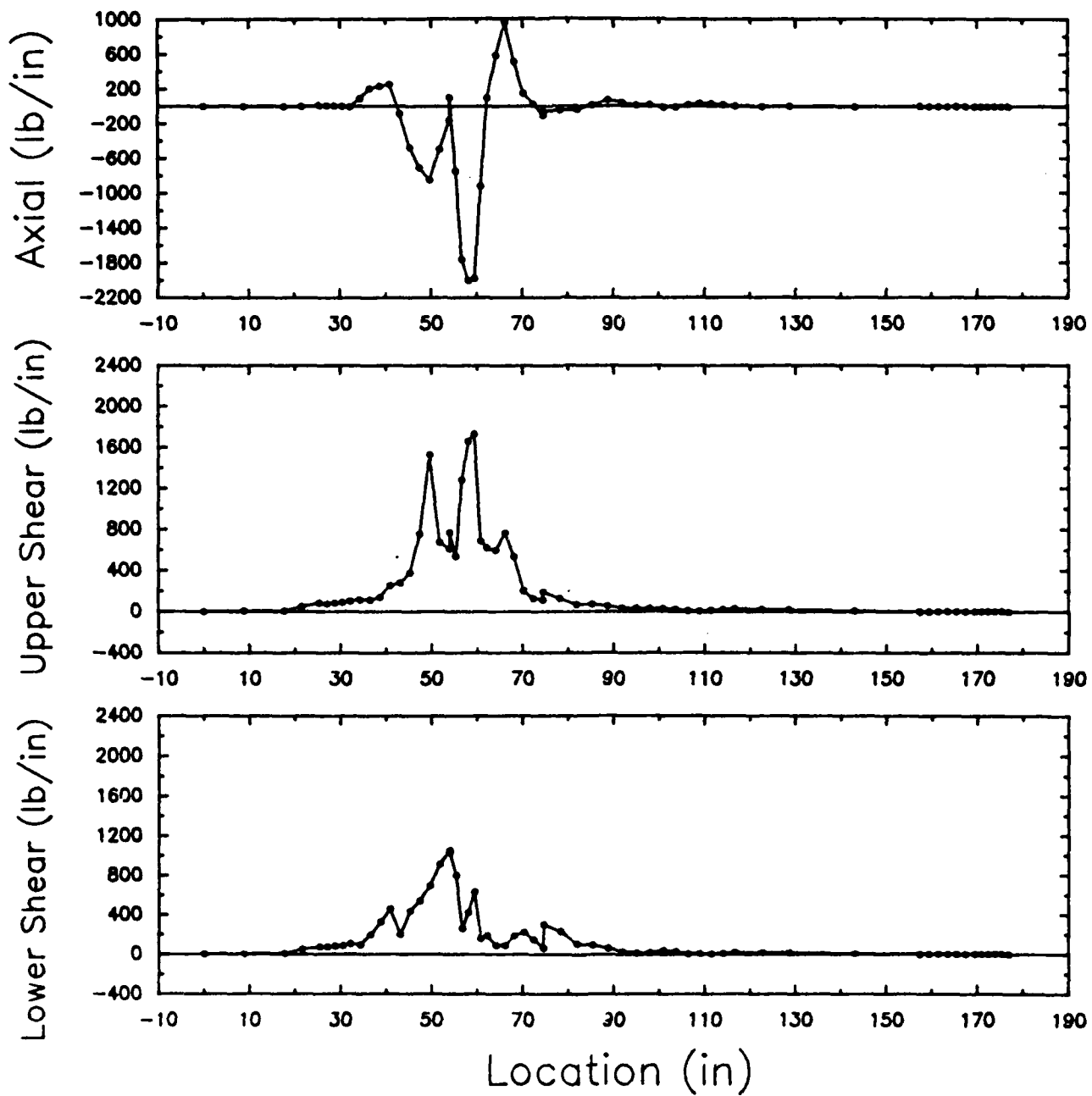


Figure 4.24. Fastener Load Distribution, Case 4.

TABLE 4.3

CRITICAL FASTENER LOADS AND SAFETY MARGINS FOR THE
BASELINE BIRDSTRIKE ANALYSIS

	Case 3	Case 4
Critical Loads		
Axial (lb/in)	700.	2010.
Upper Shear (lb/in)	860.	1740.
Lower Shear (lb/in)	970.	1060.
Safety Margins		
Fastener Tension	2.18	0.99
Fastener Shear	2.55	0.98
Transparency Bearing	3.72	1.63
Transparency Rupture	12.78	6.68
Safety Margins (50% Fastener Removal)		
Fastener Tension	0.59	-0.01
Fastener Shear	0.77	-0.01
Transparency Bearing	1.36	0.32
Transparency Rupture	15.14	8.00
Interaction Relation		
All Fasteners Present	0.12	0.38
50% Fastener Removal	0.57	2.05

Note: Safety margins < 0.0 indicate failure

Interaction relation values > 1.0 indicate failure

by the near-center impact were significantly lower than those for the upper corner impact. The minimum safety margin for fastener shear was 2.5 for Case 3, but only 0.98 for Case 4. Both were safe, but the higher stresses from the upper corner impact caused safety margins which were approximately one-half of those for the near-center impact. With every other fastener removed in the simulation, the near-center impact did not produce failure in the fasteners, but the upper corner impact did induce fastener failure adjacent to the impact area. These same trends are also indicated by the combined tension/shear interaction numbers.

In summary, the analyses indicated that the current-production windshield was capable of defeating a 4-pound bird impacting at the near-center site at 650 mi/hr. The analyses further indicated that bird impact at the upper corner location was more severe than impact at the near-center location, resulting in permanent deformation of the eyebrow frame (and possibly fracture in the eyebrow web) and the structural polycarbonate ply. Fastener margins of safety were reduced 50% compared with the near-center shot. The results of the fastener analysis showed that the fasteners of the current B-1B transparency design can withstand both near-center and upper corner impacts by a 4-pound bird at 650 mi/hr without failure. Removing every other bolt would lead to fastener failure adjacent to the impact location for upper corner impact. Removing every other bolt did not induce fastener failure for near-center impact.

4.4 Trade Study Birdstrike Results

As discussed in Section 4.3, the baseline birdstrike analyses indicated that the upper corner impact was more severe than the near-center impact in terms of the stresses applied to the windshield panel and the supporting frame members. For this reason, the upper corner impact site was used for all trade study analyses. No near-center birdstrike analyses were performed for the trade studies.

Figure 4.25 compares the displacement time histories at the same location for each trade study (node 1367 for Cases 5-7 and node 1793 for Case 9). This location was the maximum displacement location on the outer surface of the outermost structural polycarbonate ply of the windshield (see Figure 4.26). The baseline (Case 4) curve for the same location is included for comparison. The changes in displacement due to the changes in windshield configuration followed expected trends. For Case 5 and Case 6, a stiffer ply material was substituted for a more flexible baseline ply material, resulting in a stiffer windshield panel. The peak deflections therefore decreased compared to baseline, with Case 5 decreasing most (twelve percent decrease due to using acrylic instead of shattered glass, which had negligible stiffness), followed by Case 6 (seven percent due to substituting urethane for silicone). Cases 7 and 9 were more flexible than the baseline configuration, resulting in increased peak displacement. Case 7 and Case 9 resulted, respectively, in deflection increases of twelve and twenty-nine percent due to eliminating the spall ply (Case 7) and splitting the polycarbonate ply (Case 9). As Figure 4.25 demonstrates, the Case 9 change to the polycarbonate ply had the greatest effect on windshield displacement, significantly increasing the deflection and shortening the time to peak displacement. The deflection increases were due to the use of low strain rate properties for the interlayers, so that the actual change in windshield stiffness was not realized for Case 9. Deflections for all cases were relatively small, however, presenting no danger to the pilot and co-pilot.

Figures 4.27 - 4.34 present equivalent stress contours on the upper outer surface of the structural polycarbonate ply (upper surface of the upper (outer) polycarbonate ply for Case 9), which was the highest stressed windshield surface for the upper corner impact trade studies. The corresponding baseline stress contour plots are presented in Figures 4.15 and 4.16. The trade study contours were very

B-1 B Windshield Displacement Time History Trade Study

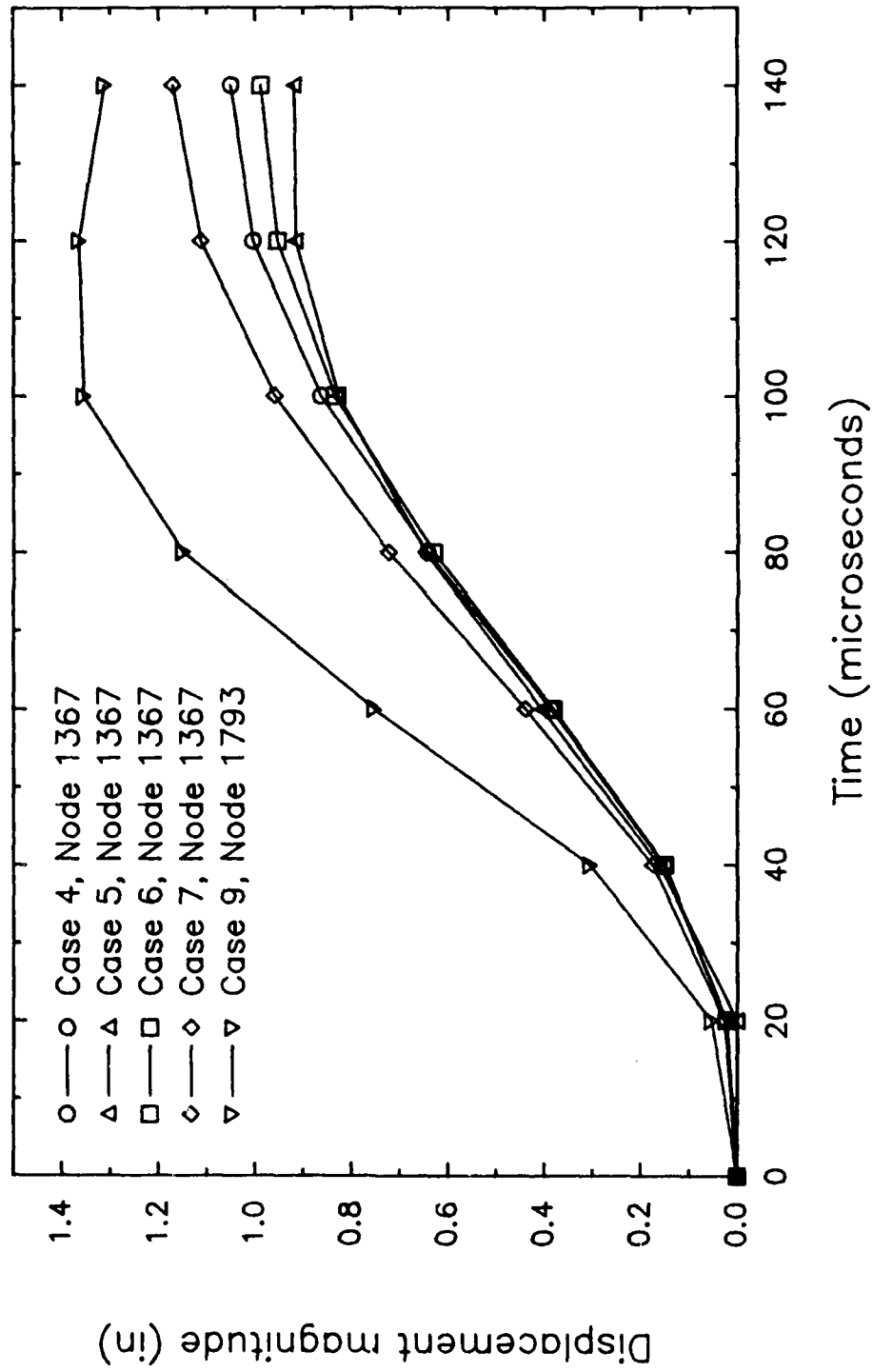


Figure 4.25. Displacement Time Histories, Cases 4, 5, 6, 7, and 9.

B = Upper Corner Impact Location
 C = Node Having Maximum
 Displacement
 (Node 1367 for Cases 4-7,
 Node 1793 for Case 9)

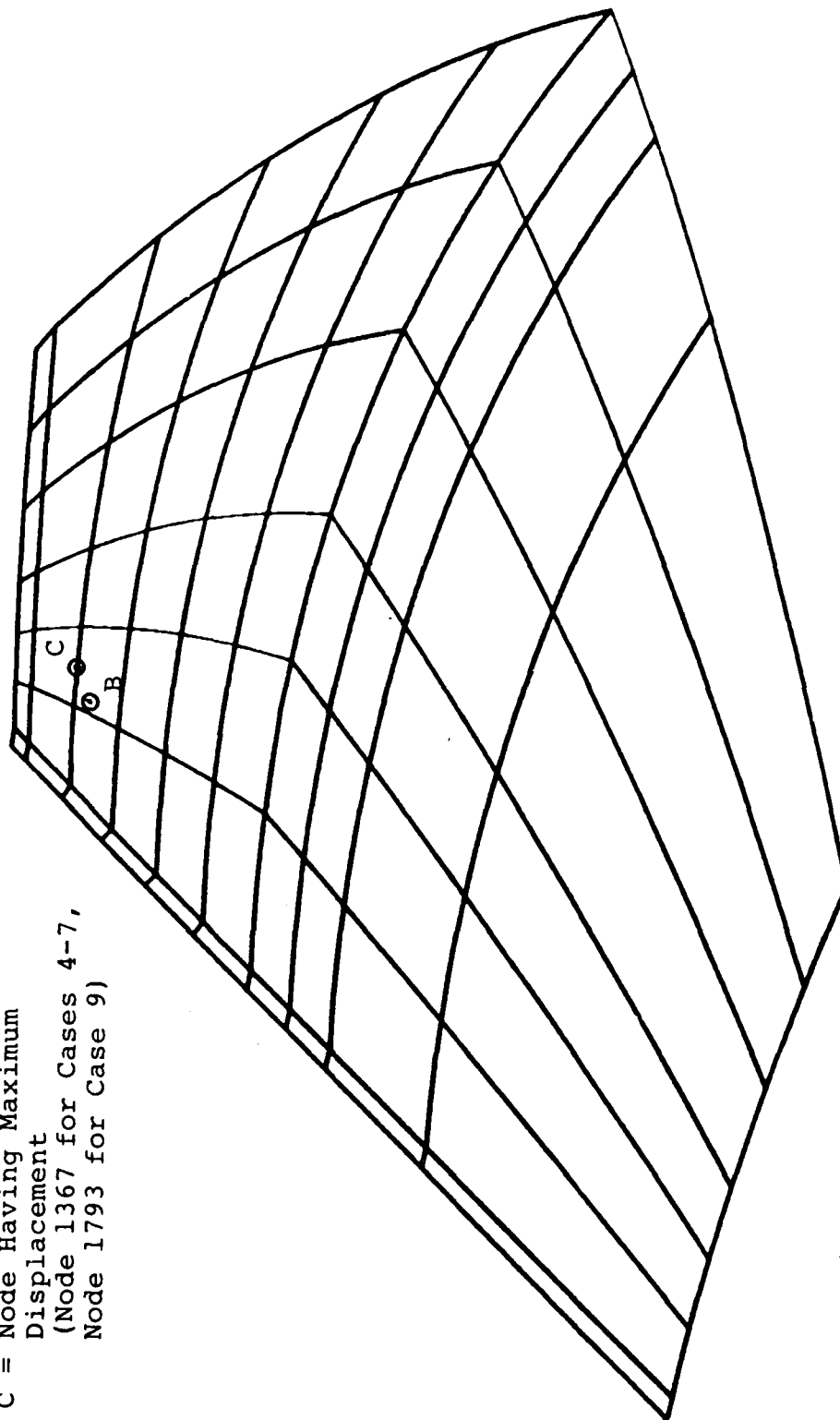


Figure 4.26. Location of Node Having Maximum Displacement Relative to Upper Surface
 of the Structural Polycarbonate Ply, Cases 4-7, 9.

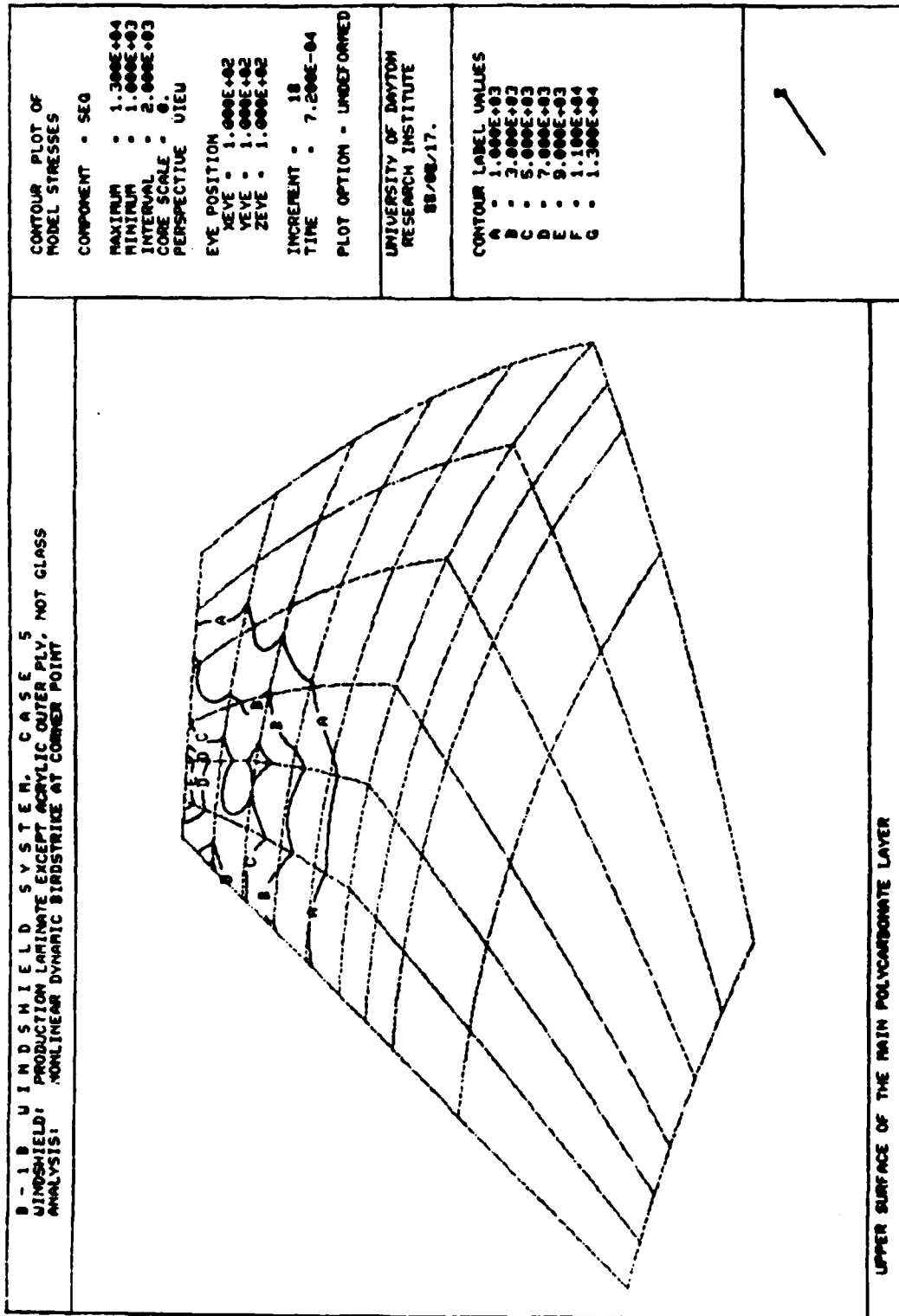


Figure 4.27. Equivalent Stress Contours on the Outer Surface of the Structural Ply, Case 5.

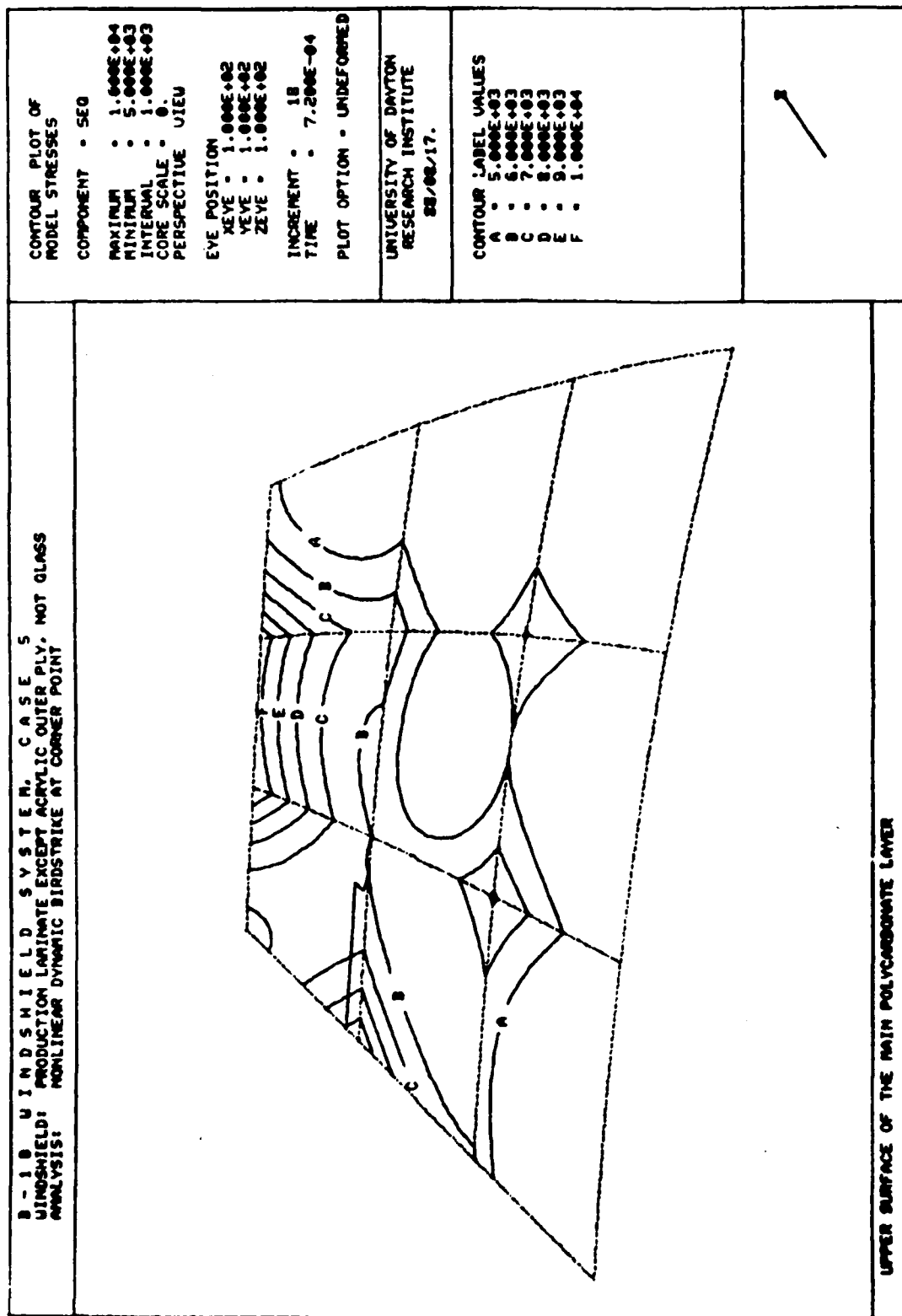


Figure 4.28. Close-up of Maximum Stress Region on the Outer Surface of the Structural Ply, Case 5.

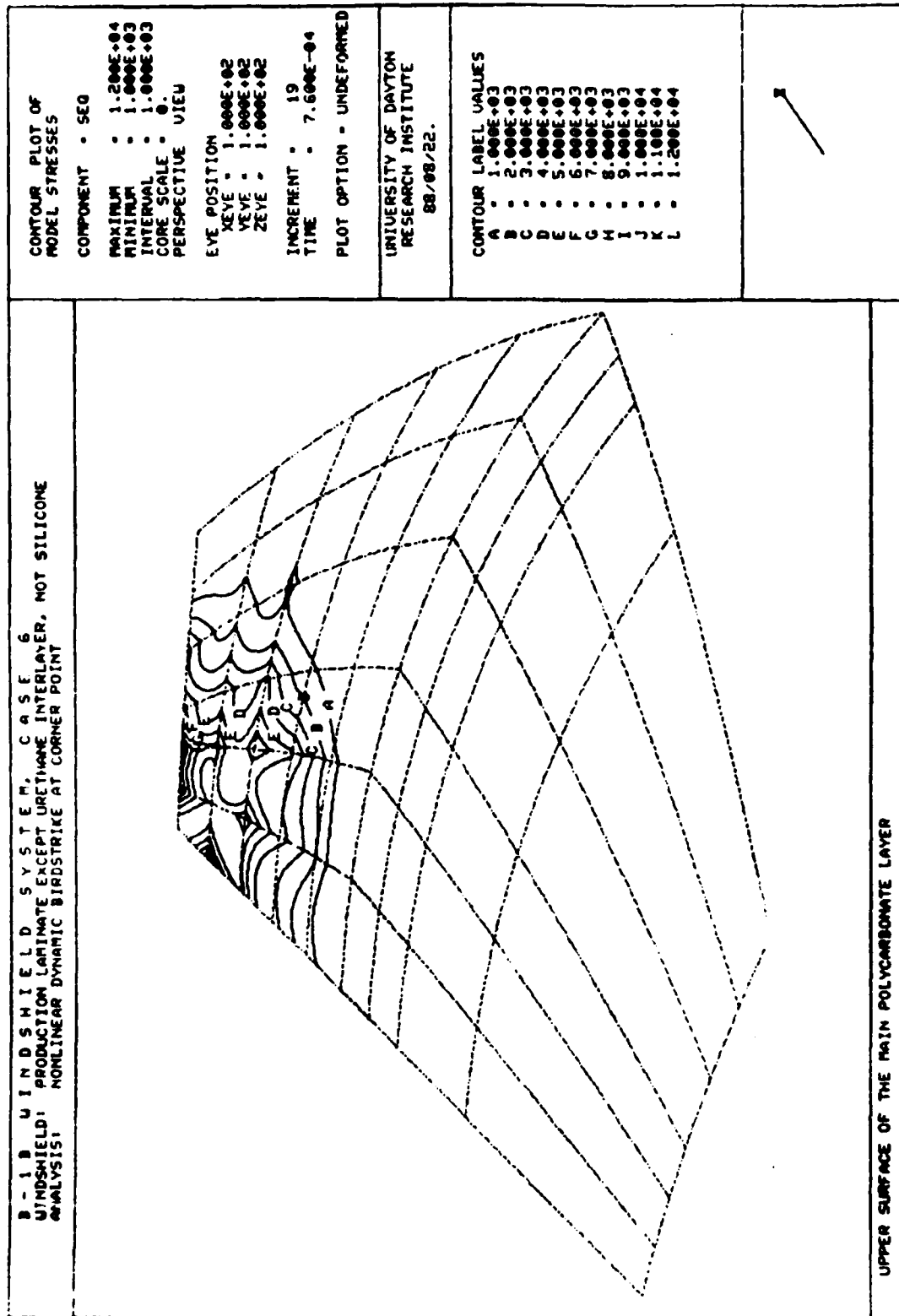


Figure 4.29. Equivalent Stress Contours on the Outer Surface of the Structural Ply, Case 6.

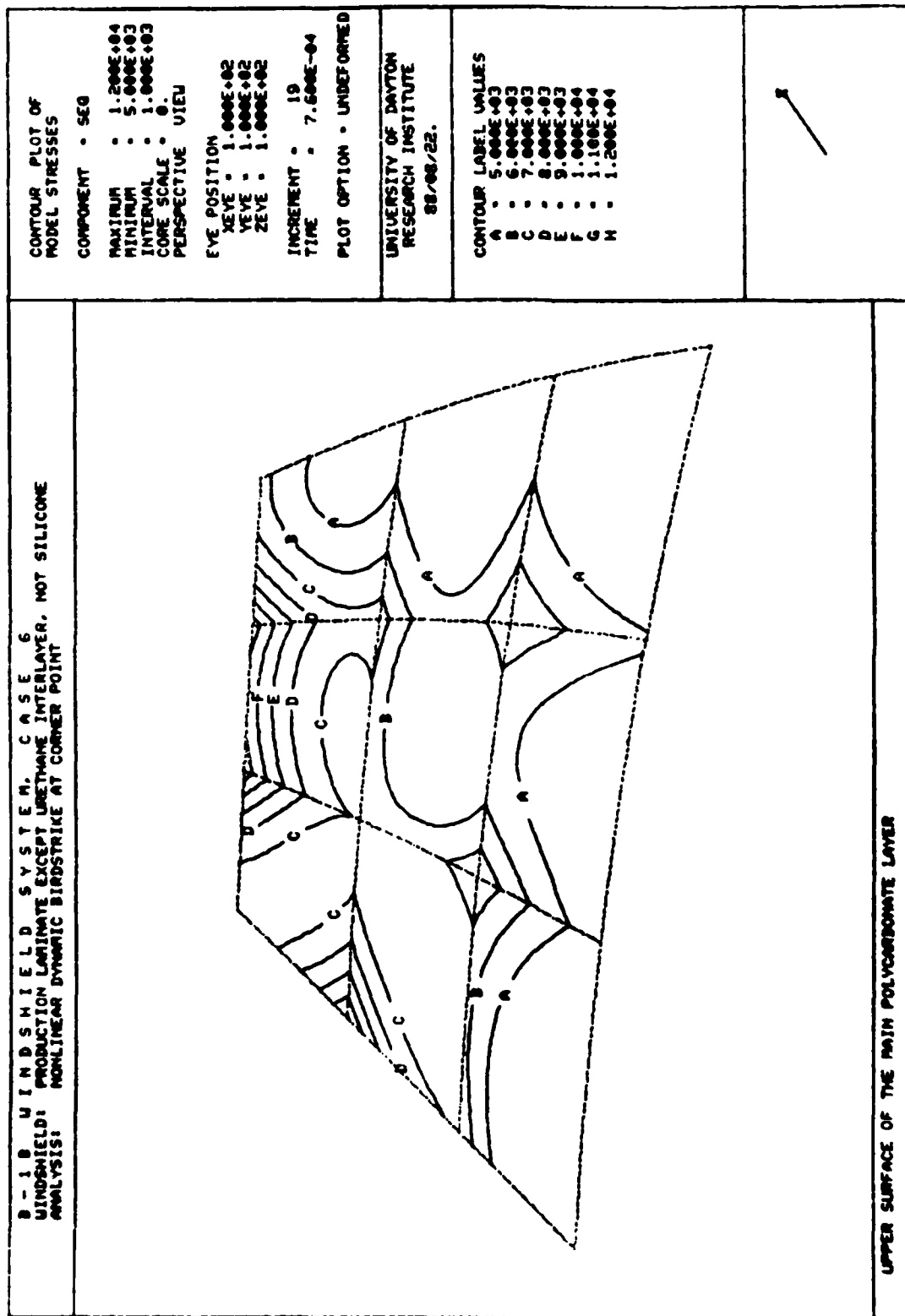


Figure 4.30. Close-up of Maximum Stress Region on the Outer Surface of the Structural Ply, Case 6.

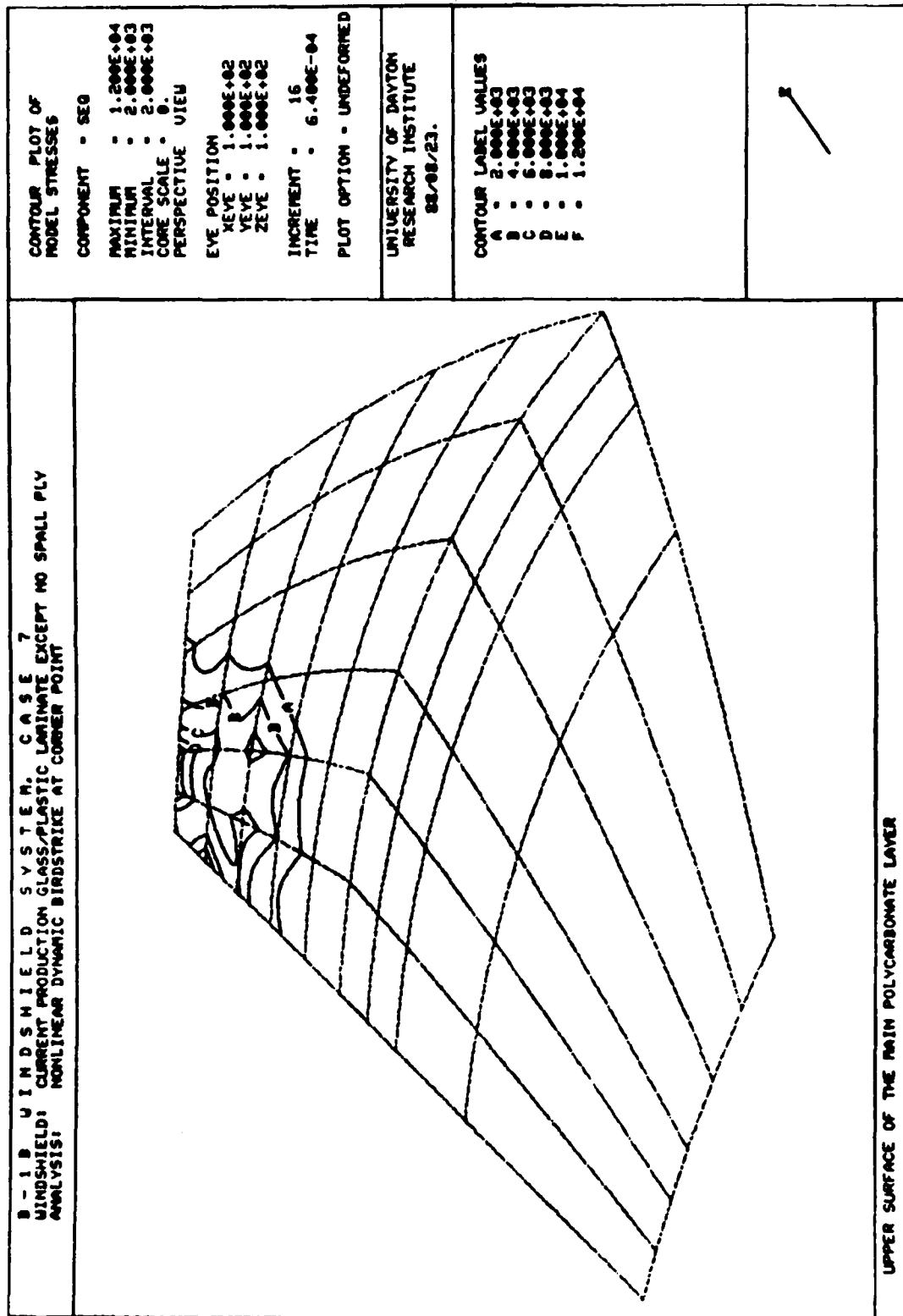


Figure 4.31. Equivalent Stress Contours on the Outer Surface of the Structural Ply, Case 7.

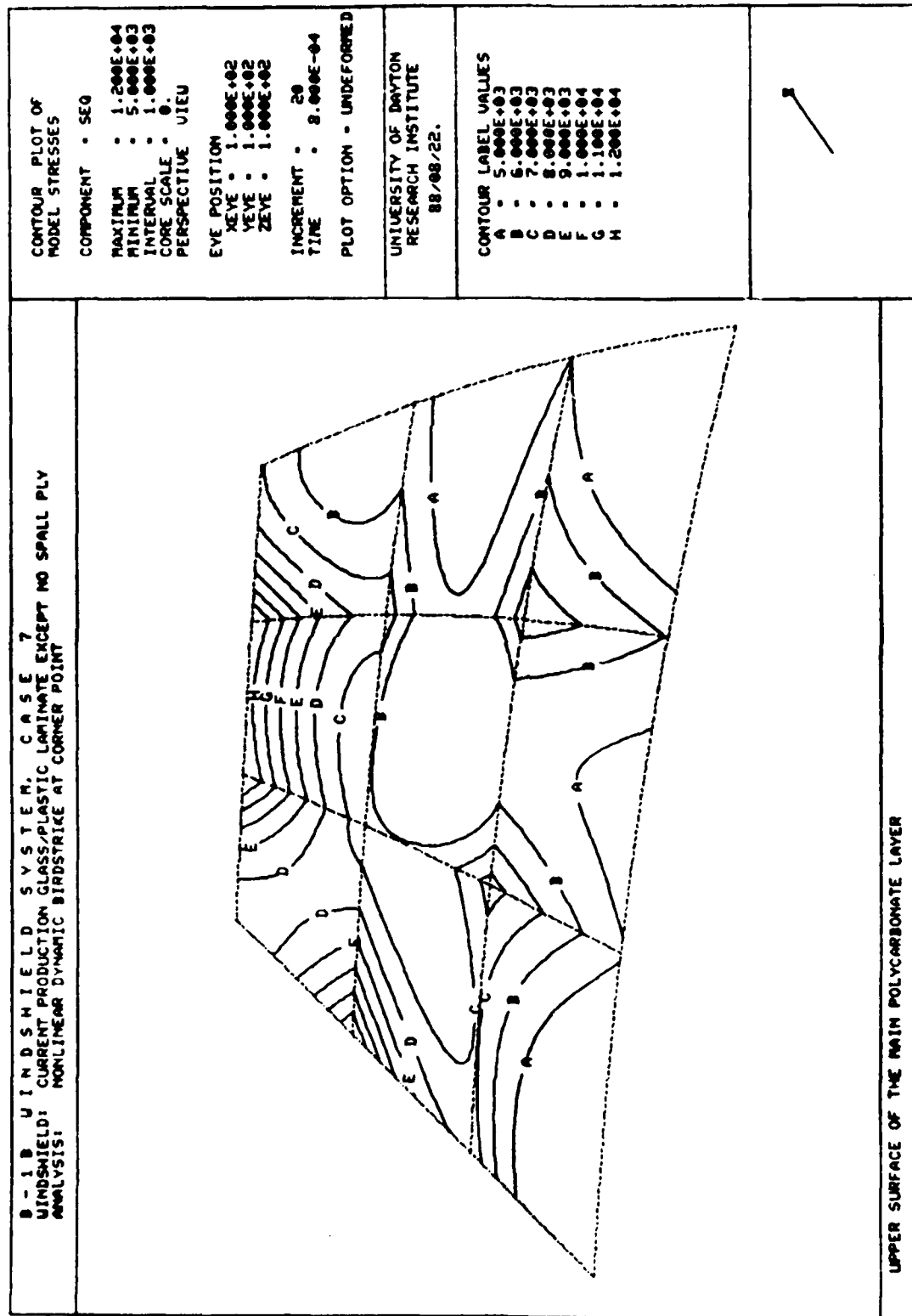


Figure 4.32. Close-up of the Maximum Stress Region on the Outer Surface of the Structural Ply, Case 7.

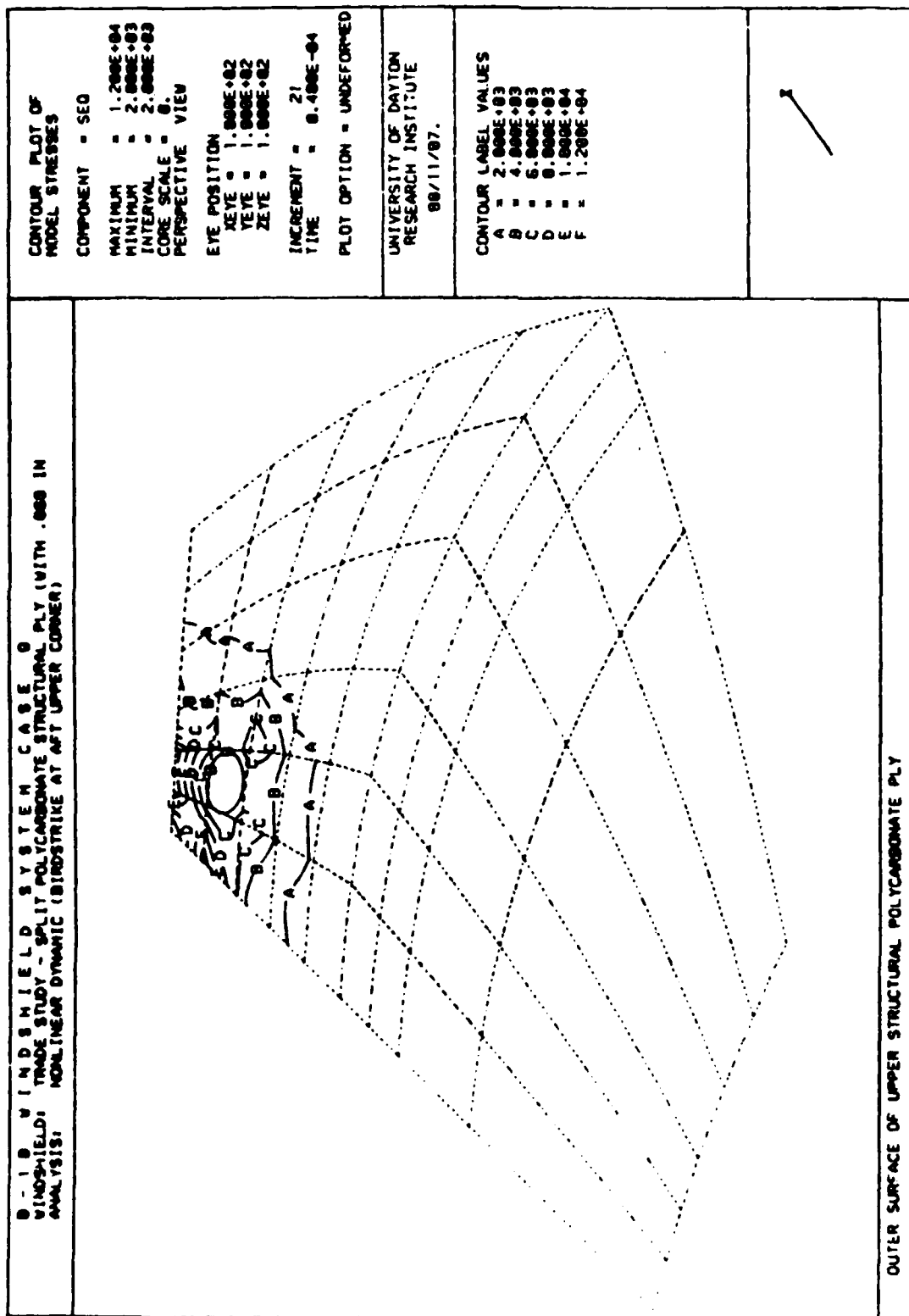


Figure 4.33. Equivalent Stress Contours on the Outer Surface of the Upper Surface Ply, Case 9.

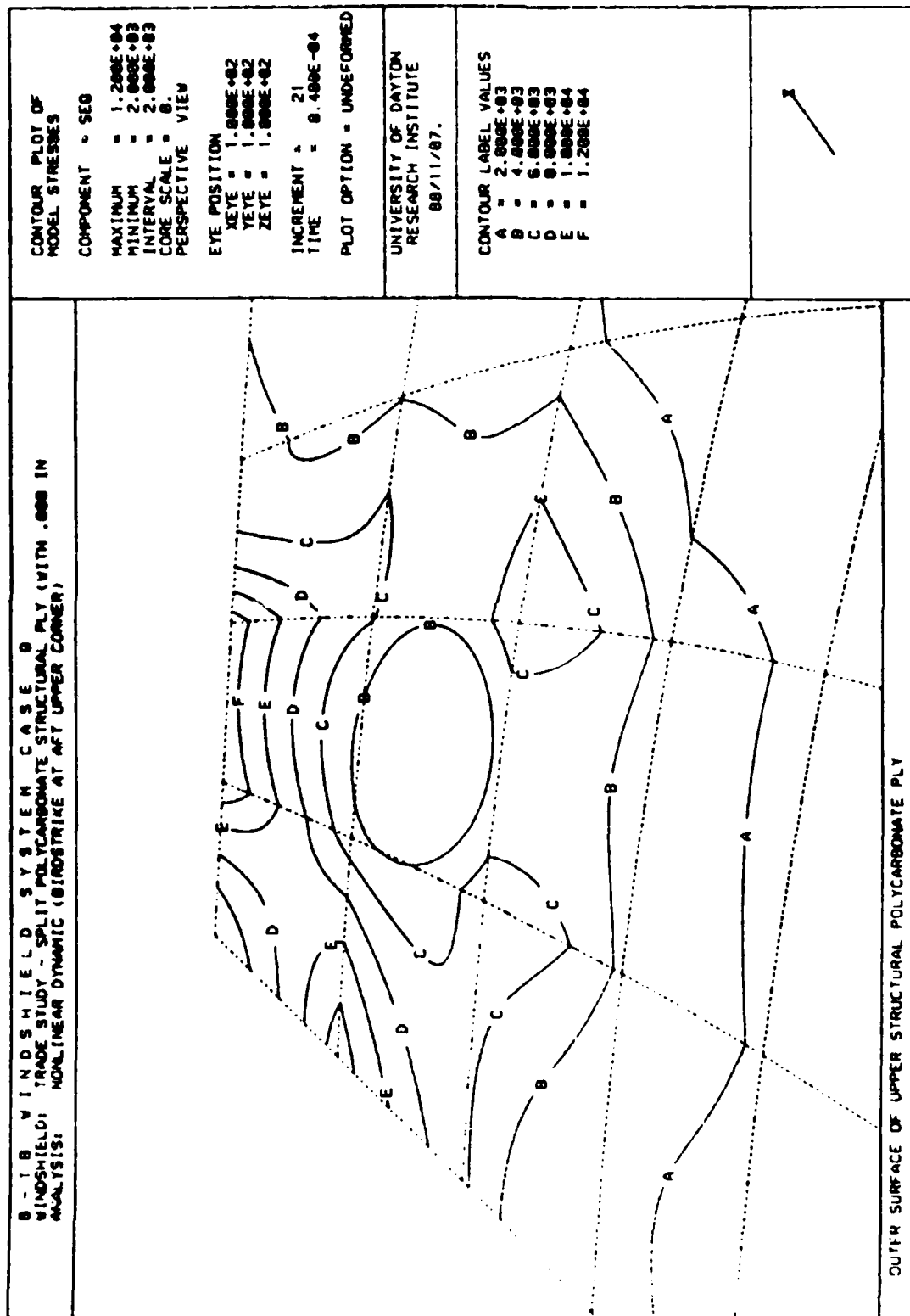


Figure 4.34. Close-up of the Maximum Stress Region on the Outer Surface of the Upper Structural Ply, Case 9.

similar to the baseline contours, showing high stresses at the windshield-eyebrow and windshield-centerpost interfaces. The contours in these regions had values of 12,000 psi, indicating that yielding of the structural polycarbonate ply has occurred. The yielded zone was larger at the eyebrow interface than at the centerpost interface, implying that the eyebrow-windshield interface was the highest stressed location on the windshield panel for the upper corner impact. Figures 4.35 - 4.38 present the equivalent strains in this region for the trade study birdstrike cases. Maximum equivalent strains were 0.075 in/in for Cases 5 and 6, 0.090 in/in for Case 7, and 0.16 in/in for Case 9, well below the strain to failure for polycarbonate (1.15 - 1.25 in/in). Maximum equivalent strain for the baseline case (Case 4 - see Figure 4.17) was 0.080 in/in. The structural polycarbonate plies therefore yielded similar to the current production configuration structural ply, but did not fracture.

Review of the output data showed that the highest stresses in the support structure occurred in the eyebrow web near the connection to the centerpost. This was true for all trade study cases as well as the baseline case. Figures 4.39 - 4.42 present the trade study eyebrow stress contours while Figure 4.20 presents the baseline contours. As was the case for the baseline upper corner impact analysis, the region of highest stresses was located in the eyebrow web between the lower, forward-facing flange and the aft-facing flange (see Figure 2.4 for the location of these flanges), with values of up to 70,000 psi. Stresses of this magnitude also occurred in the flanges at the connection with the centerpost flanges, although the extent of the highest stress region in the flanges was smaller than that of the web. Note that the reported stresses exceeded the ultimate stress of the 7075-T73 aluminum alloy, a physically impossible situation. As discussed in Section 4.3, the stresses were artificially high, and should have been equal to the yield/ultimate stress value (the same value of stress was used

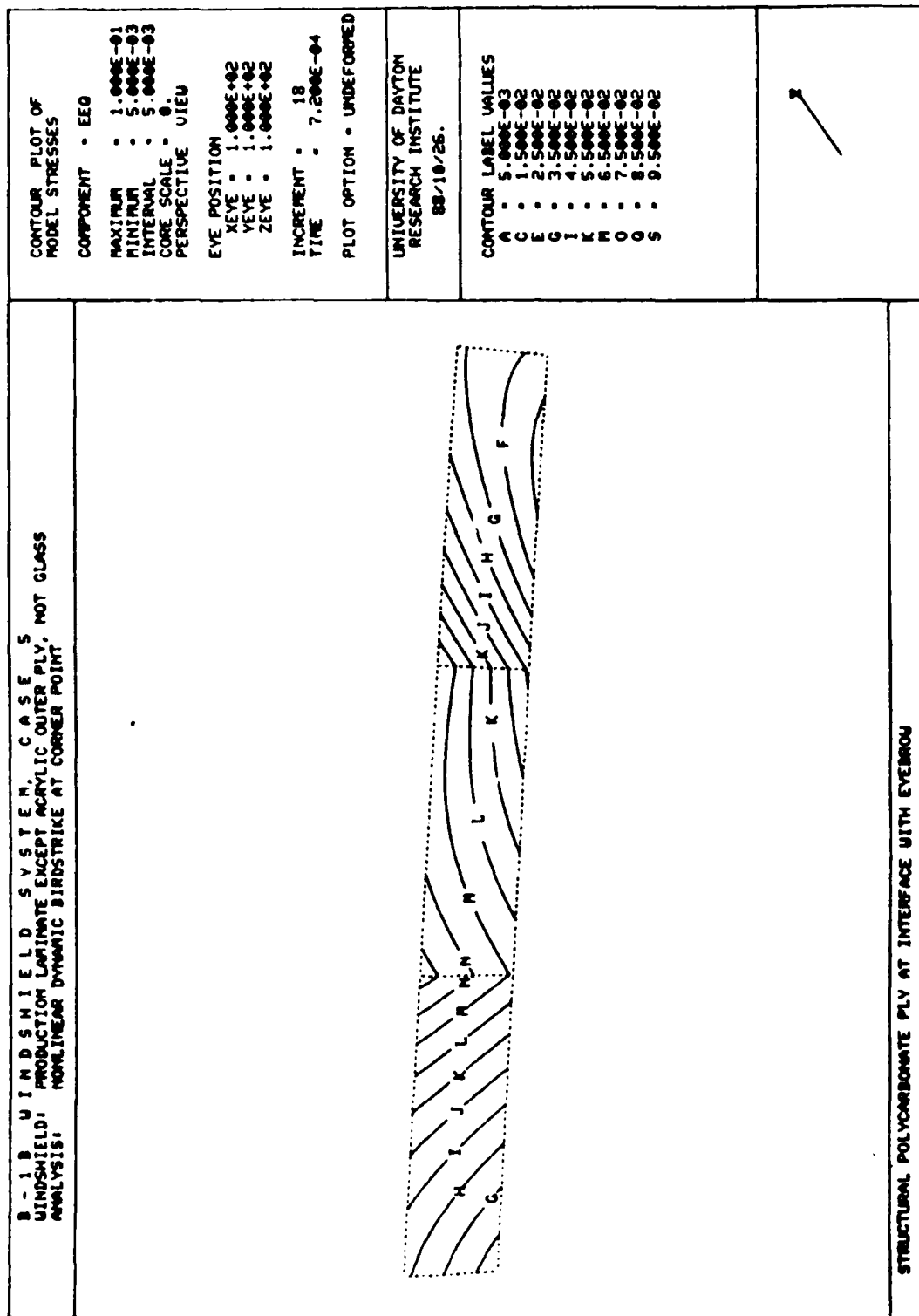


Figure 4.35. Equivalent Strain Contours Through the Thickness of the Structural Ply at the Upper Corner Windshield/Eyebrow Interface, Case 5.

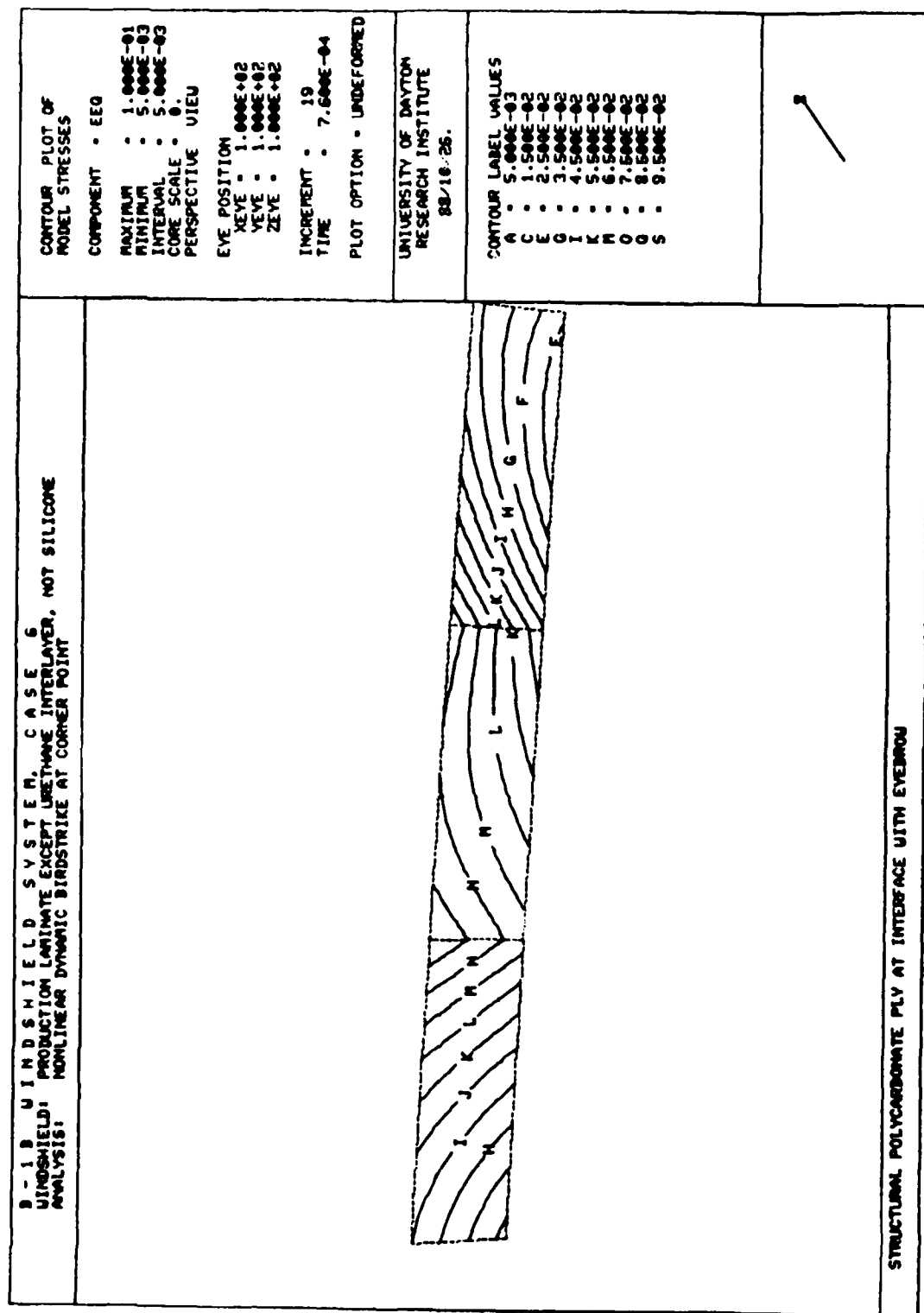


Figure 4.36. Equivalent Strain Contours Through the Thickness of the Structural Ply at the Upper Corner Windshield/Eyebrow Interface, Case 6.

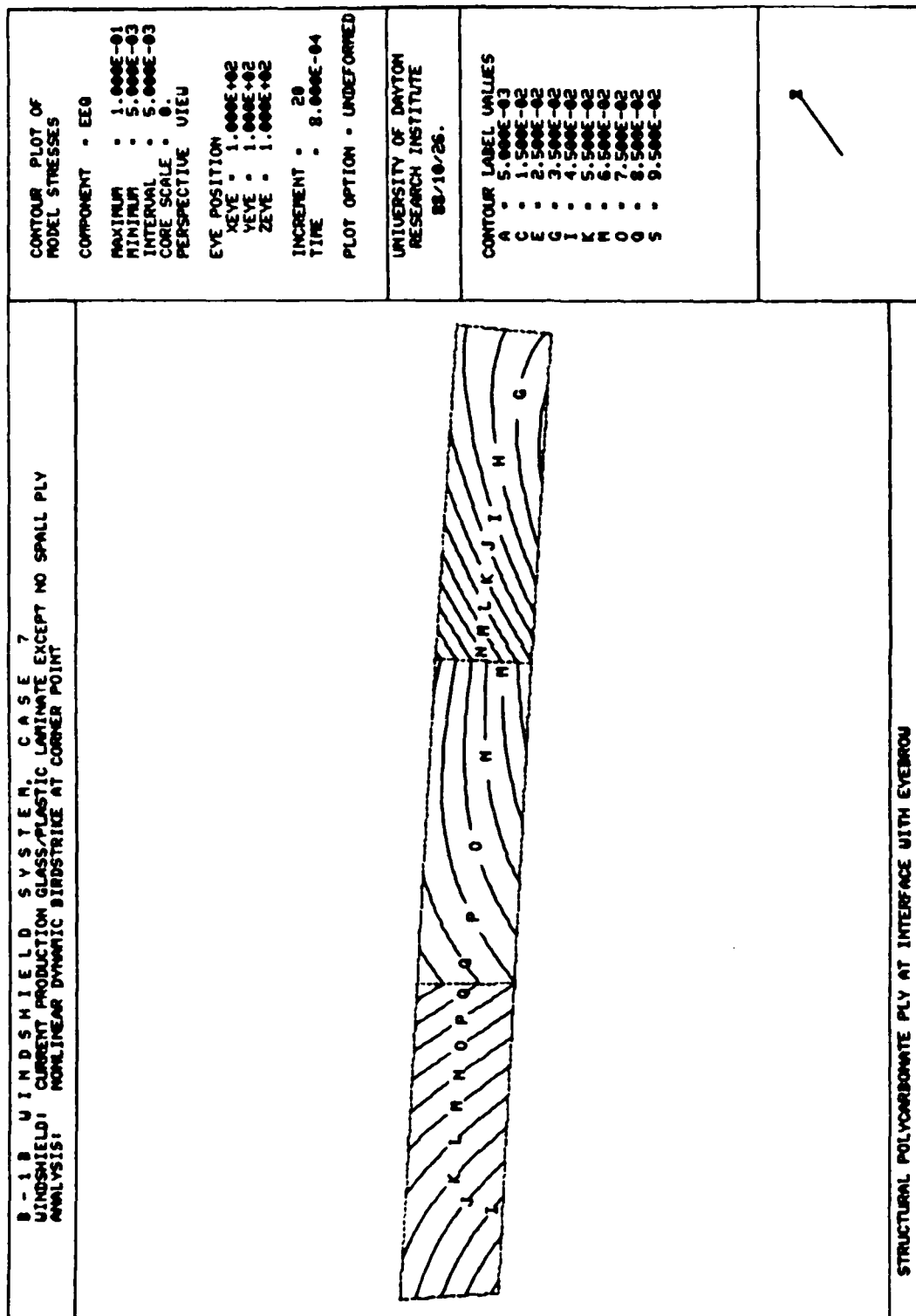


Figure 4.37. Equivalent Strain Contours Through the Thickness of the Structural Ply at the Upper Corner Windshield/Eyebrow Interface, Case 7.

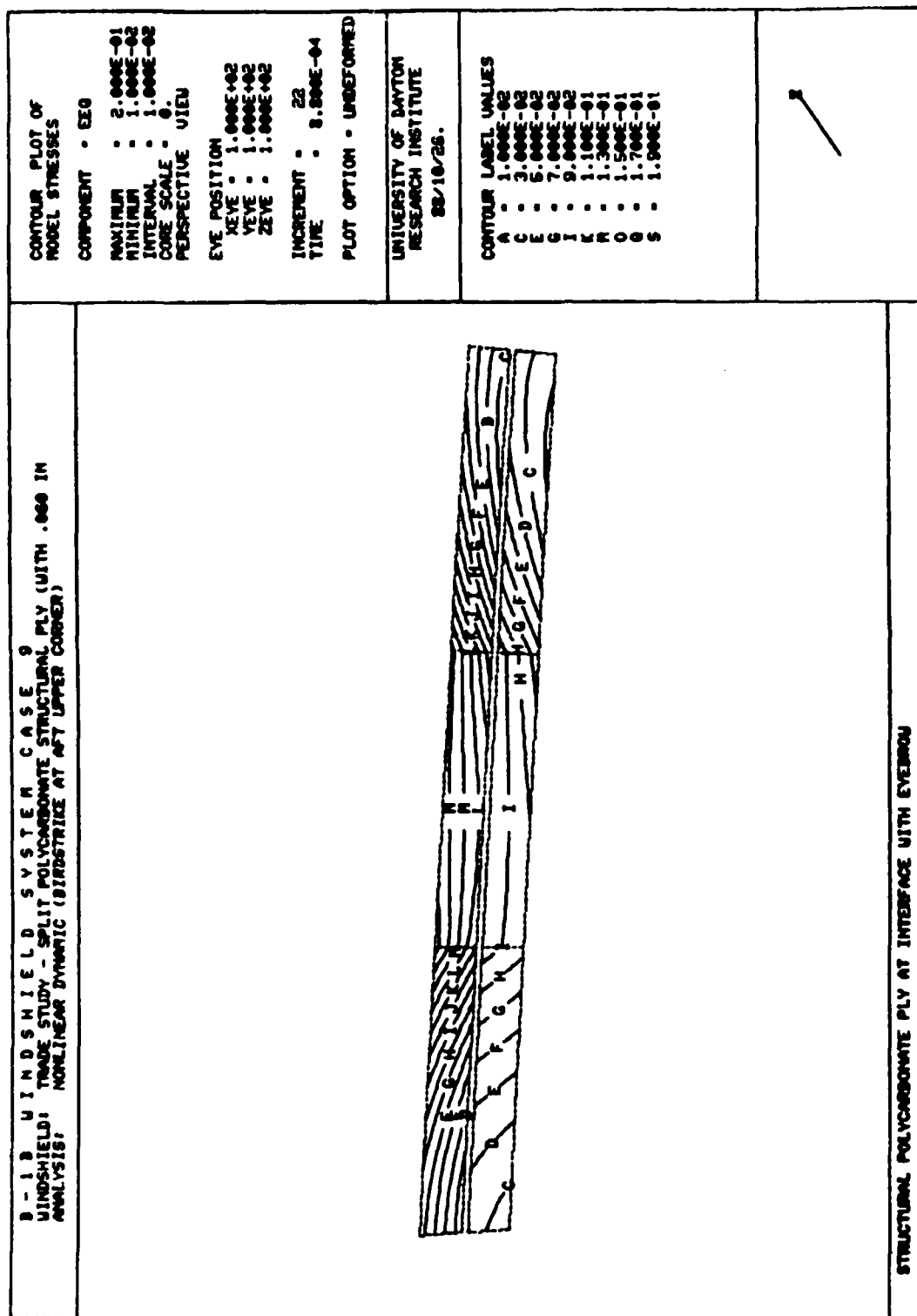


Figure 4.38. Equivalent Strain Contours Through the Thickness of the Structural Ply at the Upper Corner Windshield/Eyebrow Interface, Case 9.

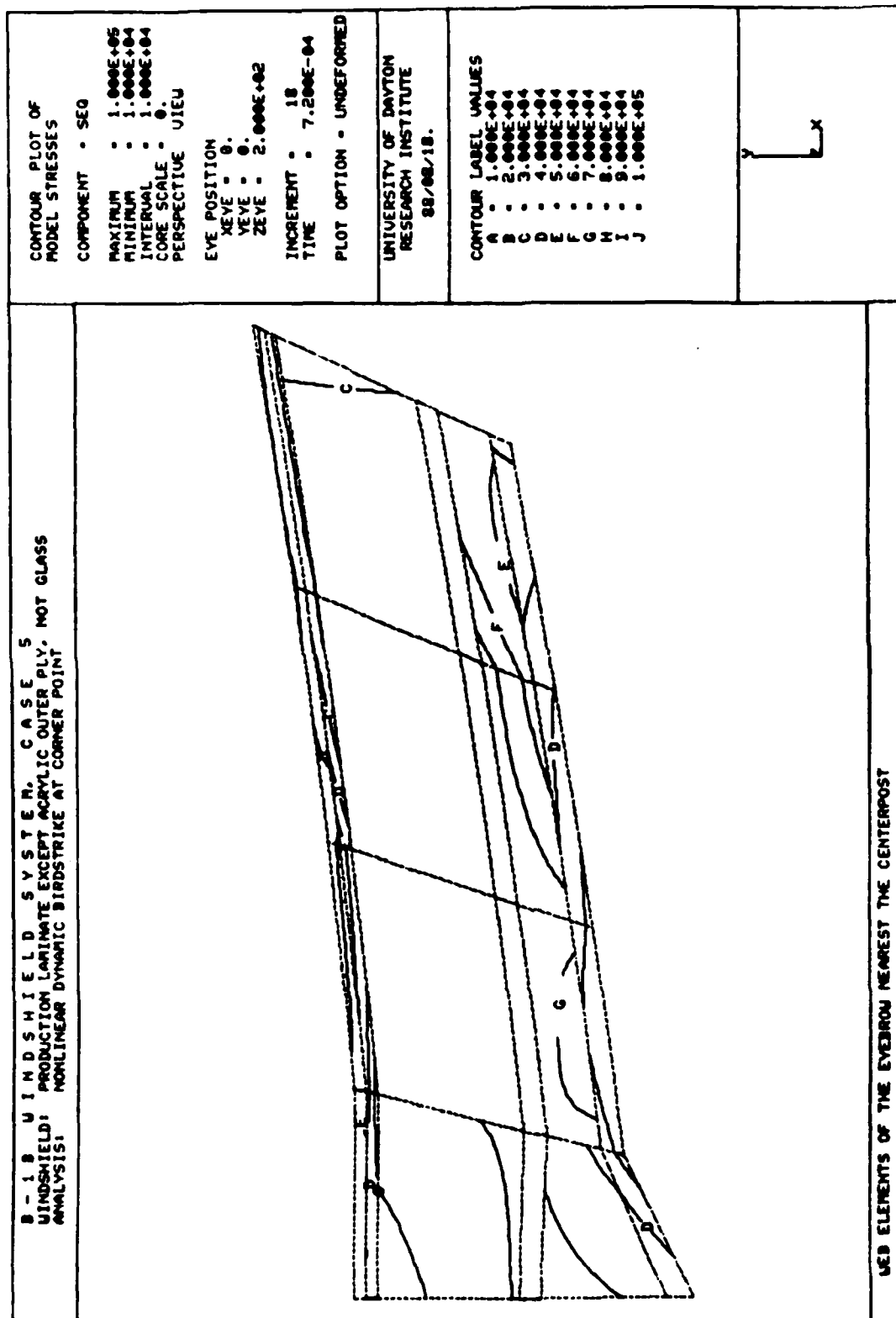


Figure 4.39. Equivalent Stress Contours on the Eyebrow Web, Case 5.

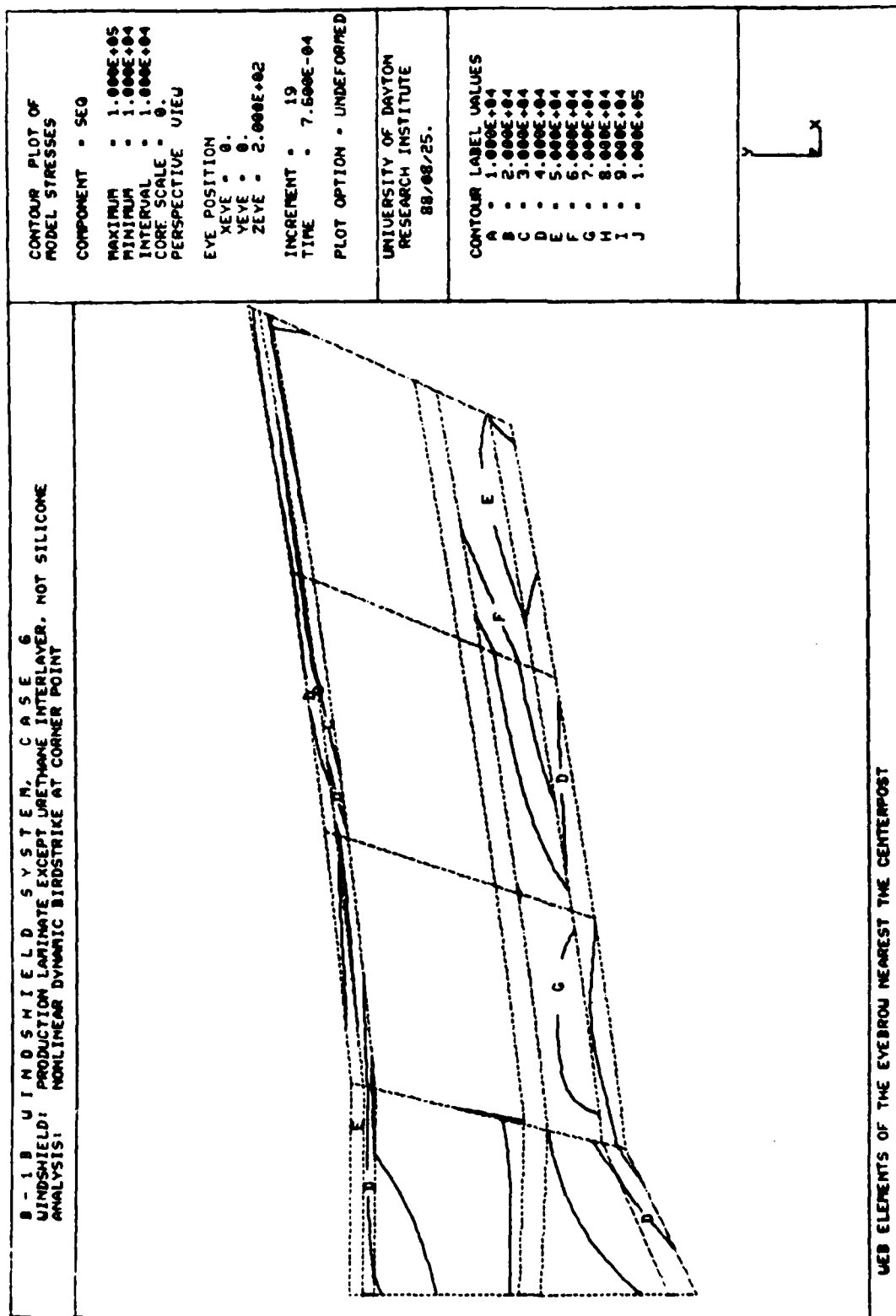


Figure 4.40. Equivalent Stress Contours on the Eyebrow Web, Case 6.

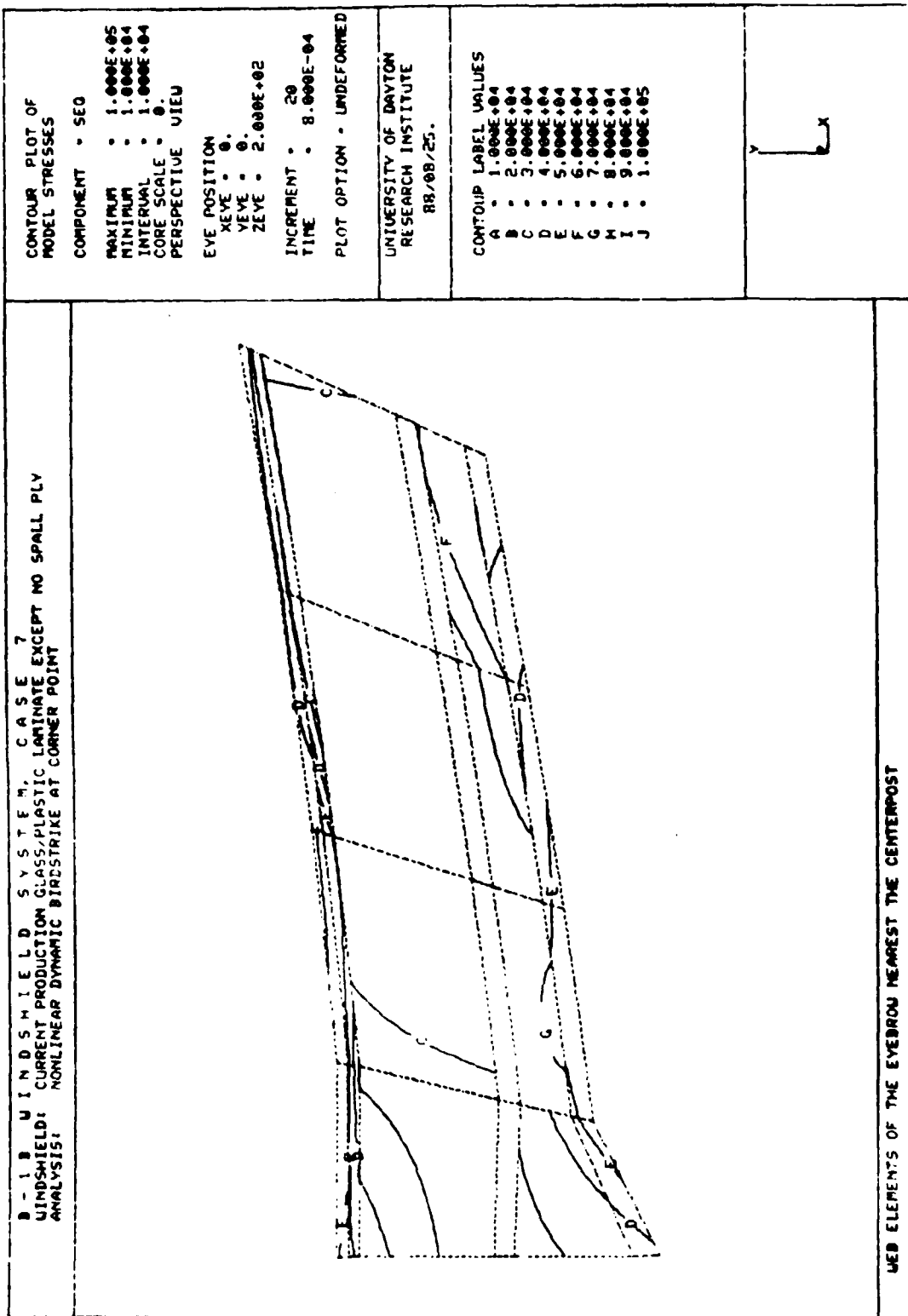


Figure 4.41. Equivalent Stress Contours on the Eyebrow Web, Case 7.

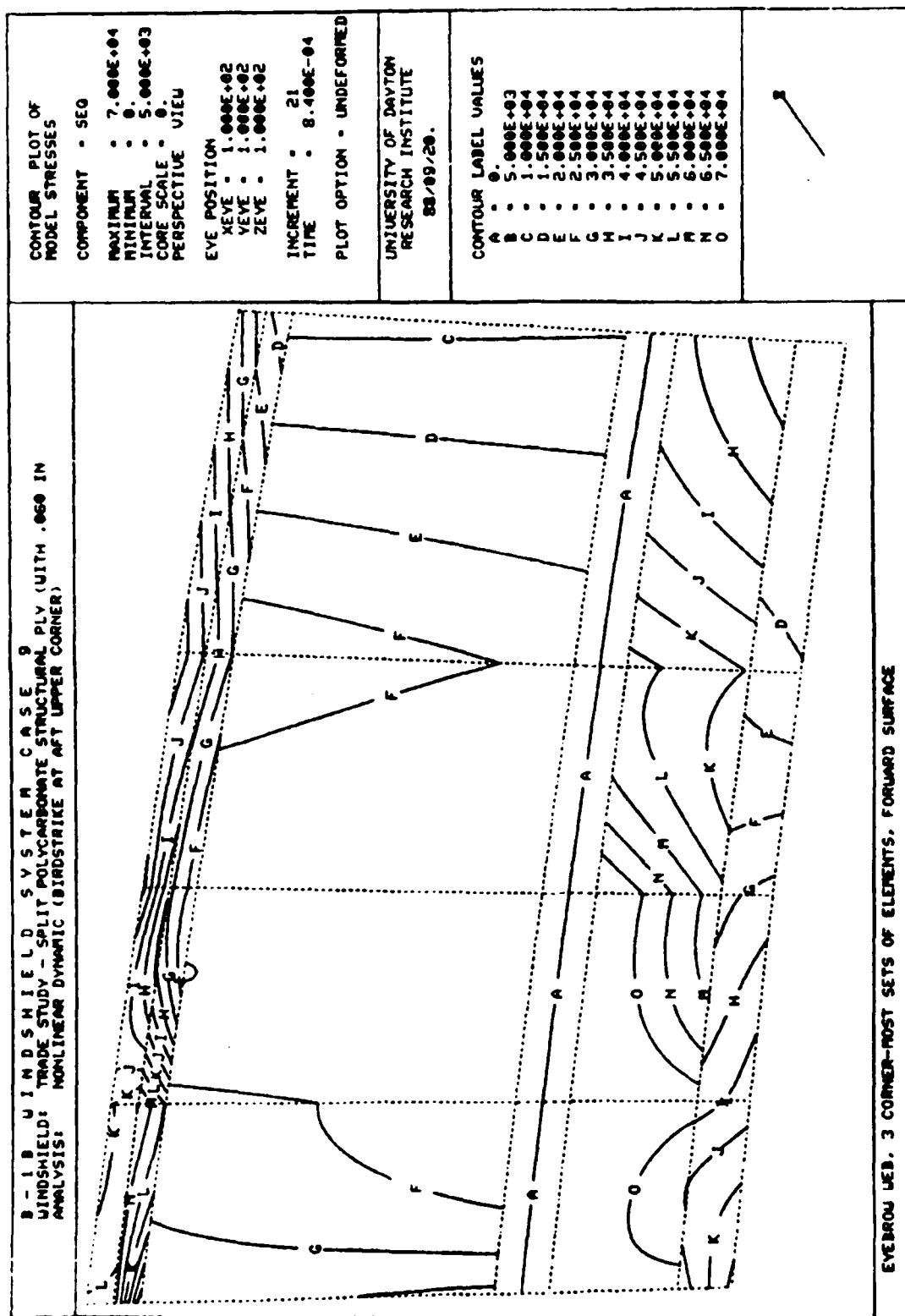


Figure 4.42. Equivalent Stress Contours on the Eyebrow Web, Case 9.

for both yield and ultimate since perfect plasticity was assumed).

Figures 4.43 - 4.46 present equivalent strain contours in the lower portion of the eyebrow web near the connection to the centerpost. The maximum equivalent strains in the high stress regions ranged from 0.035 in/in to 0.040 in/in, greater than the static transverse ultimate elongation of 0.03 in/in, but less than the static longitudinal ultimate elongation strain of 0.07 in/in. The contour values are similar to those for the current production configuration (Figure 4.22). As discussed in Section 4.3 for the current production configuration, the MAGNA results for the trade study cases indicate a marginal pass/fail (fracture) condition in the eyebrow web due to upper corner impact by a 4-pound bird at 650 mi/hr.

Review of data for the centerpost showed that the maximum centerpost stresses in the web were 40 kpsi for Cases 4, 5, and 6, 45 kpsi for Case 7, and 50 kpsi for Case 9. Thus only Case 9 showed centerpost yielding, with a total strain of 0.013 in/in, less than the strain to failure of 0.05 in/in for 2024-T62 aluminum. The centerpost was therefore adequately designed to resist impact by a 4-pound bird impacting at the upper corner location at 650 mi/hr without fracture for all configurations and without permanent deformation for all but the split structural ply configuration.

Figures 4.47 - 4.50 show the fastener load distribution curves for Cases 5, 6, 7, and 9 respectively. All the plots displayed the highly localized effect that was evident in the baseline study (see Figure 4.25). Similar characteristics were expected because the majority (70%-80%) of the impact energy was carried by the main structural ply which remained unchanged between the baseline and trade study cases (except for the split structural ply in Case 9).

Table 4.4 displays the maximum axial and shear loads and the percent change from the baseline values. Generally the

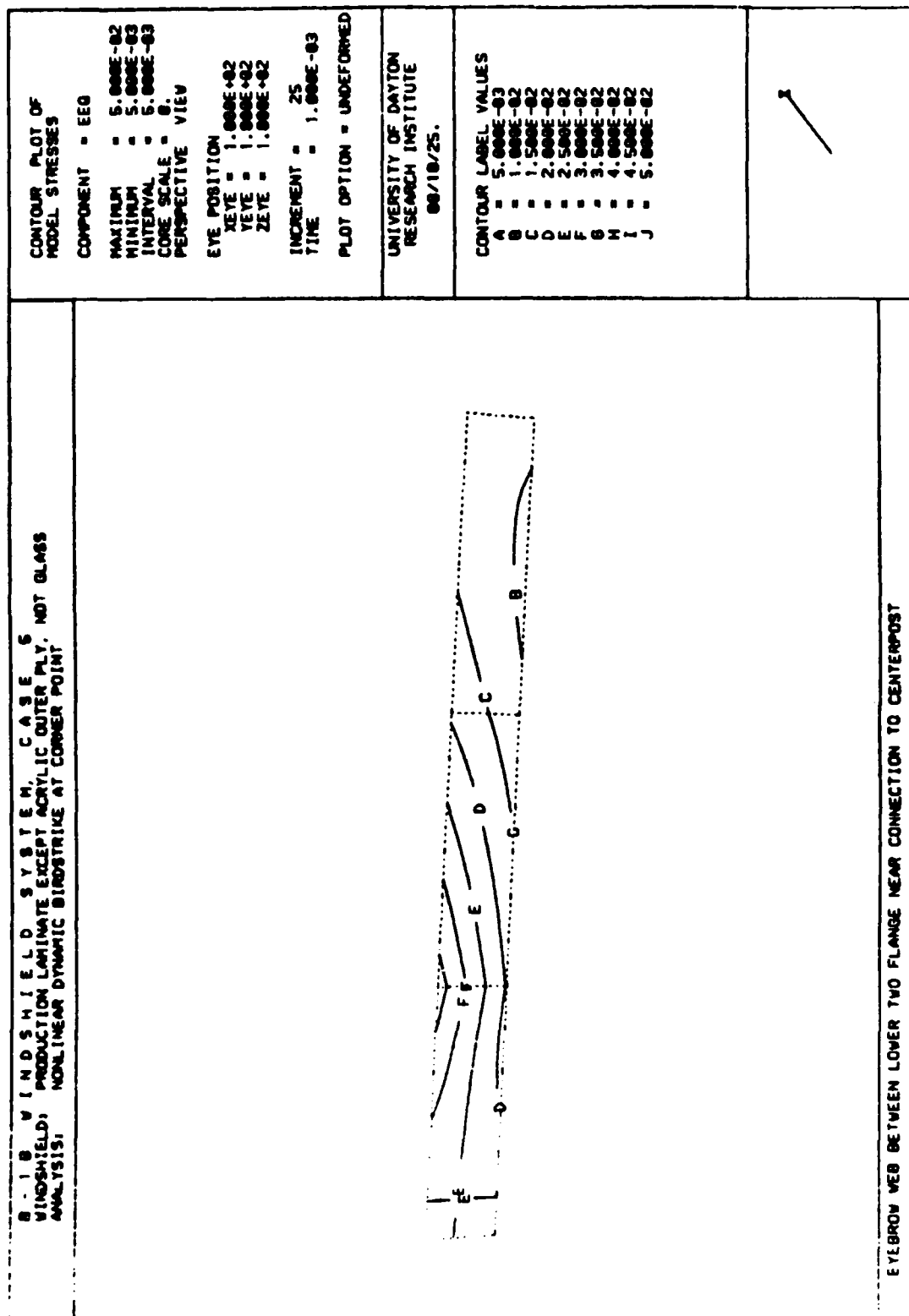


Figure 4.43. Equivalent Strain Contours on the Lower Portion of the Eyebrow Web, Case 5.

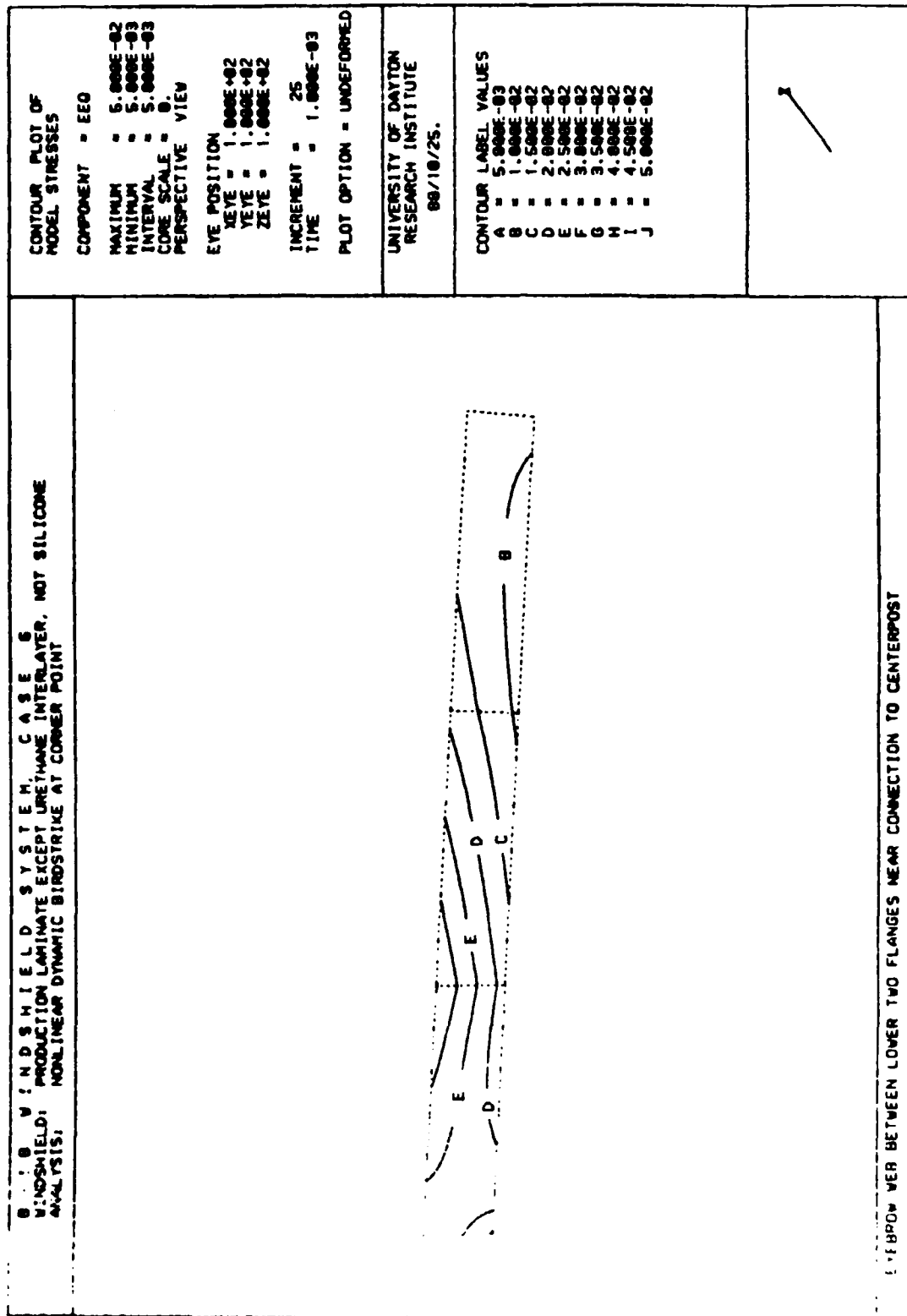


Figure 4.44. Equivalent Strain Contours on the Lower Portion of the Eyebrow Web, Case 6.

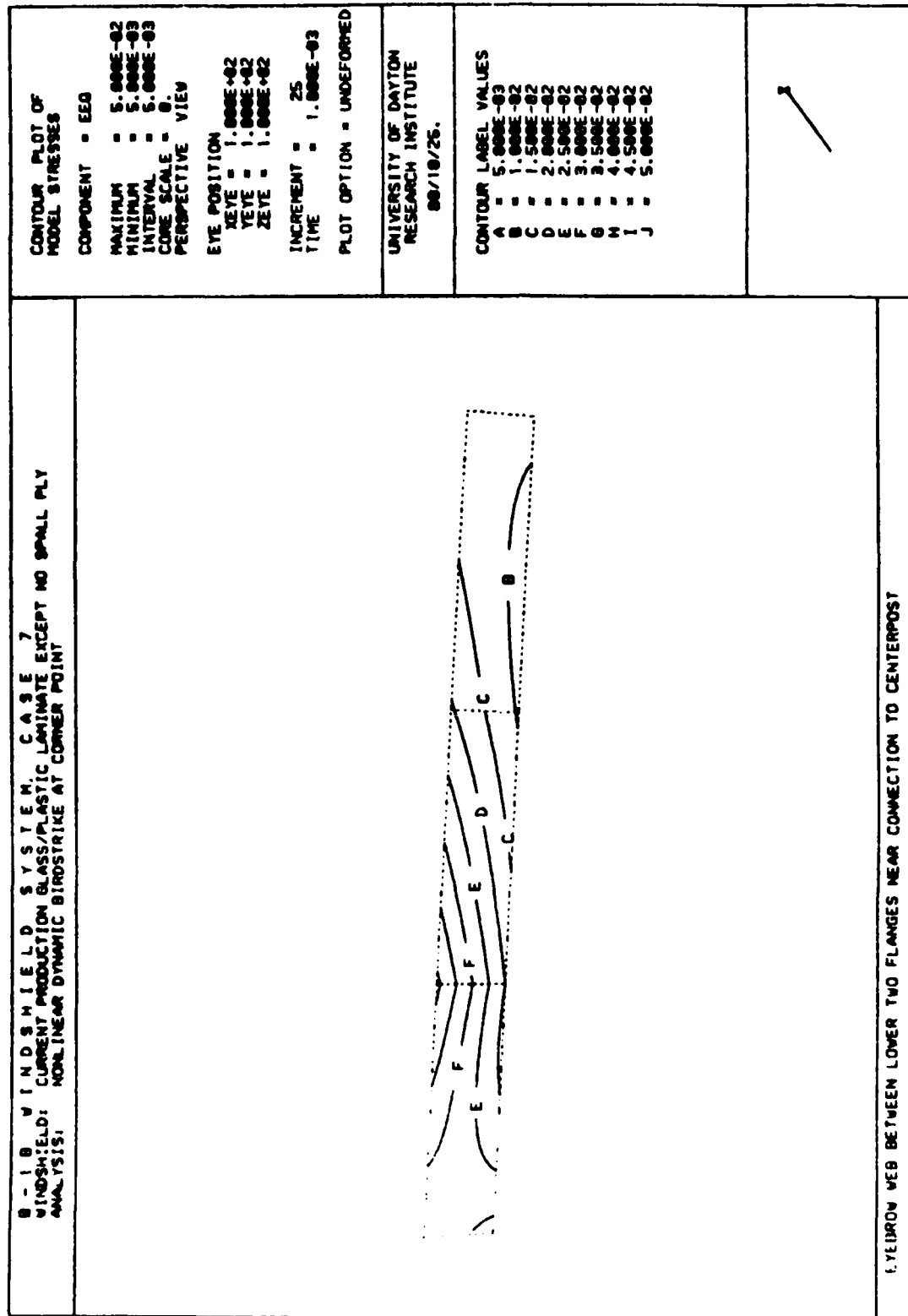


Figure 4.45. Equivalent Strain Contours on the Lower Portion of the Eyebrow Web, Case 7.

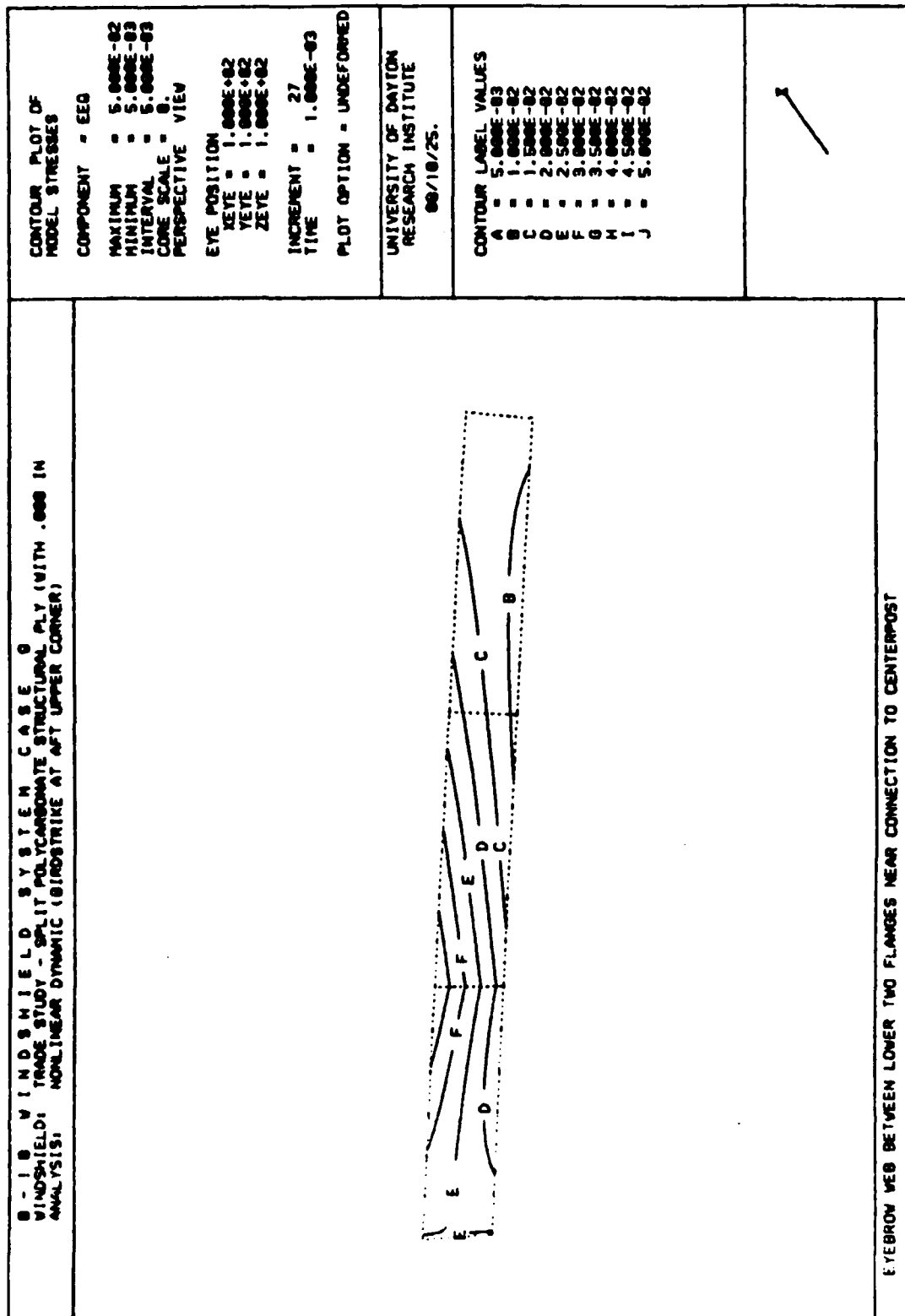


Figure 4.46. Equivalent Strain Contours on the Lower Portion of the Eyebrow Web, Case 9.

B-1 B Case 5 Incr 18

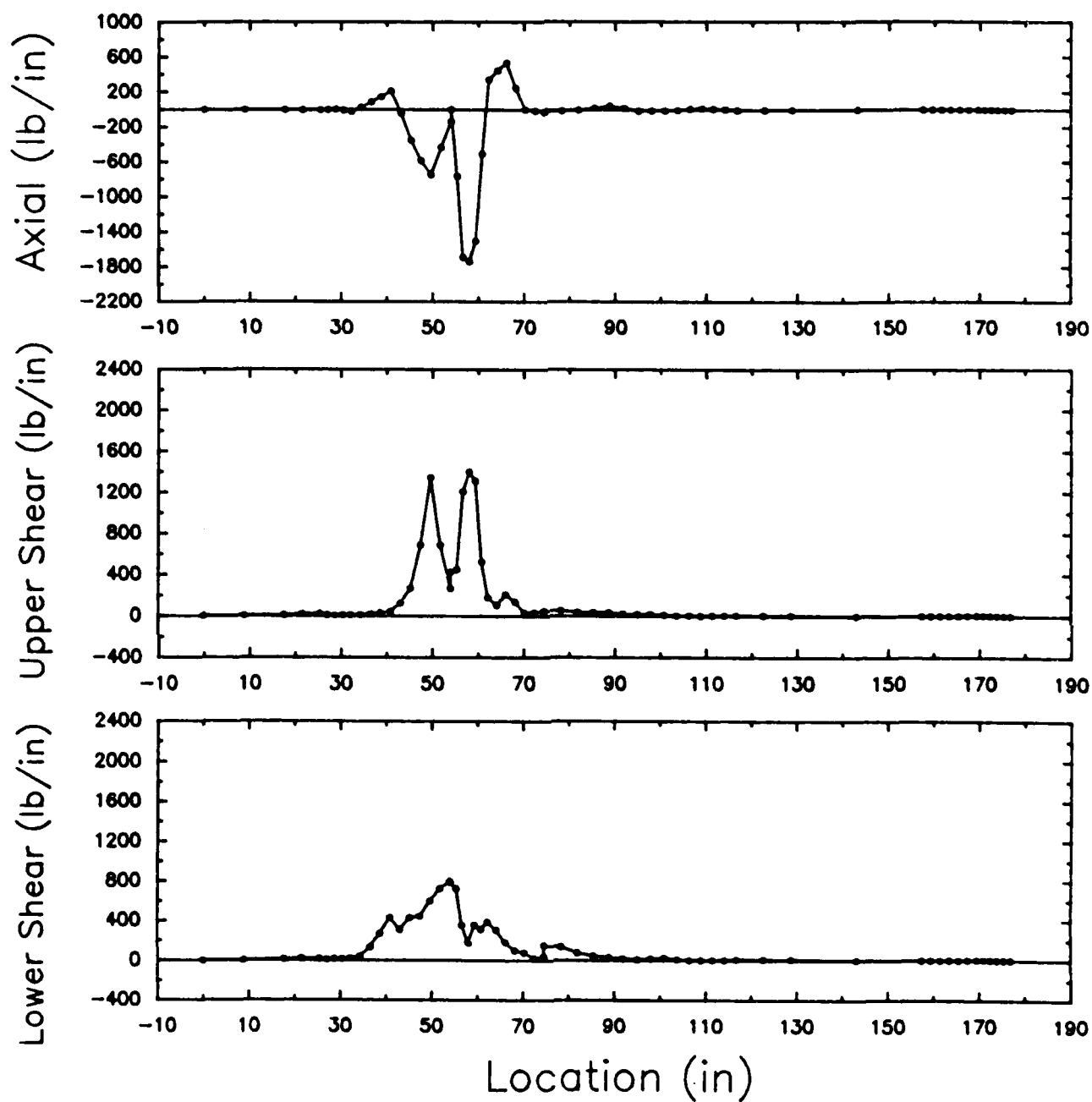


Figure 4.47. Fastener Load Distribution, Case 5.

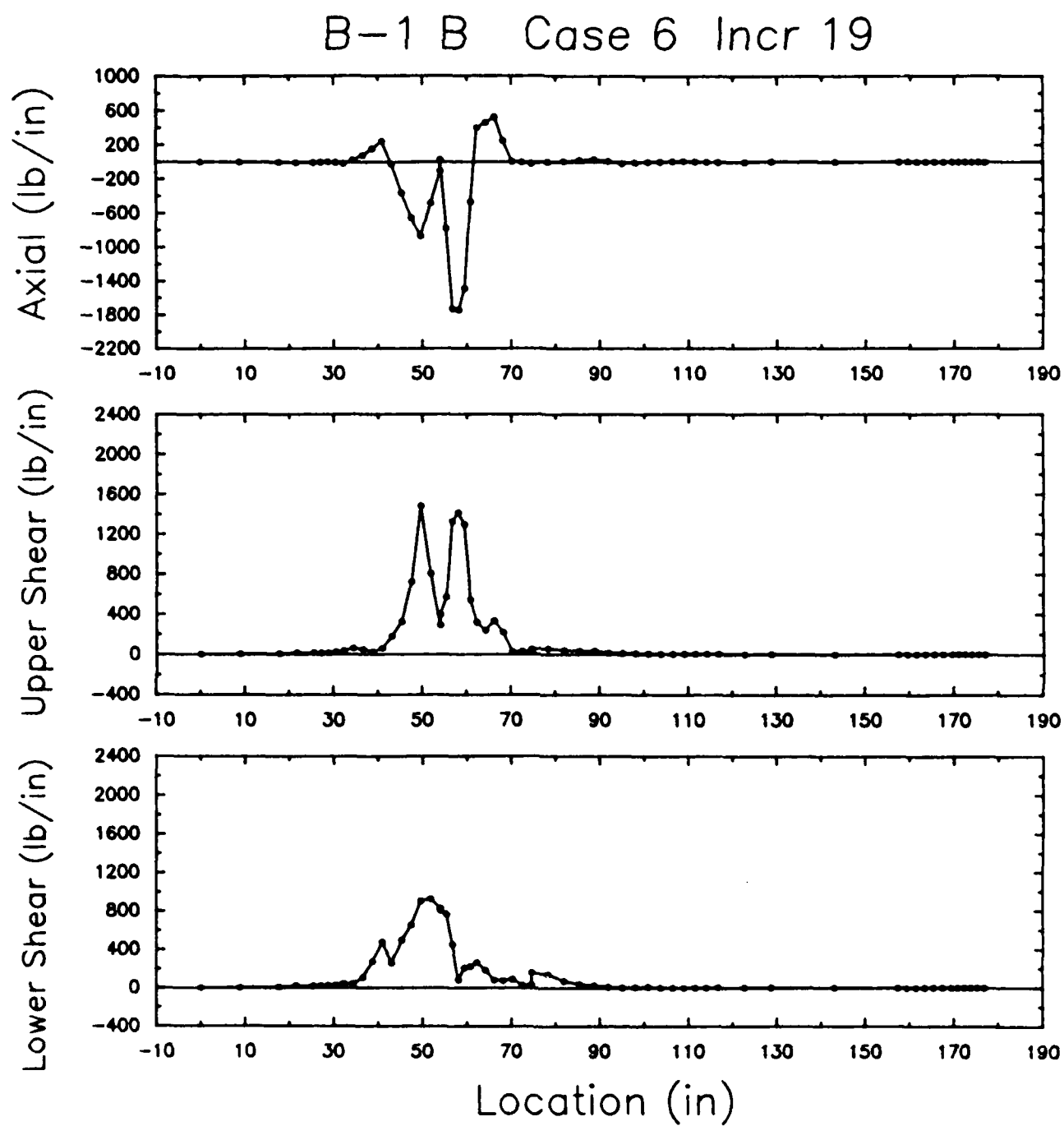


Figure 4.48. Fastener Load Distribution, Case 6.

B-1 B Case 7 Incr 20

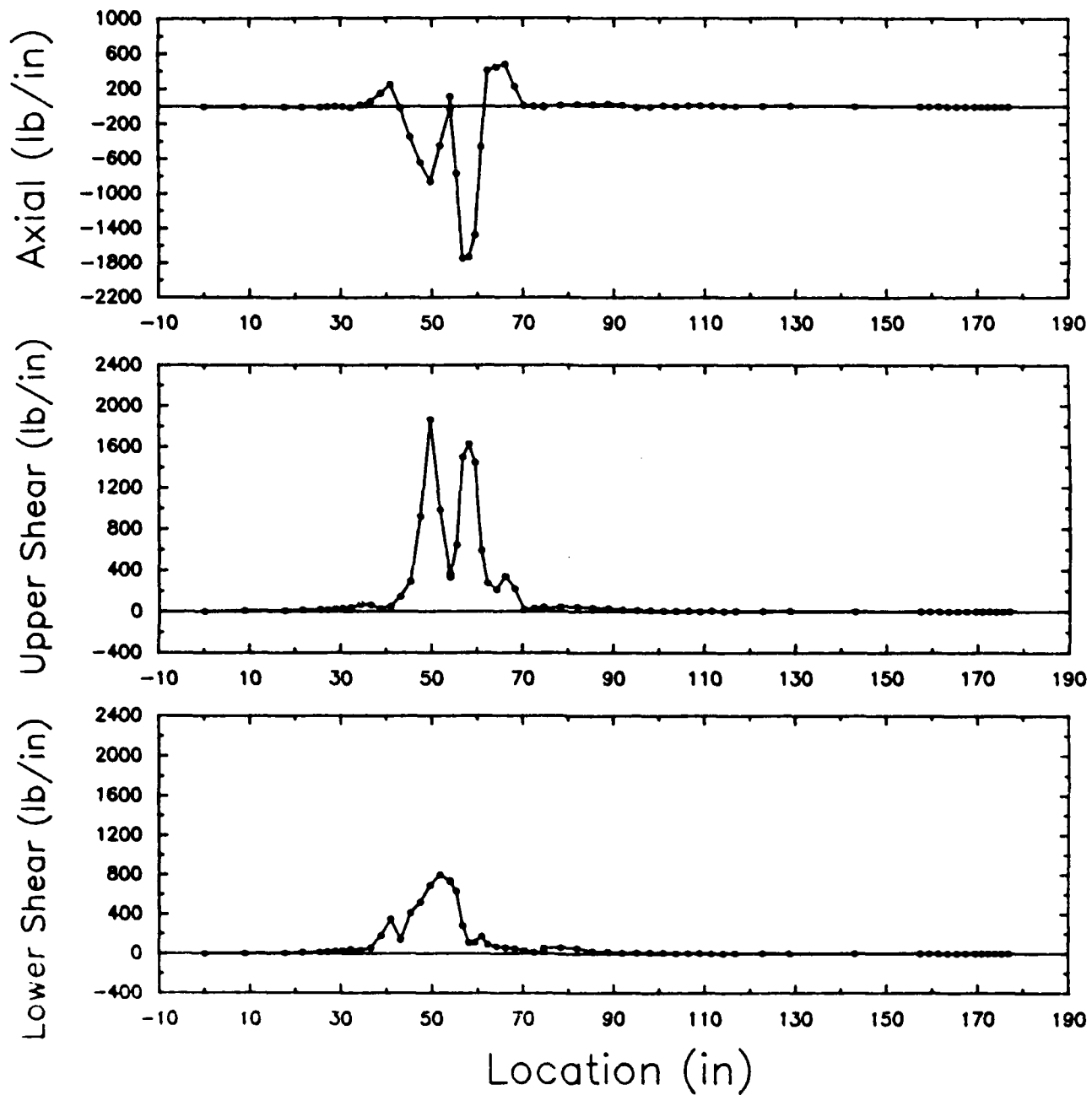


Figure 4.49. Fastener Load Distribution, Case 7.

B-1 B Case 9 Incr 21

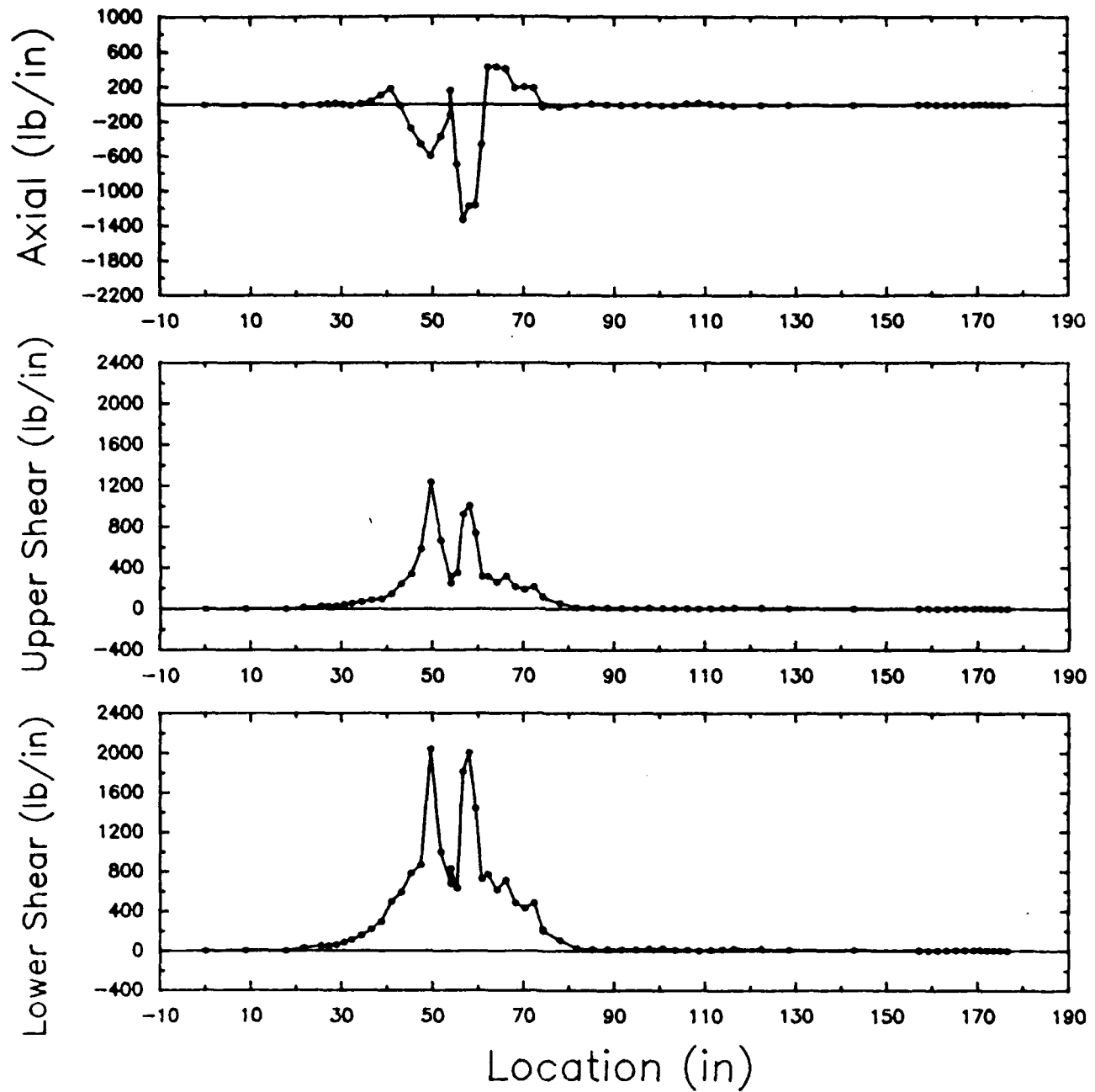


Figure 4.50. Fastener Load Distribution, Case 9.

TABLE 4.4

CRITICAL FASTENER LOADS FOR THE
UPPER CORNER IMPACT ANALYSES

Case No.	Axial (lb/in)	Upper Shear (lb/in)	Lower Shear (lb/in)	Percent Change from Baseline		
				Axial	Upper Shear	Lower Shear
4	2010.	1740.	1060.	-	-	-
5	1740.	1410.	800.	-13.4	-19.0	-24.5
6	1750	1490	930.	-12.9	-14.4	-12.3
7	1750	1870	800.	-12.9	+ 7.5	-24.5
9	1330	1240	2050.	-33.8	-28.7	+93.4

trade study values were smaller than the baseline study values but some variations increased the fastener loads. Both the acrylic outer ply (Case 5) and the urethane interlayer (Case 6) configurations reduced all three fastener loads by over ten percent. Elimination of the spall ply (Case 7) diminished the axial and lower shear loads but increased the upper shear load.

Splitting the main structural ply produced smaller fastener loads for the internal pressurization case (see Section 4.2), but did not affect the dynamic birdstrike response in the same manner. The axial and upper shear loads were significantly reduced from the baseline birdstrike values, but the lower shear load nearly doubled. However, the maximum shear load (lower shear) which was used in the safety margin calculations for Case 9 was only 18% larger than the maximum shear load (upper shear) for the baseline birdstrike study.

Table 4.5 shows the safety margins for each upper corner impact analysis. The smaller loads for Cases 5 and 6 produced larger safety margins for all eight failure modes than those of the baseline study. The safety margins for fastener shear, transparency bearing, and transparency rupture were lower for both Cases 7 and 9. The fastener shear safety margins of 0.84 and 0.68 for Cases 7 and 9, respectively, were significantly smaller than the baseline margin (0.98) and were the most critical among all the birdstrike analyses. Similar to Case 4, when every other fastener was removed, all the dynamic trade study analyses were on the verge of, if not at, failure. The combined tension/shear interaction numbers followed trends similar to the independent tension and shear margins of safety.

In summary, the MAGNA analyses indicated that all trade study configurations as well as the baseline (current production) configuration were marginally capable of defeating a 4-pound bird impacting at the upper corner location at 650 mi/hr. The MAGNA results indicated that, for the upper corner birdstrike, the structural polycarbonate ply (plies) and the

TABLE 4.5

FASTENER SAFETY MARGINS FOR THE
UPPER CORNER IMPACT ANALYSES

	Case 4	Case 5	Case 6	Case 7	Case 9
Safety Margins					
Fastener Tension	0.99	1.16	1.15	1.15	1.47
Fastener Shear	0.98	1.44	1.31	0.84	0.68
Transparency Bearing	1.63	2.25	2.07	1.45	1.23
Transparency Rupture	6.68	8.48	7.97	6.15	5.52
Safety Margins (50% fastener removal)					
Fastener Tension	-0.01	0.08	0.07	0.07	0.23
Fastener Shear	-0.01	0.22	0.15	-0.08	-0.16
Transparency Bearing	0.32	0.62	0.54	0.22	0.12
Transparency Rupture	8.00	10.10	9.51	7.37	6.64
Interaction Relation					
All Fasteners Present	0.38	0.28	0.30	0.38	0.38
50% Fastener Removal	2.05	1.42	1.52	2.15	2.35

Note: Safety margins < 0.0 indicate failure

Interaction relation values > 1.0 indicate failure

eyebrow frame permanently deformed, with the eyebrow frame exhibiting a marginal pass/fail (fracture) condition. The location of the highest strains and stresses in the eyebrow frame (in the web between the bottom two flanges) was the same location where fracture occurred during upper corner birdstrike testing of the B-1A. No definite conclusion can be drawn regarding whether or not the B-1B eyebrow frame will pass upper corner birdstrike by a 4-pound bird at 650 mi/hr. The results indicate that fracture in the eyebrow web is possible under such conditions. Fracture of the B-1B structural polycarbonate ply (plies) should not occur unless the elongation to failure of the polycarbonate is degraded (due to, for example, improper material processing, embrittlement, or stress concentration).

The performance of the various configurations was similar, although the use of low strain rate interlayer material properties for the split polycarbonate ply configuration resulted in increased windshield deflection and structural ply yielding, and permanent deformation of the centerpost. Since the upper corner location was determined to be more severe than the near-center impact site, all windshield configurations should be capable of defeating a 4-pound bird impacting at the near-center site at 650 mi/hr.

The fastener analysis of the trade study cases determined that the current fastener design was adequate for surviving an upper corner impact birdstrike at 650 mi/hr by a 4-pound bird. The acrylic outer ply and the urethane interlayer configurations improved the fastener safety margins, but the removal of the spall ply and the split structural ply did not. The safety margins determined when every other fastener was removed were bordering on failure. It is therefore recommended, based on the load distribution plots in Figures 4.24 and 4.47 - 4.50, that all existing fasteners be retained within 10 inches of either side of the eyebrow-to-centerpost corner

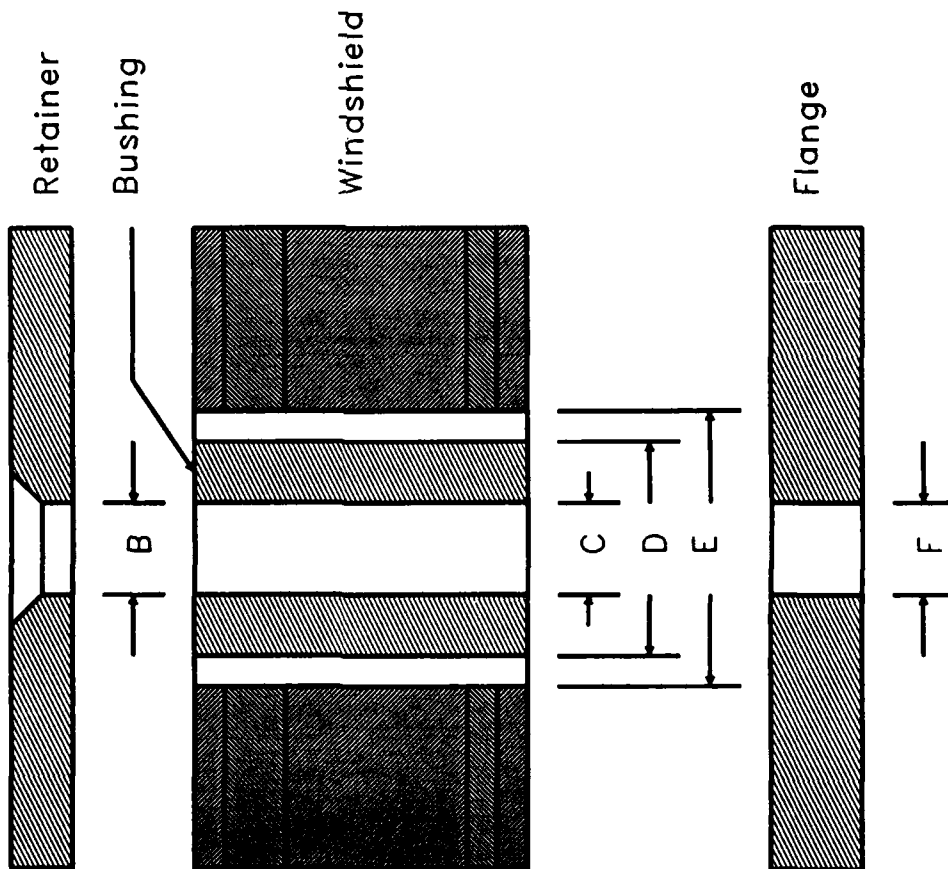
connection (that is, do not delete every other fastener in this region. The decision on whether or not to delete fasteners in other regions should be based in part on additional birdstrike analyses with impact sites located near each region of interest, since such impact conditions result in the highest birdstrike-induced loads in the fasteners of interest.

4.5 Fastener Tolerances

Concern had been expressed that the hole tolerance for the windshield fasteners was too restrictive, making windshield changeout slow and tedious. Specifically, it was thought that the hole tolerance was plus or minus 0.0005 inch, which, due to alignment mismatches caused by thermal expansion effects, required that changeout be accomplished in a narrow temperature range of 72°F +/- 5°F. To alleviate the alignment problems, it was desired to increase the tolerance to a target value of 0.010 inch. An objective of the current study was to determine if the increased tolerance would adversely affect the structural performance of the windshield system.

Figure 4.51 presents a sketch of the B-1B fastener system geometry. Note that the hole tolerance is actually +0.005, -0.0043 inch. The hole reaming operation is performed in a controlled environment during the fabrication process, and is not performed at the field or depot level as part of the windshield changeout process. Note further that the fasteners are not inserted directly into these holes. Rather, bushings are inserted first and then the bolts are inserted into the bushings. The critical tolerance for windshield changeout is therefore the clearance between the fastener and the bushing. As Figure 4.51 indicates, a total of 0.015 to 0.017 inch fastener-to-bushing tolerance is present in the existing B-1B fastener system (based on a nominal fastener diameter of 0.25 inch). In addition, the tolerance between the fastener and the support structure flange or retainer is 0.01 to 0.015 inch. Both of these tolerances are

NAS1580C4
Fastener



Dimensions for B-1B (inches)

- A = 0.2490 - 0.2495
- B = 0.261 +.004/-0.001
- C = 0.266 +/-0.001
- D = 0.4005 +/-0.0010
- E = 0.4063 +.0005/-0.0043
- F = 0.261 +.004/-0.001

Note: C = 0.257 for B-1A

Figure 4.51. B-1B Fastener System Dimensions.

equal to or larger than the previously mentioned target tolerance of 0.010 inch. In addition, the B-1A fastener-to-bushing tolerance was only 0.007 inch.¹⁶ The current B-1B windshield fastener-to-bushing tolerance, which is larger than the target and B-1A tolerances, is therefore believed to be adequate for facilitating windshield changeout.

Birdstrike tests of the B-1A windshield had been performed in an effort to evaluate the effect of increasing the fastener-to-bushing tolerance.^{16,17} As mentioned previously, the B-1A standard tolerance was 0.007 inch. The enlarged tolerance was 0.050 to 0.073 inch, considerably larger than the current B-1B maximum tolerance of 0.017 inch. The test results for shots BM004 and BM006 indicated that the enlarged holes did not degrade the structural performance of the windshield system. Deflections were nearly equal (within five percent) and no damage to the polycarbonate structural plies or the supporting frames was observed. In light of these test results, and because the existing B-1B tolerance is less than the enlarged B-1A test tolerance, the results of the fastener analyses are believed to be representative of the performance of the current production windshield system fasteners. In other words, the tolerance does not change the reported results.

4.6 Summary of Results

Table 4.6 summarizes the MAGNA results for the baseline (current production) and trade study (split structural polycarbonate ply) internal pressurization analyses. Because the other trade study configurations utilized the same structural ply as the baseline, and because this ply bears 70% - 80% of the applied load, the performance of these other trade studies was judged to be similar to that of the baseline configuration. The results therefore showed that the current production windshield system and each of the trade study windshield system configurations were sufficiently designed to resist internal

TABLE 4.6
SUMMARY OF RESULTS FOR MAGNA PRESSURIZATION ANALYSES

Case Number	2	8
Category	Baseline	Trade Study
Model Description	Current Production Windshield	Split Structural Ply
Maximum Deflection (in)	0.104	0.107
Maximum Polycarbonate Structural Ply Stress (kpsi)	0.5 (12)	0.5 (12)
Glass Ply Stress (psi)	11.9 (18)	9.9 (18)
Maximum Centerpost Stress (kpsi)	5. (50)	4. (50)
Maximum Eyebrow Stress (kpsi)	4.5 (56)	6.5 (56)
Maximum Aft Arch Stress (kpsi)	5.8 (56)	2.9 (56)

NOTE: Numbers in parentheses are yield stresses, in kpsi,
for the indicated windshield system component.

cabin pressures of up to 21.2 psi above outside atmospheric pressure without permanent deformation to any of the windshield components.

Table 4.7 and Figures 4.52-4.54 summarize the MAGNA results for the baseline and trade study birdstrike analyses. The baseline (current production) analyses indicated that the current-production windshield was capable of defeating a 4-pound bird impacting at the near-center site at 650 mi/hr. The analyses further indicated that bird impact at the upper corner location was more severe than impact at the near-center location, resulting in permanent deformation of the eyebrow frame (and possibly fracture in the eyebrow web) and the structural polycarbonate ply.

The marginal condition is indicated in Figure 4.54 by the region between 3% and 7% strains, which coincides with ultimate elongation in the transverse and longitudinal directions, respectively. The maximum MAGNA equivalent strains for all upper corner impact cases fall in this region. Additional MAGNA data verified that the state of strain/stress in the eyebrow web due to upper corner impact was marginal.

Table 4.8 and Figure 4.55 summarize the results of the baseline and birdstrike fastener analyses for both the pressurization and birdstrike loading. Note that values inside (below) the curve of Figure 4.55 indicate fastener pass, while values outside the curve indicate fastener failure. The safety margins for the pressurization analyses were large, indicating that the current production and trade study windshield fasteners were sufficiently designed to resist internal cabin pressures of up to 21.2 psi above the outside atmospheric pressure. (Note that the trade study configurations for which no pressurization margins are given were expected to give similar results since they utilized the same structural polycarbonate ply, which transfers 70% - 80% of the applied load to the fasteners.)

TABLE 4.7

SUMMARY OF RESULTS FOR MAGNA BIRDSTRIKE ANALYSES

Case Number Category	3 Baseline	4 Current Production	5 Trade Study	6 Trade Study	7 Trade Study	9 Trade Study
Model Description	Current Production	Current Production	Acrylic Outer Ply	Urethane Interlayer	Remove Spall Ply	Split Structural Ply
Impact Site	A	B	B	B	B	B
Maximum Deflection (in.)	1.399	1.05	0.919	0.988	1.171	1.364
Maximum Structural Polycarbonate Stress (kpsi) (Yield = 12 kpsi)	5	12	12	12	12	12
Maximum Structural Polycarbonate Strain (%) (Yield = 3.38%, Failure = 120%)	1.4	8	7.5	7.5	9.	16.
Maximum Centerpost Stress (kpsi) (Yield = 50 kpsi)	14.	40.	40.	40.	45.	50.
Maximum Centerpost Strain (%) (Yield = 0.47%, Failure = 5.0%)	0.13	0.38	0.38	0.38	0.42	1.3
Maximum Eyebrow Stress (kpsi) (Yield = 65 kpsi)	7.	70	70	70	70	70
Maximum Eyebrow Strain (%) (Yield = 0.56%, Failure = 8.0%)	0.06	3.5	3.5	3.5	4.0	4.0

NOTE: Site A is the near-center location
Site B is the upper-corner location

STRUCTURAL PLY STRAIN SUMMARY

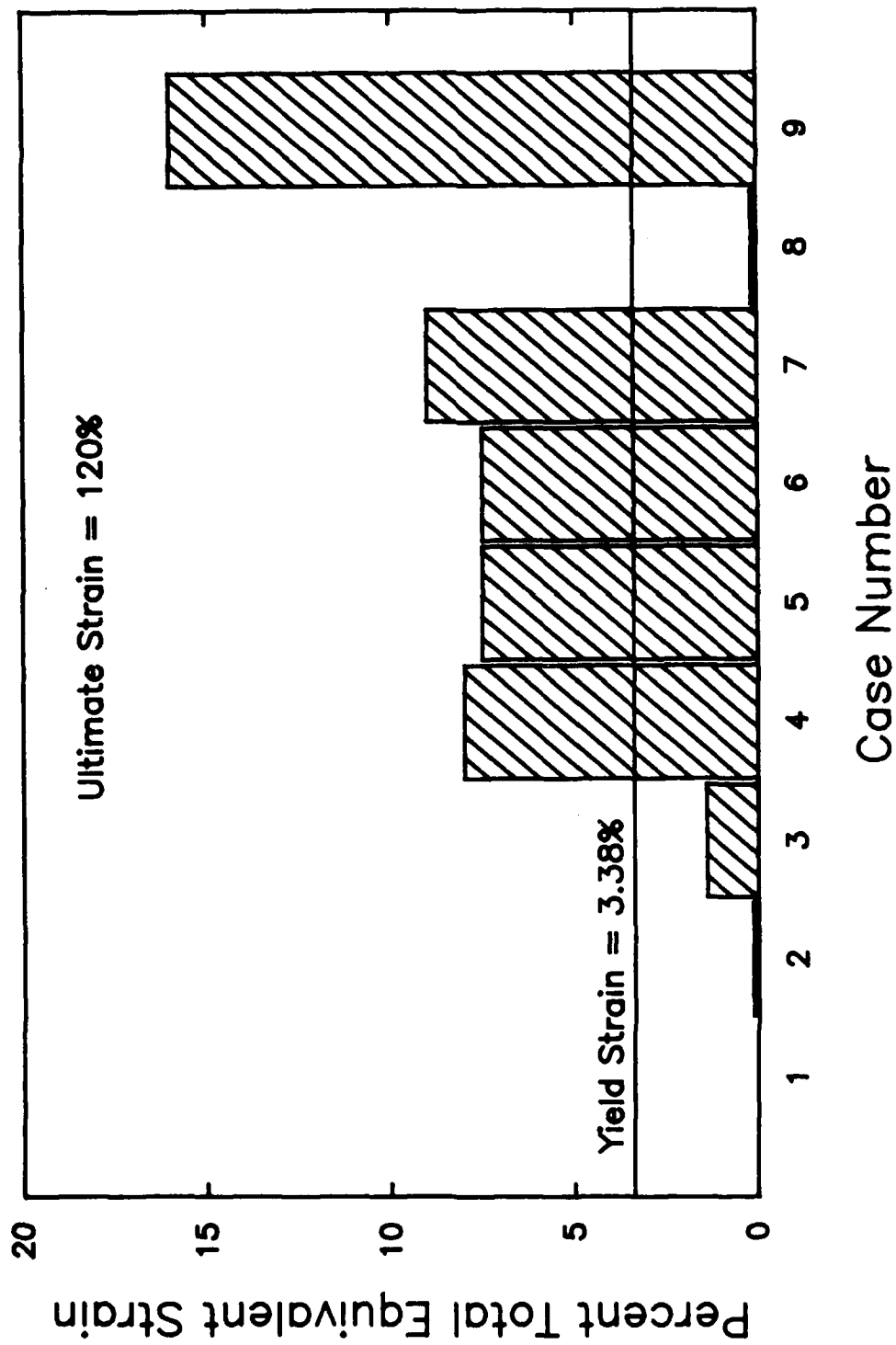


Figure 4.52. Strain Summary, Polycarbonate Structural Ply.

CENTERPOST STRAIN SUMMARY

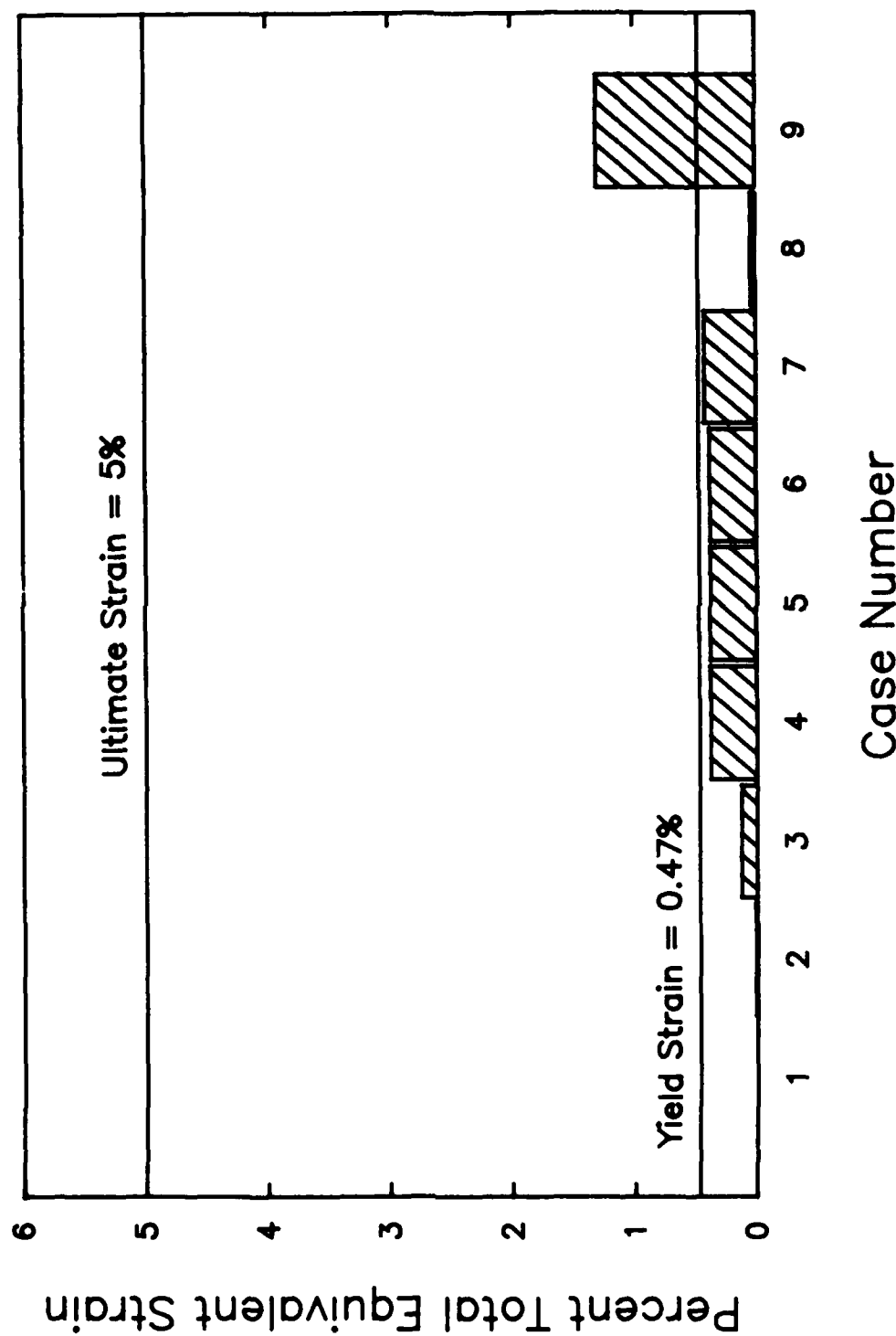


Figure 4.53. Strain Summary, Centerpost.

EYEBROW STRAIN SUMMARY

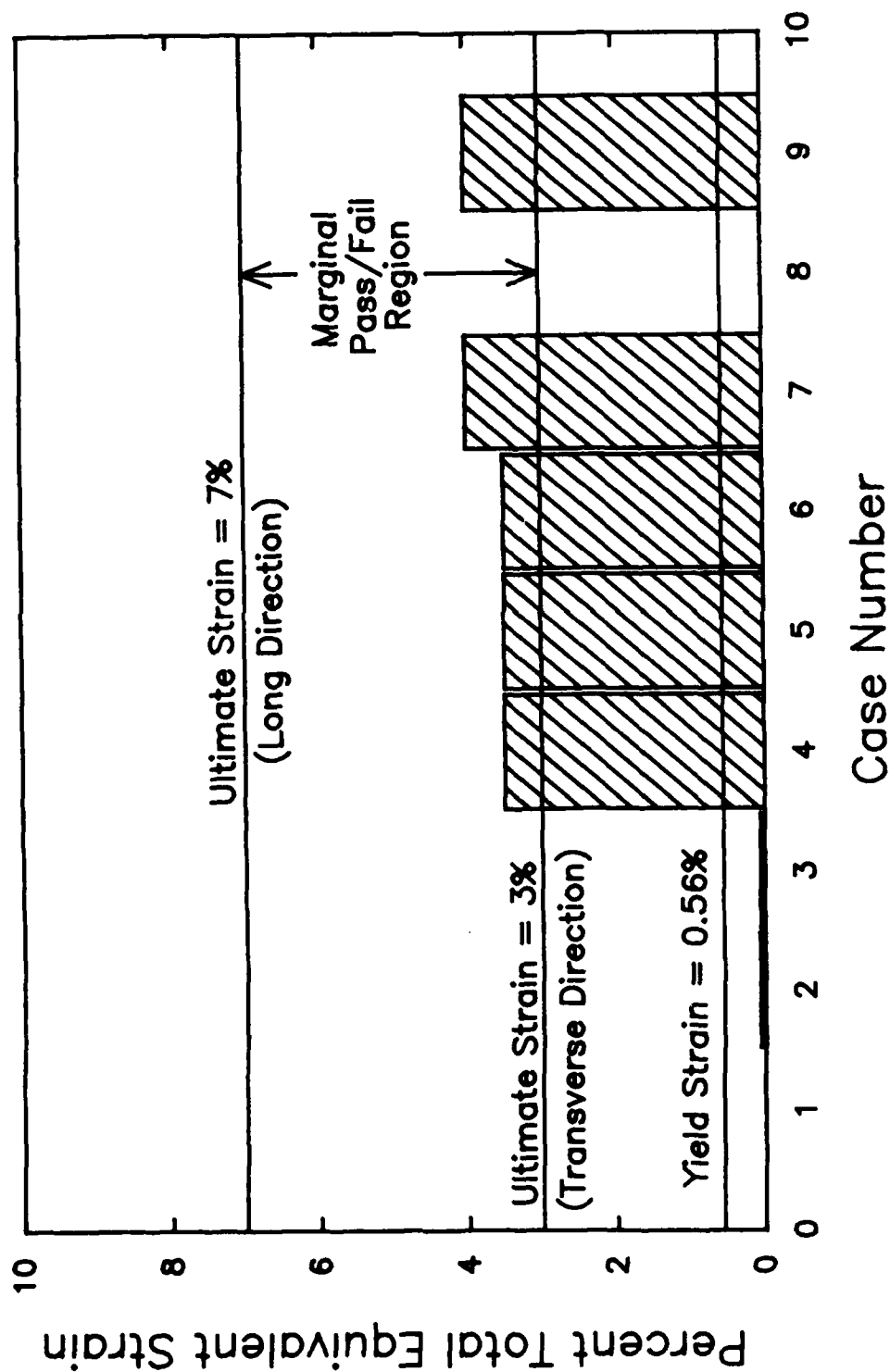


Figure 4.54. Strain Summary, Eyebrow.

TABLE 4.8
FASTENER ANALYSIS SUMMARY

Case No.	Category	Model Description	Loads	Safety Margins ^c			Safety Margins (50% fastener removal)			Interaction Relation Values ^d			
				Tension	Shear	Bearing Rupture	Tension	Shear	Bearing Rupture	All Present	50% Removal		
1	Baseline	Current Production Windshield	Natural Frequency	-	-	-	-	-	-	-	-		
2	Baseline	Current Production Windshield	Internal Pressure	3.12	4.64	6.50	20.91	1.06	1.82	2.75	24.66	0.06	0.28
3	Baseline	Current Production Windshield	Impact at A	2.18	2.55	3.72	12.78	0.59	0.77	1.36	15.14	0.12	0.57
4	Baseline	Current Production Windshield	Impact at B	0.99	0.98	1.63	6.68	-0.01	-0.01	0.32	8.00	0.38	2.05
5	Trade Study	Acrylic Outer Ply	Impact at B	1.16	1.44	2.25	8.48	0.08	0.22	0.62	10.10	0.28	1.41
6	Trade Study	Urethane Interlayer	Impact at B	1.15	1.31	2.07	7.97	0.07	0.15	0.54	9.51	0.30	1.52
7	Trade Study	Remover Inner (Spall) Ply	Impact at B	1.15	0.84	1.45	6.15	0.07	-0.08	0.22	7.37	0.38	2.15
8	Trade Study	Split Main Structural Ply	Internal Pressure	3.30	6.17	8.53	21.84	1.15	2.58	3.77	31.61	0.06	0.24
9	Trade Study	Split Main Structural Ply	Impact at B	1.47	0.68	1.23	5.52	0.23	-0.16	0.12	6.64	0.38	2.35

Notes:

- a. Point A is near-center location of windshield
- b. Point B is adjacent to the corner connection between the centerpost and eyebrow.
- c. Safety margins < 0.0 indicate failure
- d. Interaction Relation values > 1.0 indicate failure

FASTENER STRESS SUMMARY

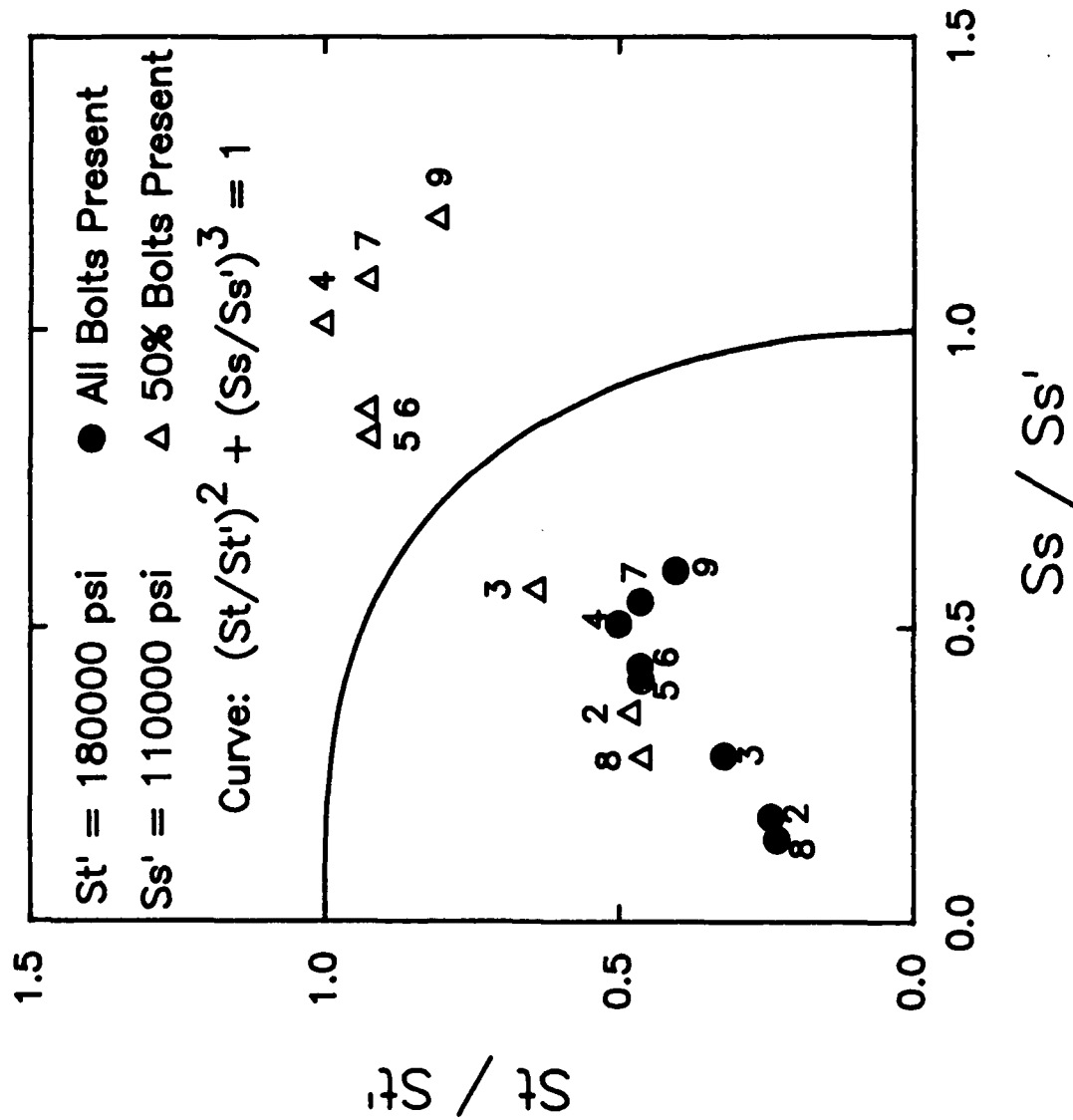


Figure 4.55. Fastener Stress Summary.

With all fasteners present, all birdstrike fastener margins are positive, indicating that the fasteners were sufficient to resist both near-center and upper corner birdstrikes without failure. (Note that, since the upper corner impact was more critical than the near-center impact, and since the fastener performance was acceptable for all upper corner impacts, it was inferred that the fastener performance would also be acceptable for near-center impact on those trade study configurations that were not explicitly analyzed for this impact condition.) The use of acrylic for the outer ply or urethane for the interlayers improved the fastener margins somewhat, while removing the spall ply or splitting the structural ply reduced the margins somewhat. With every other fastener removed, the safety margins and interaction numbers were still acceptable for the near-center impact, but were approximately the critical values (0 for margin of safety, 1 for interaction) for upper corner impact, meaning that fastener failure occurred. It is therefore recommended, based on the MAGNA results, that all fasteners be retained within 10 inches of either side of the eyebrow-to-centerpost corner connection (that is, do not delete every other fastener in this region). The decision on whether or not to delete fasteners in other regions should be based in part on additional birdstrike analyses with impact sites located near each region of interest, since such impact conditions result in the highest birdstrike-induced loads in the fasteners of interest.

Finally, based on a review of B-1B and B-1A fastener system drawings, it appears that the existing B-1B fastener-to-bushing tolerance is adequate to facilitate windshield changeout. Based on B-1A birdstrike test results for windshields having bushings with the as-specified fastener-to-bushing tolerance and windshields having bushings with an oversize tolerance, the existing B-1B tolerance should not change the structural behavior of the windshield system. All results reported herein should therefore be representative of the full-scale B-1B windshield system performance.

SECTION 5

CONCLUSIONS AND RECOMMENDATIONS

As a result of the MAGNA analyses, the following conclusions concerning the structural performance of the current production and alternate configuration B-1B windshield systems were reached:

1. The current production and the split polycarbonate structural ply windshield configurations resisted internal cabin pressures of up to 21.2 psig (ultimate pressure) without permanent deformation to the windshield panel or the immediate support structure. Similar performance is to be expected for all of the other trade study configurations.

2. The current production windshield configuration was capable of resisting impact by a 4-pound bird at the near-center location at 650 mi/hr without fracture of the windshield panel or immediate support structure. Similar performance is to be expected for the trade study configurations.

3. All windshield configurations were marginally capable of resisting impact by a 4-pound bird at the upper corner location at 650 mi/hr. All windshield system components passed without fracture except for the eyebrow frame, which exhibited a marginal pass/fail condition (see Conclusion 6).

4. The upper corner impact location was more critical than the near-center location, resulting in higher stresses and yielding in the windshield structural ply (plies) and the supporting framework.

5. All of the various windshield configurations demonstrated similar resistance to upper corner birdstrike, although the use of low strain rate interlayer material properties led to the split polycarbonate ply configuration exhibiting somewhat more windshield deflection and polycarbonate yielding, and exhibiting yielding in the centerpost.

6. The stresses and strains present in the MAGNA B-1B model indicated that a marginal pass/fail (fracture) condition in the eyebrow resulted from upper corner birdstrike. The high stress region in the eyebrow frame (the web between the bottom two flanges near the connection to the centerpost) due to upper corner birdstrike was the same region that fractured in upper corner birdstrike testing of the B-1A windshield system. Apparently the redesign of the crew enclosure from B-1A to B-1B did not eliminate potentially critical stresses (strains) in this region. No definite conclusion can be drawn whether or not the B-1B eyebrow frame will pass upper corner birdstrike by a 4-pound bird at 650 mi/hr. The results indicate that fracture in the eyebrow web is possible under such conditions.

7. The total strain present in the structural polycarbonate ply (plies) due to upper corner birdstrike was well below the elongation to failure for polycarbonate. Fracture of these plies during upper corner bird impact should therefore not occur unless the polycarbonate elongation is degraded (due to, for instance, improper material processing, embrittlement, or stress concentration).

8. The current production and trade study fasteners resisted internal cabin pressures up to 21.2 psig without failure.

9. Analysis of the current production windshield revealed that the upper corner impact produced fastener safety margins which were 50% less than those resulting from the near-center impact.

10. All fasteners in the current production and trade study windshield configurations withstood near-center and upper corner impact by a 4-pound bird at 650 mi/hr without failure.

11. With every other fastener deleted, the remaining fasteners were sufficiently strong to resist failure when the current production windshield was subjected to impact by a 4-pound bird at the near-center location. Similar fastener performance is to be expected for the trade study configurations.

12. When every other fastener was removed from the current production and trade study windshield configurations, the resulting safety margins for upper corner impact were reduced to approximately zero, implying that fastener failure was probable.

13. The critical fastener tolerance for windshield changeout was identified to be the fastener-to-frame tolerance. This tolerance (0.010 - 0.015 inch) was larger than the B-1A tolerance (0.007 inch) and was judged to be adequate to facilitate windshield changeout. The existing B-1B tolerance does not change the results reported herein, that is, the structural performance is not degraded or improved by this tolerance.

Based on the above conclusions, the following are recommended:

1. To prevent upper corner fastener failure, it is recommended that all fasteners be retained within 10 inches of either side of the eyebrow-to-centerpost corner connection (that is, do not delete every other fastener in this region).

2. The decision on whether or not to delete fasteners in other regions should be based in part on additional birdstrike analyses with impact sites located near the regions of interest, since such impact conditions result in the highest birdstrike-induced loads in the fasteners of interest.

REFERENCES

1. Sanders, Eugene J., Results of Qualification Testing of Bird Resistant Windshields for the B-1 Aircraft, AEDC-DR-75-87, Arnold Engineering Development Center, Arnold Air Force Station, Tennessee, September 1975.
2. Brockman, R.A., MAGNA (Materially and Geometrically Nonlinear Analysis, Part I - Finite Element Analysis Manual, AFWAL-TR-82-3098, Part I, Air Force Wright-Aeronautical Laboratories, Wright-Patterson Air Force Base, Ohio, March 1984.
3. Bruner, T.S., Brockman, R.A., and Primrose, K.A., MAGNA (Materially and Geometrically Nonlinear Analysis, Part II - Preprocessor Manual, AFWAL-TR-82-3098, Part II, Air Force Wright-Aeronautical Laboratories, Wright-Patterson Air Force Base, Ohio, March 1984.
4. McCarty, R.E. and Hart, 2nd Lt. J.L., "Validation of the MAGNA Computer Program for Nonlinear Finite Element Analysis of Aircraft Transparency Bird Impact," AFWAL-TR-83-4154, Proceedings for Conference on Aerospace Transparent Materials and Enclosures, pp. 921-972, Air Force Wright Aeronautical Laboratories, December 1983.
5. Hoit, Marc and Wilson, E. L., "An Equation Numbering Algorithm Based on a Minimum Front Criteria," Computers and Structures, Vol. 16, Nos. 1-4, pp. 225-239, 1983.
6. Brockman, R.A., Simple Finite Elements for Layered Plates and Shells, UDR-TR-87-111, University of Dayton Research Institute, Dayton, Ohio, August 1987.
7. Sanders, Eugene J., Results of Further Tests to Evaluate the Bird Impact Resistance of Windshields for the B-1 Aircraft, AEDC-DR-76-43, Arnold Engineering Development Center, Arnold Air Force Station, Tennessee, May 1976.
8. Sanders, Eugene J., Results of Bird Impact Testing of Prototype B-1 Windshields and Supporting Structure Design, AEDC-DR-76-100, Arnold Engineering Development Center, Arnold Air Force Station, Tennessee, December 1976.

9. Brockman, R.A. and West, B.S., Bell-Boeing V-22 Birdstrike Loads Estimation, UDR-TM-86-12, University of Dayton Research Institute, Dayton, Ohio, July 1986.
10. Barber, John P., Taylor, Henry T., and Wilbeck, James S., Bird Impact Forces and Pressures on Rigid and Compliant Targets, AFFDL-TR-77-60, Air Force Wright Aeronautical Laboratories, Wright-Patterson Air Force Base, Ohio, May 1978.
11. West, Blaine S. and Brockman, Robert A., Evaluation of Bird Load Models for Dynamic Analysis of Aircraft Transparencies, AFWAL-TR-80-3092, Air Force Wright Aeronautical Laboratories, Wright-Patterson Air Force Base, Ohio, August 1980.
12. Braisted, W. R., Transparency Fastener Analysis Based on MAGNA Finite Element Analysis Results, UDR-TR-88-146, University of Dayton Research Institute, Dayton, Ohio., December 1988.
13. Brockman, R.A., Bruner, T.S., Hecht, M.J., Bouchard, M.P., and Wright, M.E., MAGNA (Materially and Geometrically Nonlinear Analysis, Part III - Postprocessor Manual, AFWAL-TR-82-3098, Part III, Air Force Wright-Aeronautical Laboratories, Wright-Patterson Air Force Base, Ohio, March 1984.
14. Rubenstein, Steve, Norby, John, and Mitchell, Dick, Sigma Plot - Scientific Graph System, Version 3.0, Jandel Scientific, Sausalito, California, 1986.
15. Popov, E.P., "Thin-Walled Pressure Vessels," from Mechanics of Materials, 2nd Ed., Prentice-Hall, Inc., pp. 288-290, 1976.
16. _____, Merlon Polycarbonate Design Manual, Plastics Division, Mobay Chemical Corporation, Pittsburgh, Pennsylvania.
17. Magnusson, R.H., High Speed Bird Impact Testing of Aircraft Transparencies, AFFDL-TR-77-98, Air Force Wright Aeronautical Laboratories, Wright-Patterson Air Force Base, Ohio, June 1978.
18. _____, Military Standardization Handbook - Metallic Materials and Elements for Aerospace Vehicle Structures, MIL-HDBK-5D, Volume 1, Department of Defense, Washington, D.C., June 1983.
19. Lawrence, James A. Jr., Guidelines for the Design of Aircraft Windshield/Canopy Systems, AFWAL-TR-80-3003, Air Force Wright Aeronautical Laboratories, Wright-Patterson AFB, OH, February 1980.

20. Greene, F. E., Testing for Mechanical Properties of Monolithic and Laminated Polycarbonate Materials--Part I: Test Results and Analysis, AFFDL-TR-77-96, Part I, Air Force Wright Aeronautical Laboratories, Wright-Patterson AFB, OH, October 1978.
21. _____, Military Standardization Handbook, Plastics for Aerospace Vehicles--Part II: Transparent Glazing Materials, MIL-HDBK-17A, Part II, June 1977.
22. Rockwell B-1B Drawing L 3051091, note for Parts -007 and -008.
23. Clayton, Kenneth I., Milholland, John F., and Stenger, Gregory J., Experimental Evaluation of F-16 Polycarbonate Canopy Material, AFWAL-TR-81-4020, Air Force Wright Aeronautical Laboratories, Wright-Patterson AFB, OH, April 1981.
24. Rajendran, A. M. and Bless, S. J., High Strain Rate Material Behavior, AFWAL-TR-85-4009, Air Force Wright Aeronautical Laboratories, Wright-Patterson AFB, OH, December 1985.